Imperial College London

The synergy of modelling and experimental imaging in soil mechanics research

Prof. Catherine O'Sullivan
Dept. Civil and Environmental Engineering
Imperial College London

cath.osullivan@imperial.ac.uk

https://www.imperial.ac.uk/people/cath.osullivan

Outline

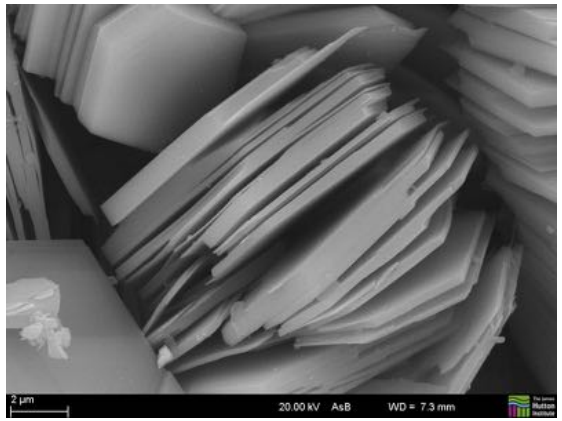

Part 1: Clay

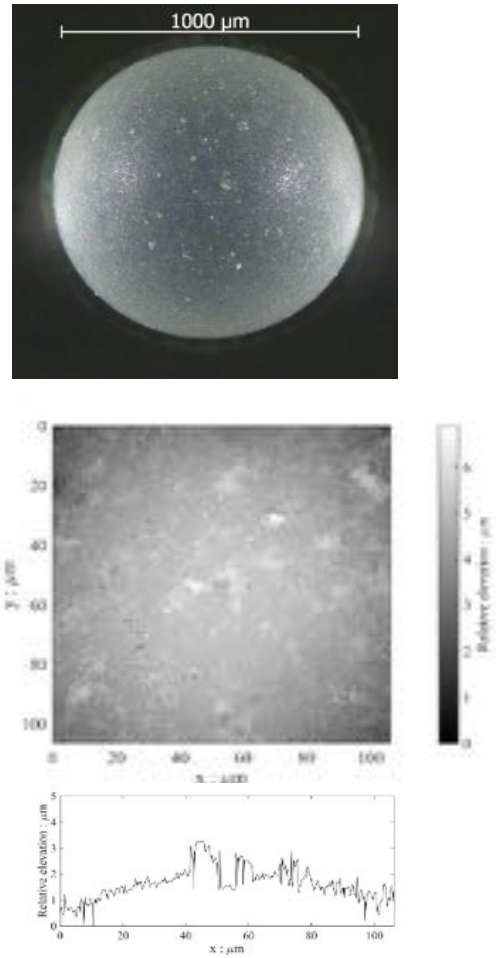

Part 2: Surface roughness

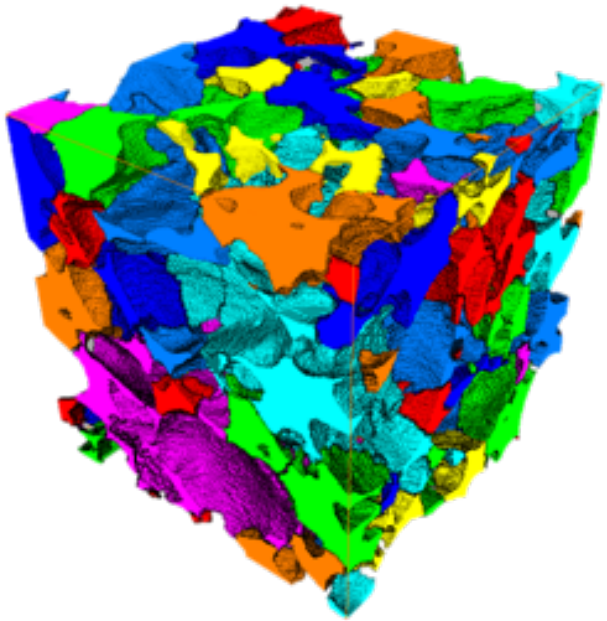

Part 3: Void space topology and fluid flow

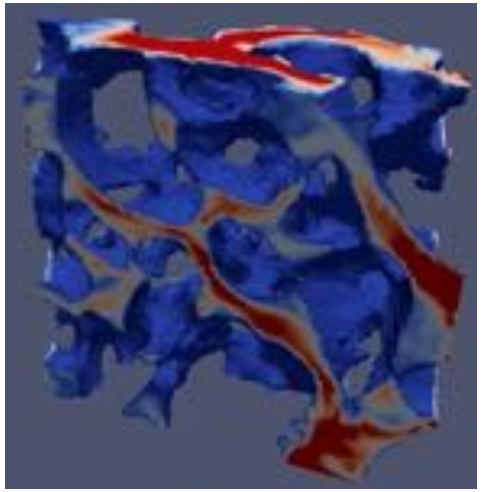

Part 4: Semi-solid metals

Part 1: Clay behaviour

AFM and SEM

Clay – challenges posed

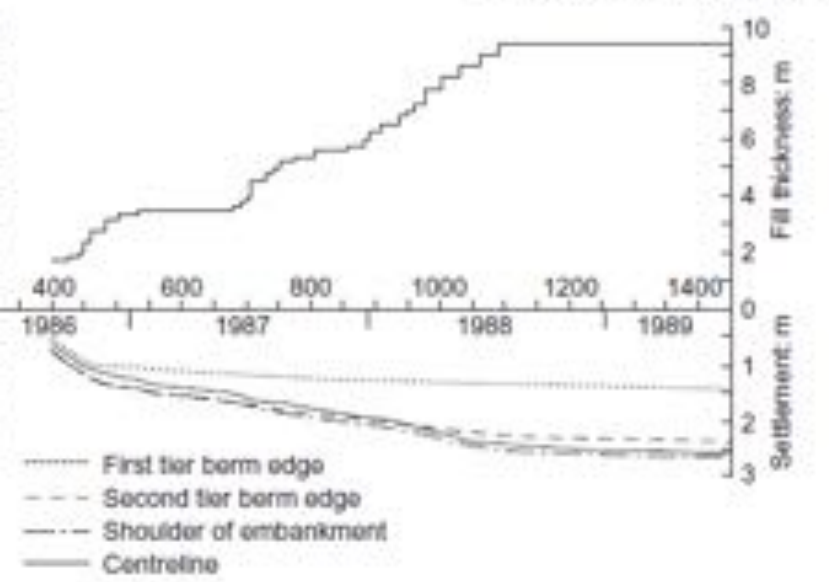

Large, time dependant settlement observed at Athlone road embankment in Ireland (Long and O'Riordan, 2001)

Quick clay landslide at Lyngseidet, Norway September 3, 2010 (220,000 m^3) (Geological survey of Norway, 2015)

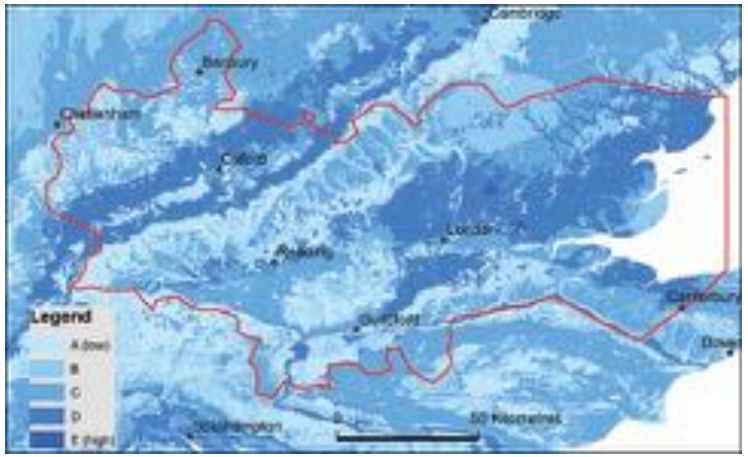

Hazard potential for shrink–swell clay in the Thames basin (British Geological Survey, 2019)

Particle scale model of kaolinite

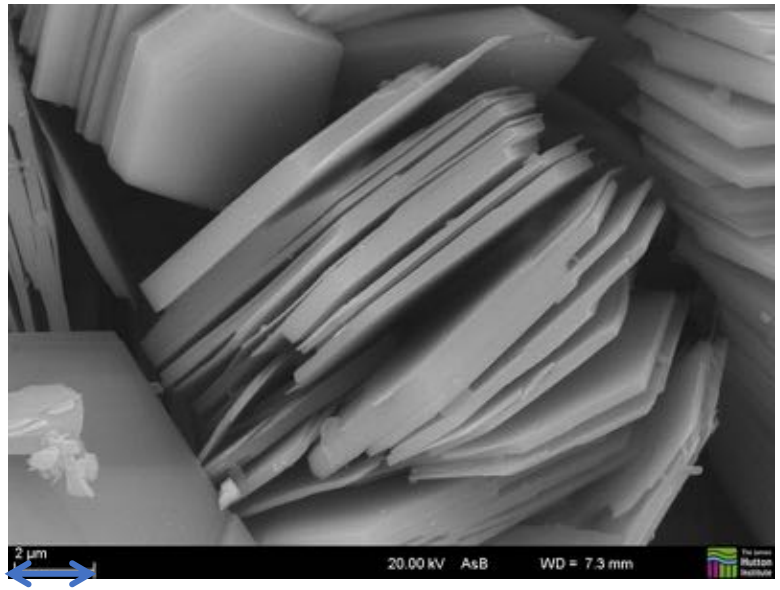

2µm

https://www.minersoc.org/images-of-clay.html

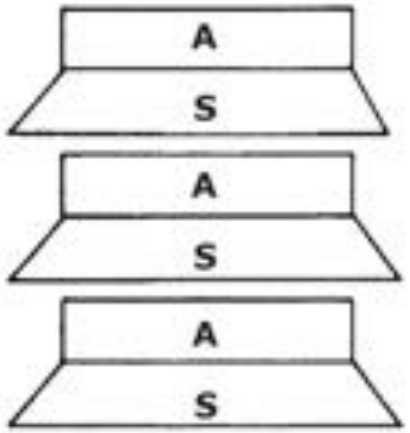

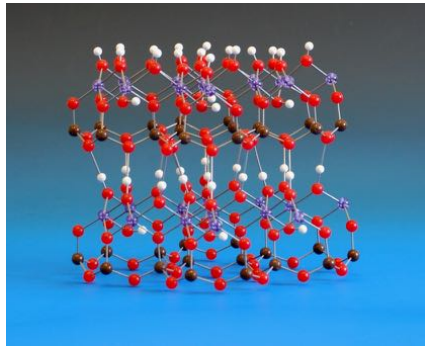

Silicon tetrahedra and aluminium octahedra structural units (Mitchell and Soga, 2005, https://www.miramodus.com)

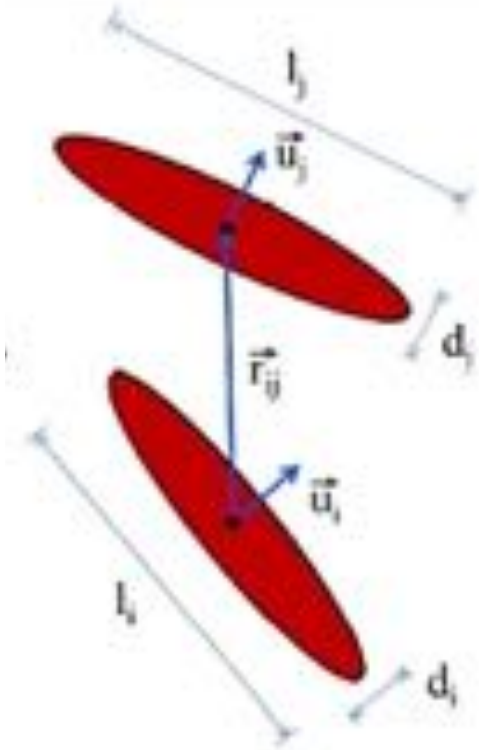

Simulate interactions using Gay – Berne Potential – generalization of Lennard Jones Potential for ellipsoids

DLVO model

- Derjaguin-Landau-Vervey-Overbeek Model
- Developed to explain colloidal behaviour- equilibrium of colloids in solution
- Dates from 1950s
- Generally accepted in soil mechanics
- Gives force / energy per unit area

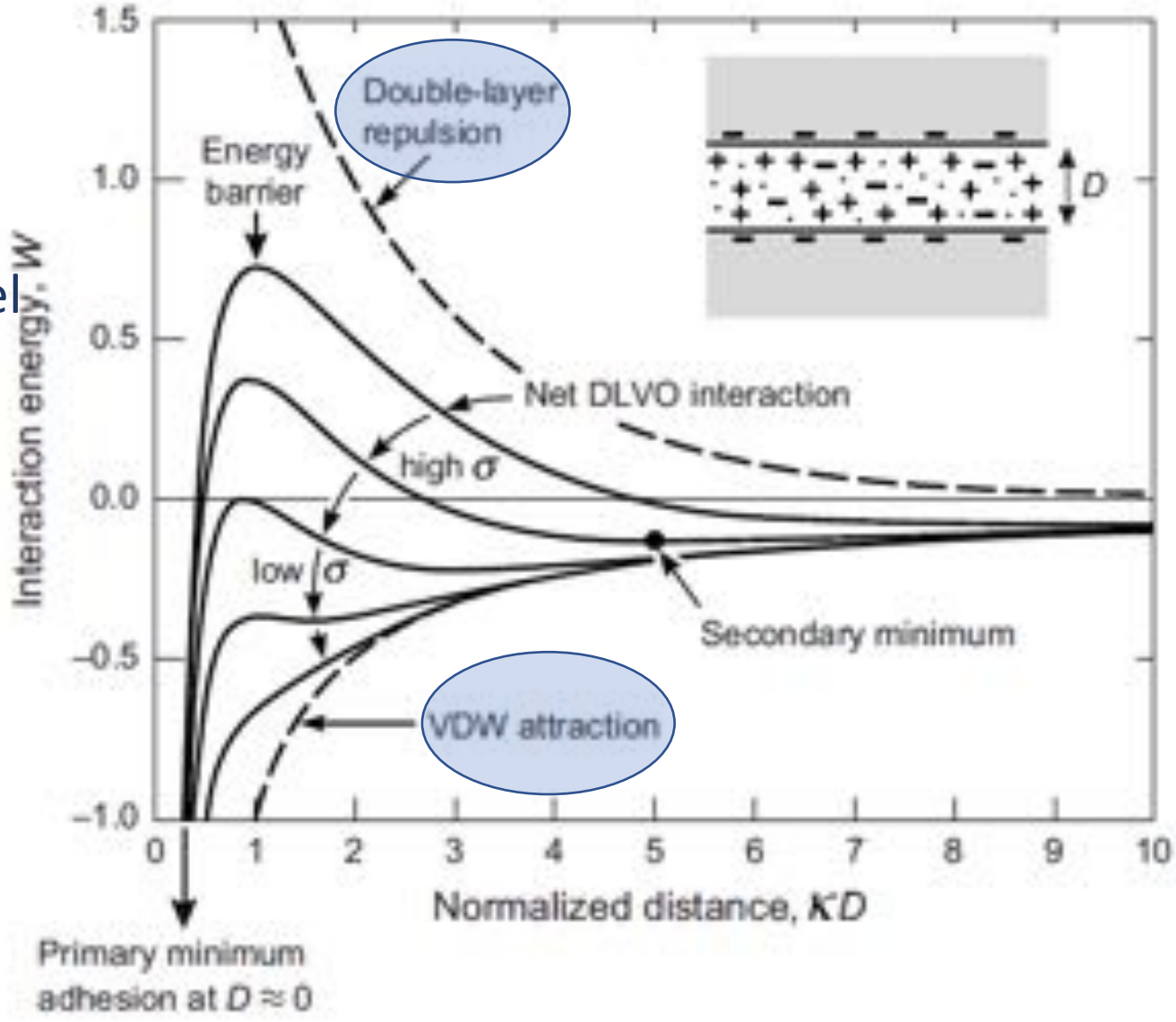

Israelavhvili (2011)

Van der Waals Energy

- Attractive force (in case of colloids)

$$E_{vdv} = \frac{\boldsymbol{A_H}}{12\pi}\left[\frac{1}{h^2} + \frac{1}{(h+\boldsymbol{\delta_1}+\boldsymbol{\delta_2})^2} - \frac{1}{(h+\boldsymbol{\delta_1})^2} - \frac{1}{(h+\boldsymbol{\delta_2})^2}\right]$$

Assume two infinite parallel plates

- h = separation distance
- Mineralogy of the clay considered and type of solvent through Hamaker Constant A_H
- Thickness of interacting particles δ_i

Model parameters √

Electrostatic Energy

$$\mathrm{E}_{\mathrm{Coulumb}} = \boldsymbol{\varepsilon_r \epsilon_0 \kappa} \left[\frac{2\boldsymbol{\psi_1 \psi_2} \exp(\kappa h) - \psi_1^2 - \psi_2^2}{\exp(2\kappa h) - 1} \right]$$

- Dielectric permittivity ε_r **√**
- κ - Debye length which depends on salt concentration ρ_s **√**
- Surface potential ψ_i ***Challenging to determine accurately***

Atomic Force Microscopy (AFM`

System to determine cantilever bending moment

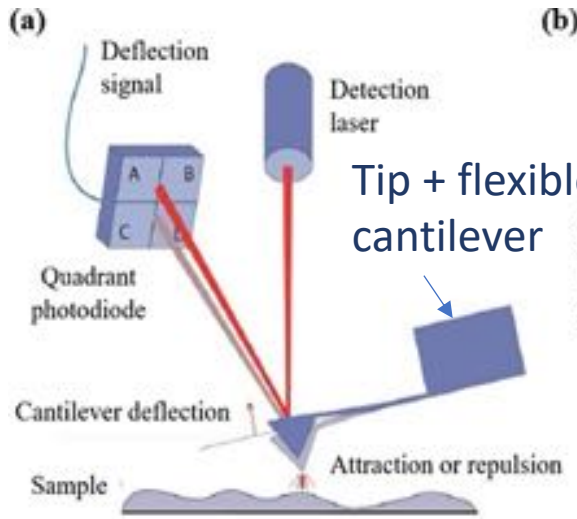

Tip + flexible cantilever

Silicon nitride tip on mica in air

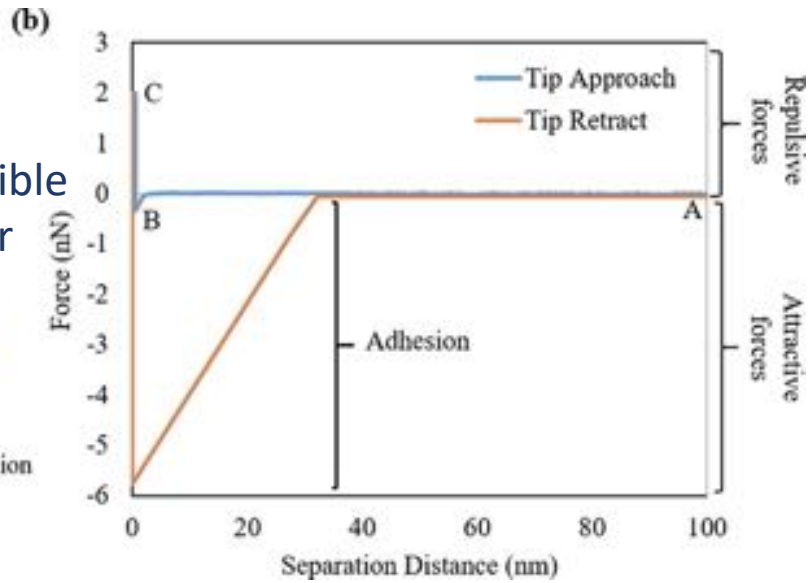

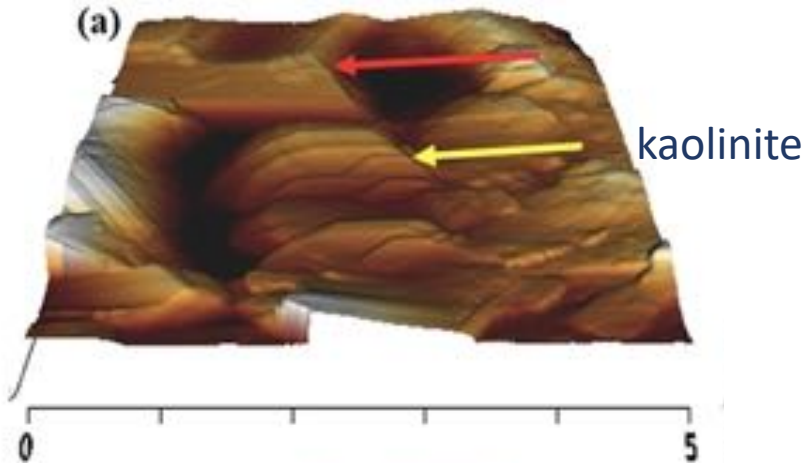

kaolinite

Clay edges

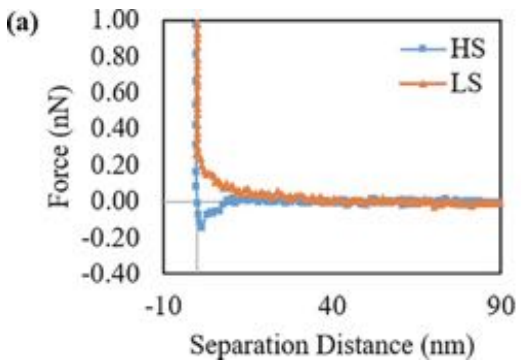

Clay basal planes

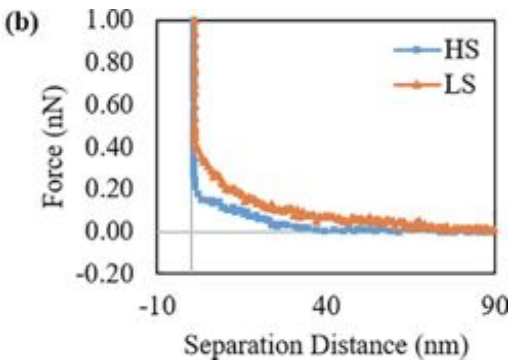

Forces on kaolinite:
HS – high salinity, LS -Low salinitiy

AFM→ topography, stiffness and adhesion

Yesufu-Rufaia et al. (2020)
https://doi.org/10.1016/j.fuel.2020.117807

Particle-scale measurements

- Atomic Force Microscopy measurements of surface charge
- Gupta (2011) and Liu (2015) working with Miller at the University of Utah
- Kumar (2017) University of Twente
- Both highlight different pH sensitivity of alumina and silica faces

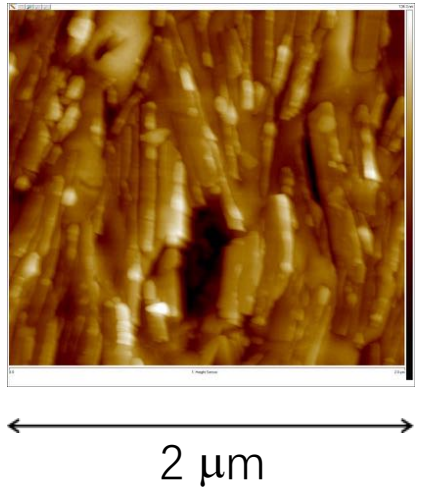

AFM image of kaolinite particle edges (Liu, 2015)

Surface charge

- Influenced by salt concentration and acidity of environment

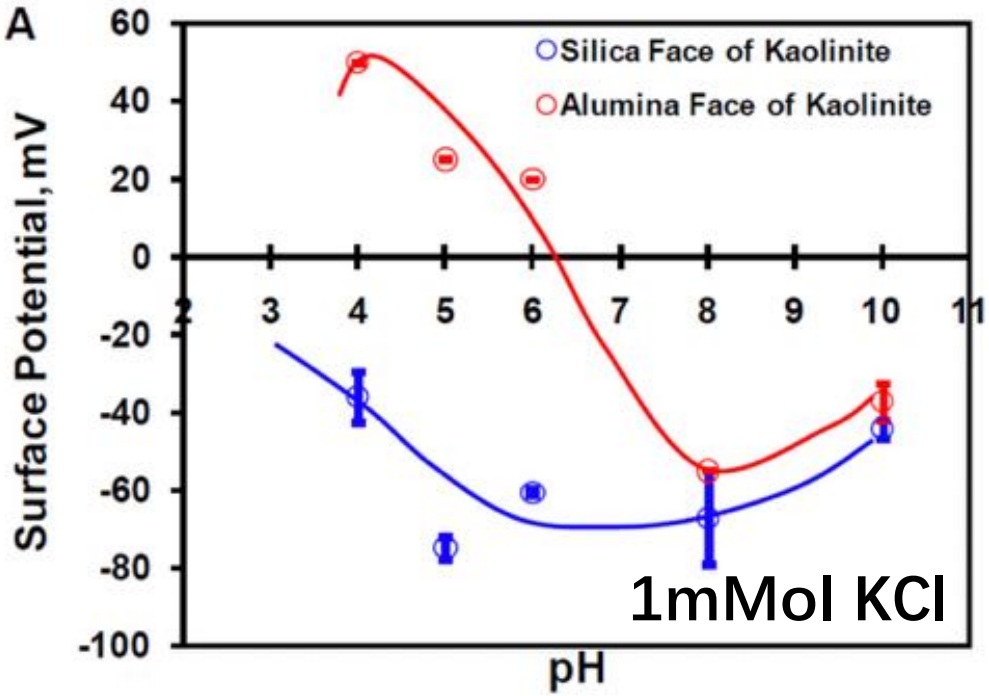

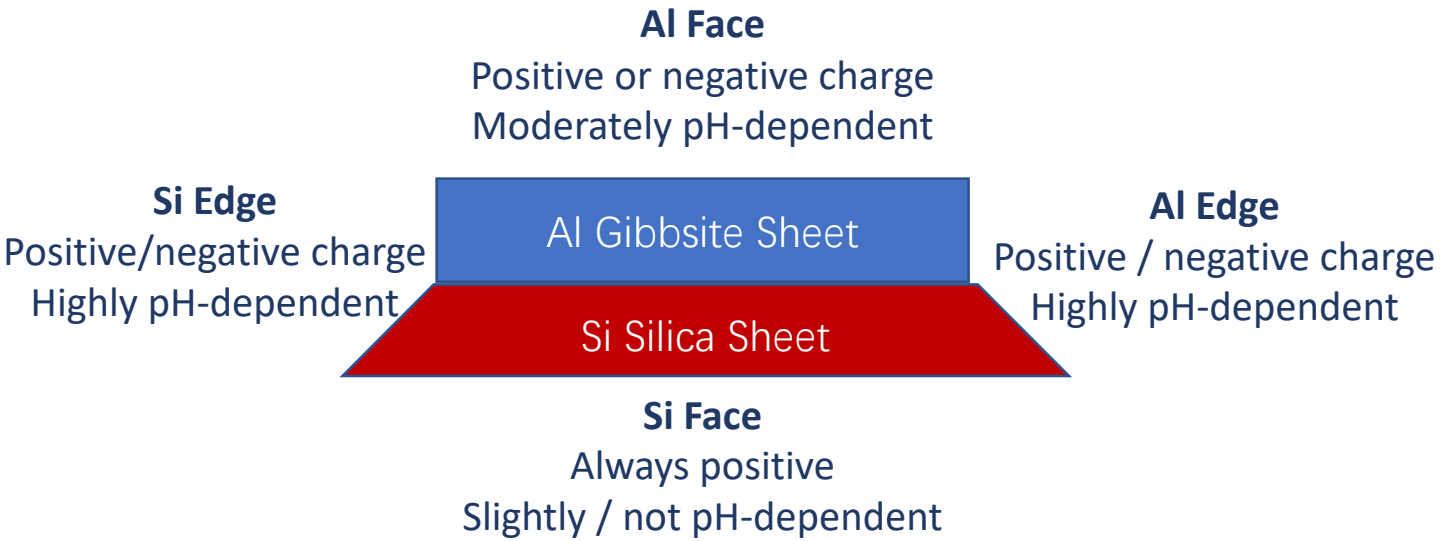

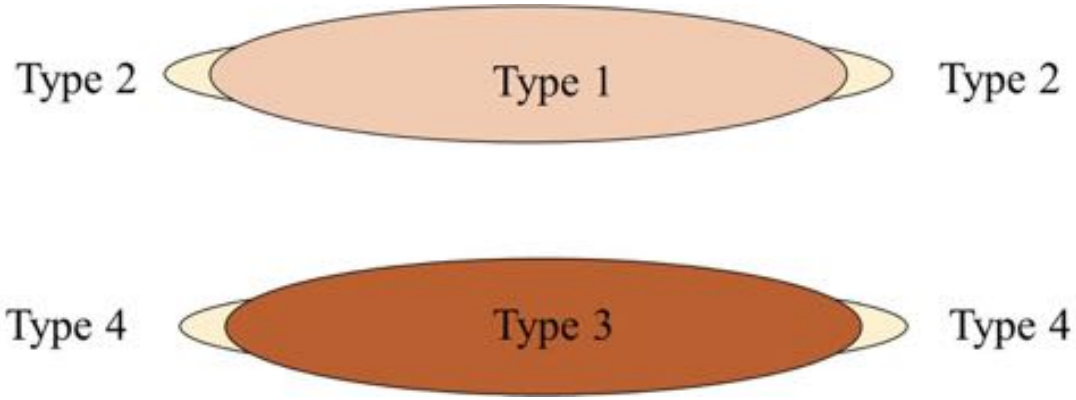

- Atomic Force Microscpy (AFM) measurements from Gupta (2011)

- Additional measurements Liu (2015)

Required system size

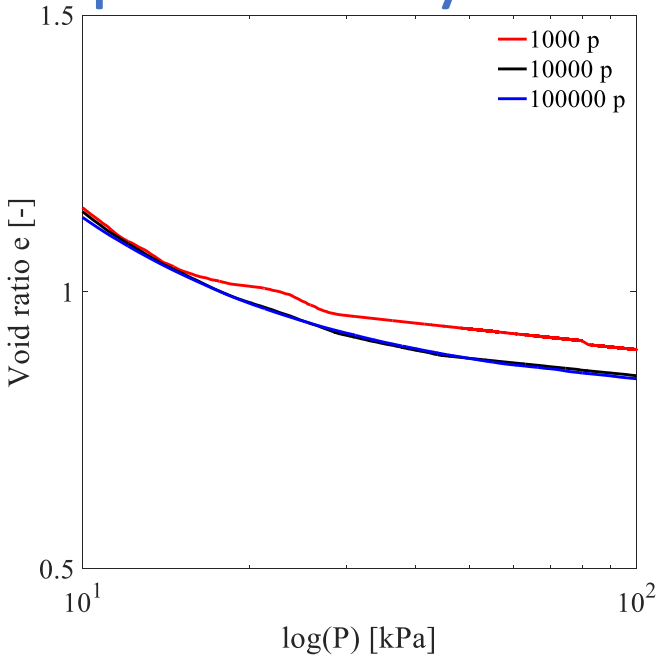

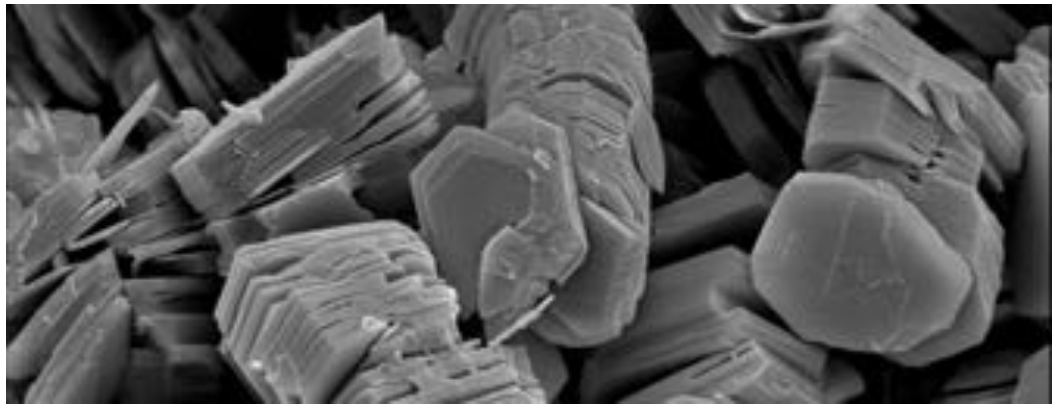

SEM image of kaolinite
(Mineralogical Society of Great Britain and Ireland)

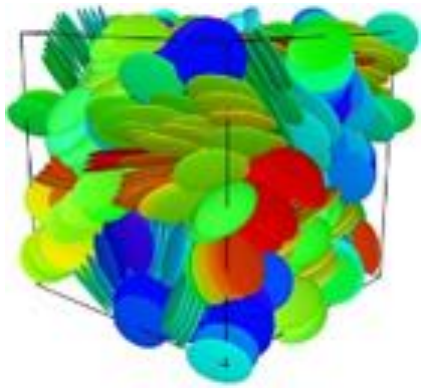

1,000 particle system

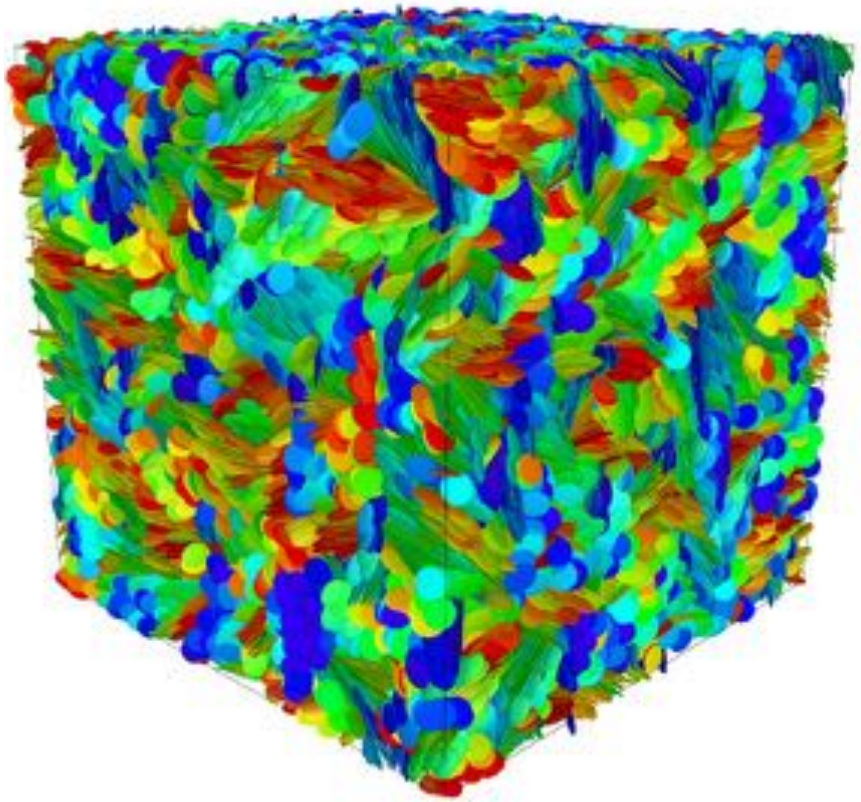

100,000 particle system

Part 2: Granular soils

Interferometry and surface roughness

Stiffness

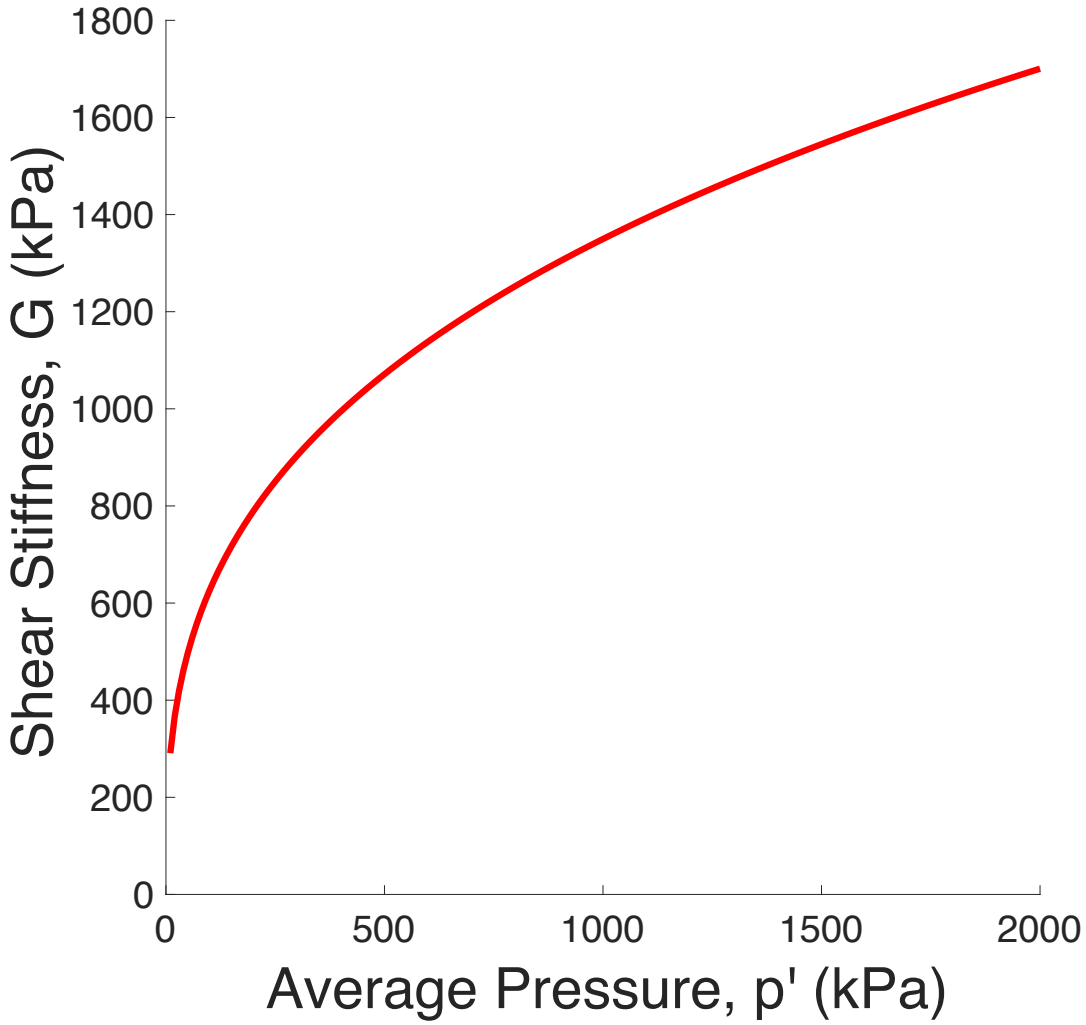

https://centralpiling.com/case-studies/harbour-central-isle-of-dogs-london/

Stiffness

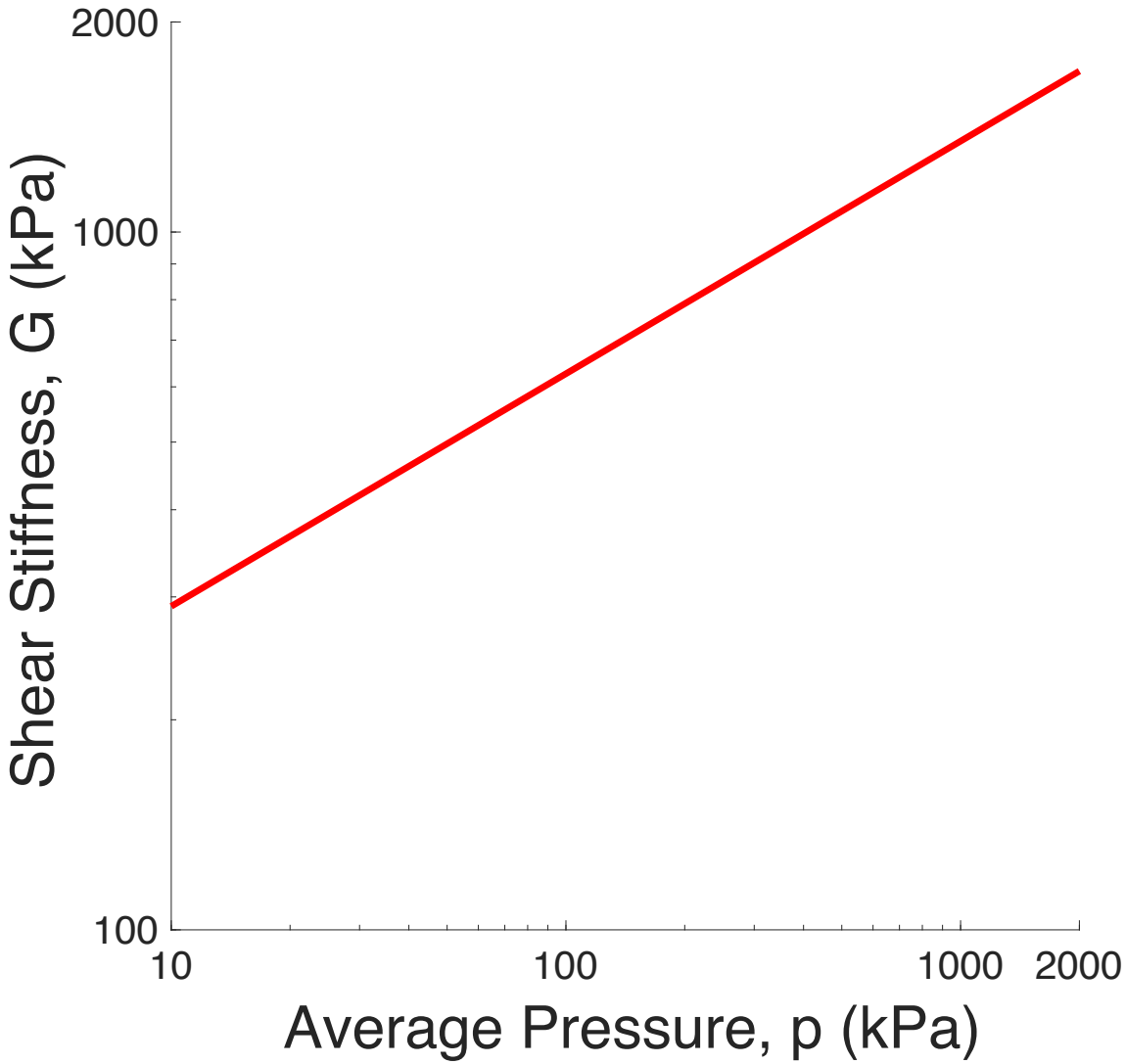

https://centralpiling.com/case-studies/harbour-central-isle-of-dogs-london/

Pressure-Stiffness Relationship

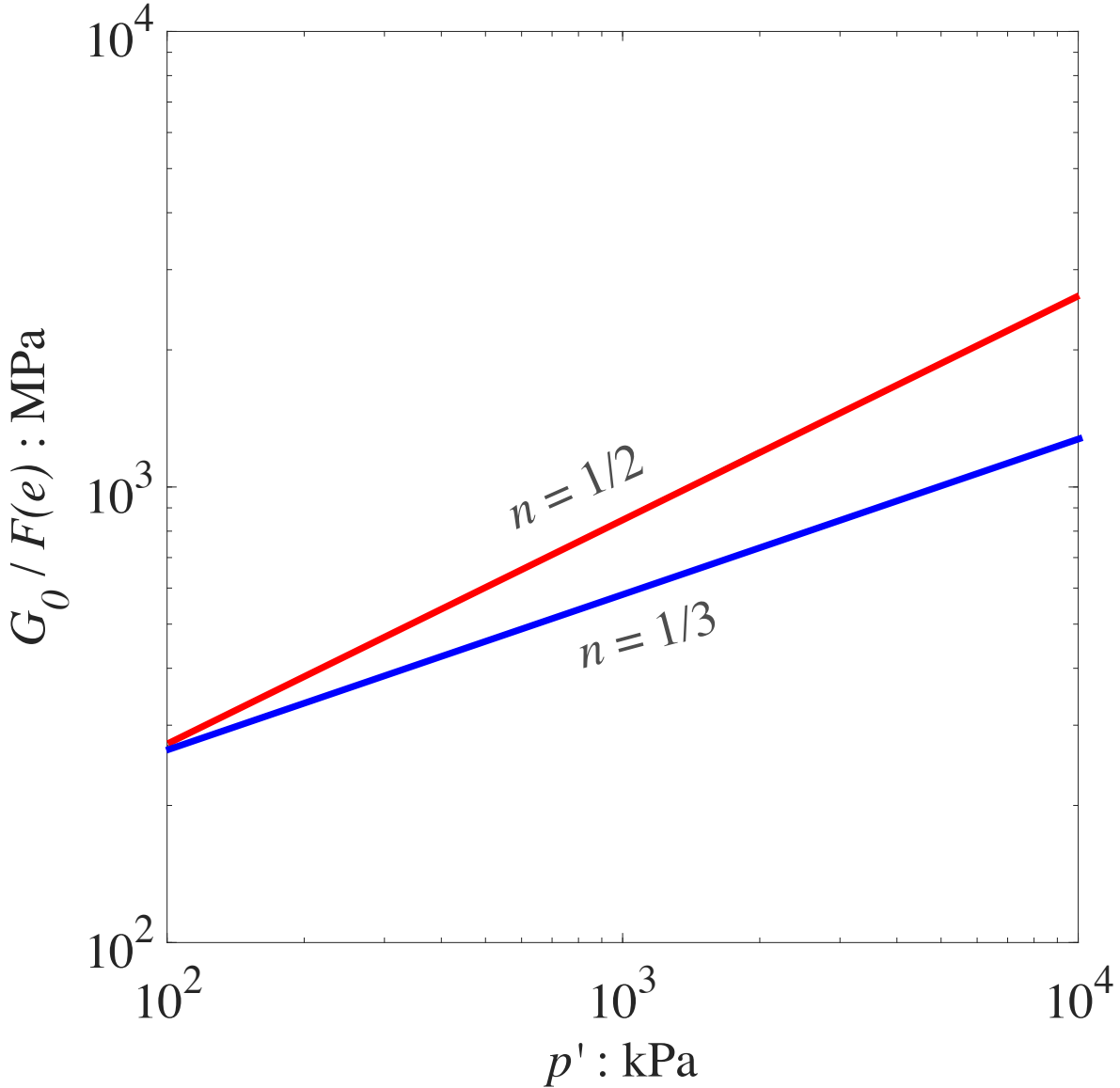

- Elastic theory explains pressure dependency: contact area increases as pressure increases – larger area gives a larger stiffness
- Elastic theory predicts that $G_0 \propto (p')^{1/3}$
- Experimental data for sand gives $G_0 \propto (p')^{1/2}$

Otsubo and O'Sullivan S+F (2018)

Roughness-dependant contact behaviour

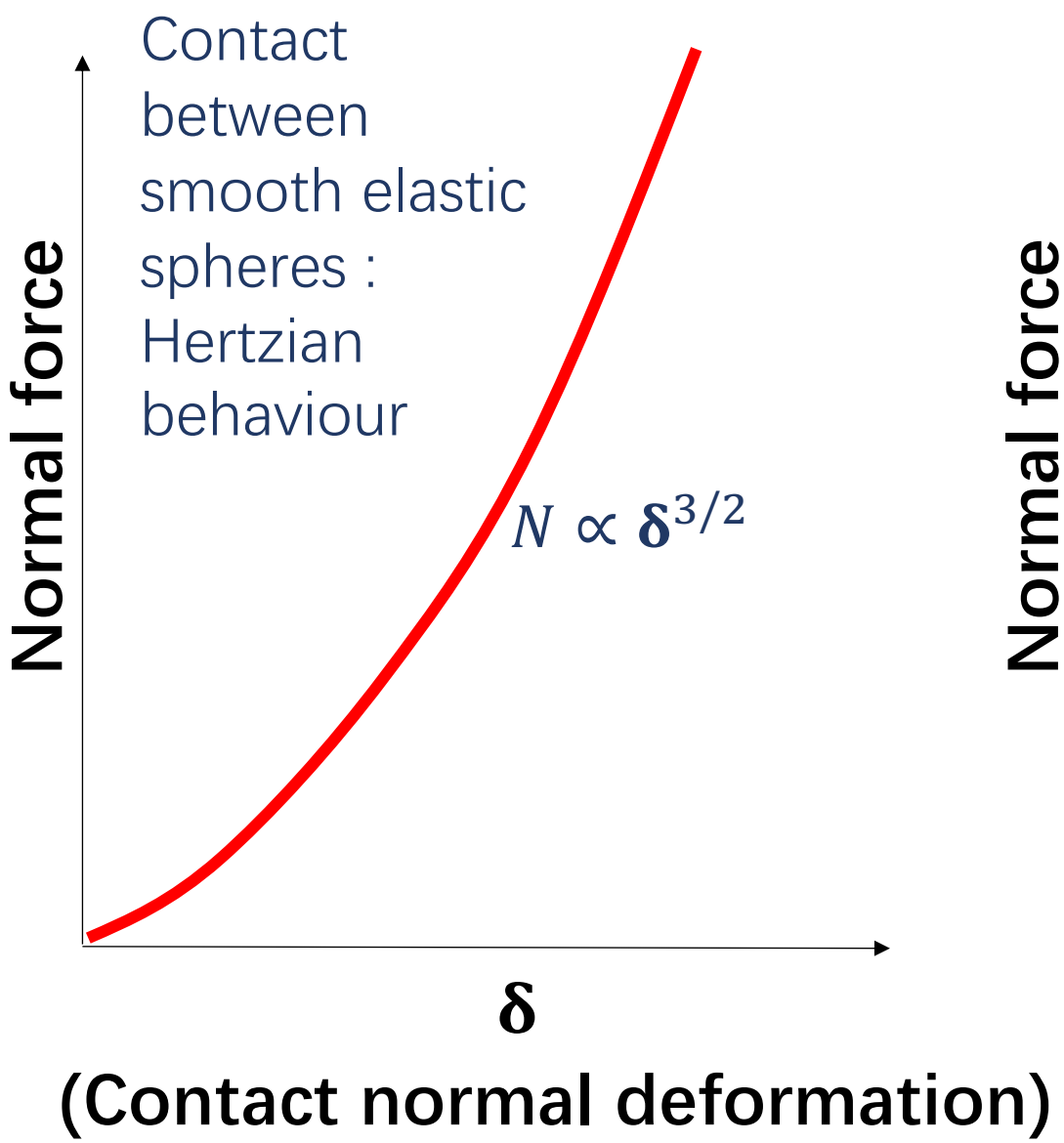

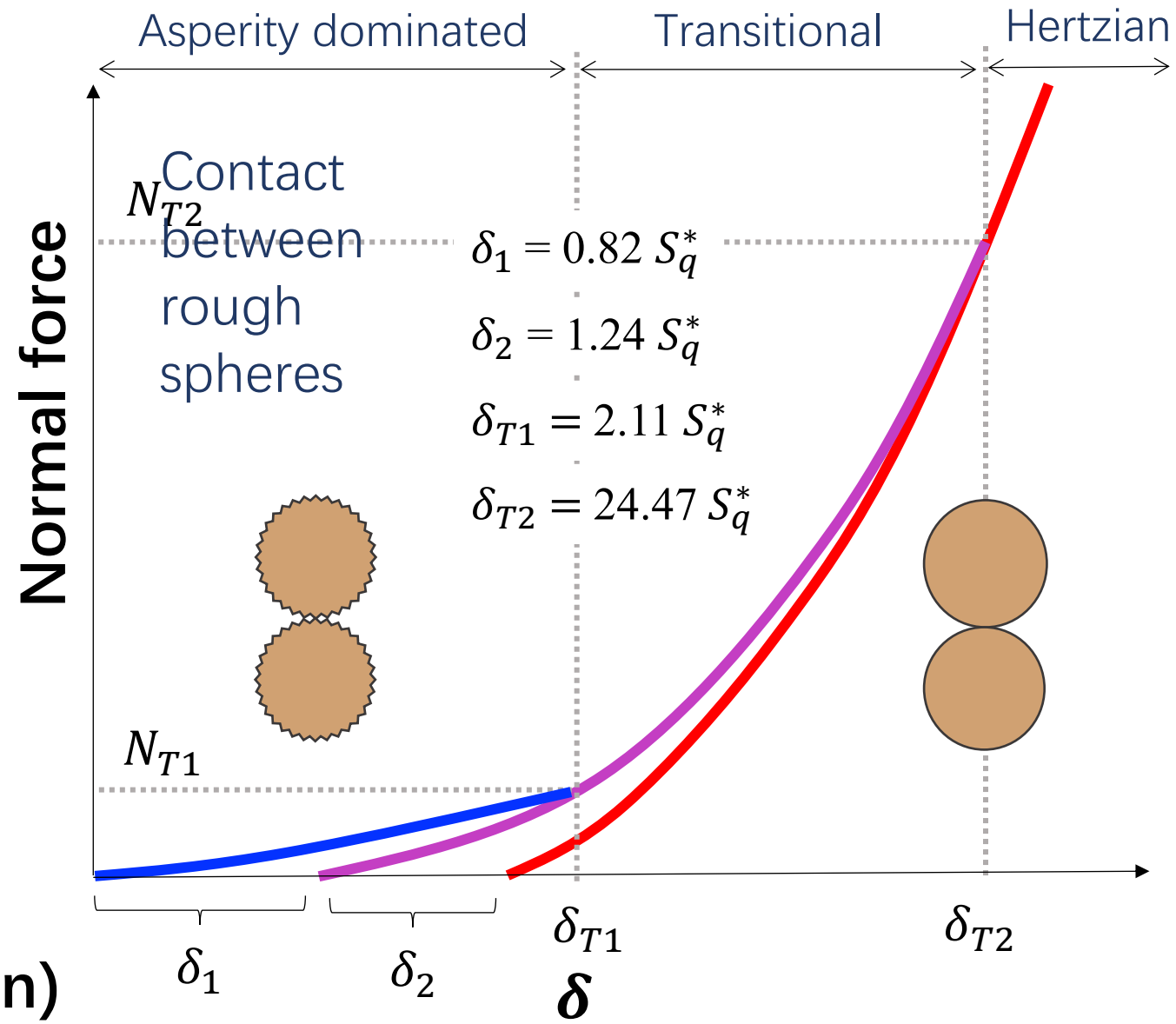

Controlling and Surface Roughness

Ballotini + Toyoura Sand

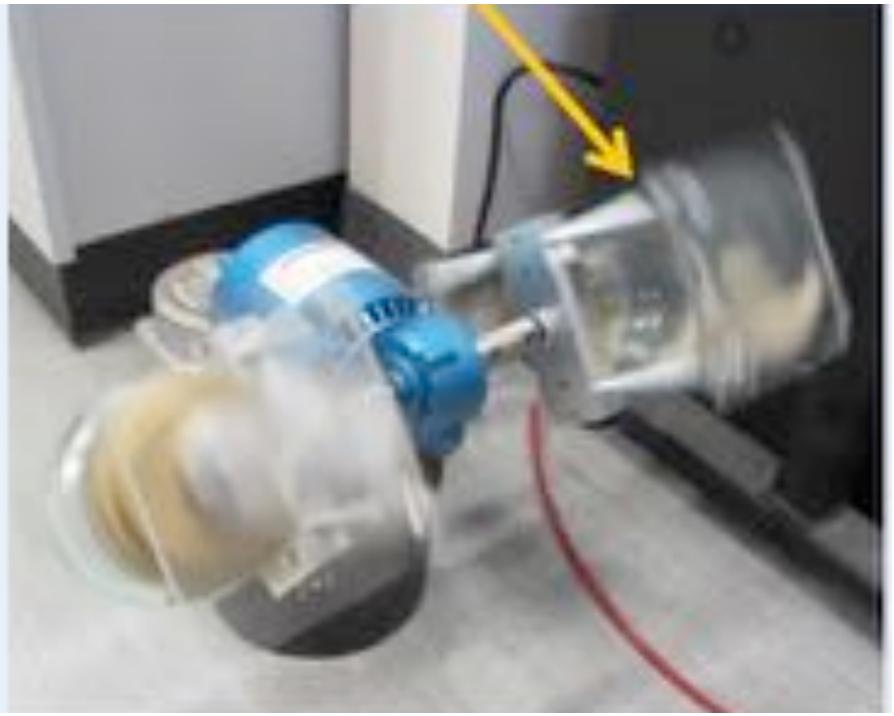

Used spherical glass beads to isolate roughness from shape (form) effects

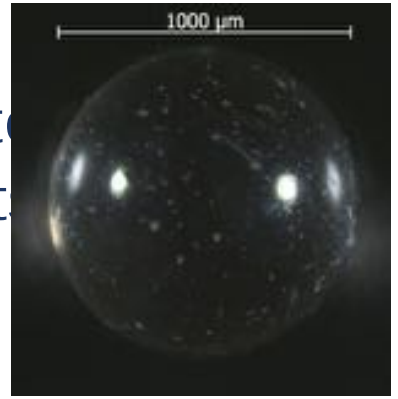

Measured roughness using interferometry

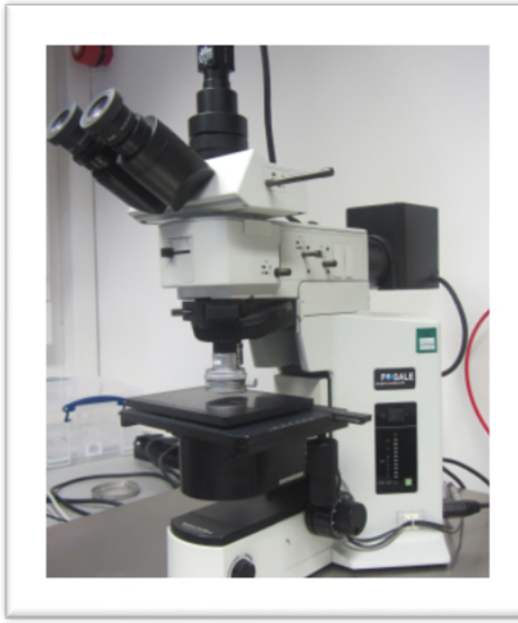

Surface roughness measurement

Optical interferometry

Quantify surface roughness

RMS roughness

$$S_q = \sqrt{\frac{1}{n}\sum_{i=1}^{n} Z_i^2}$$

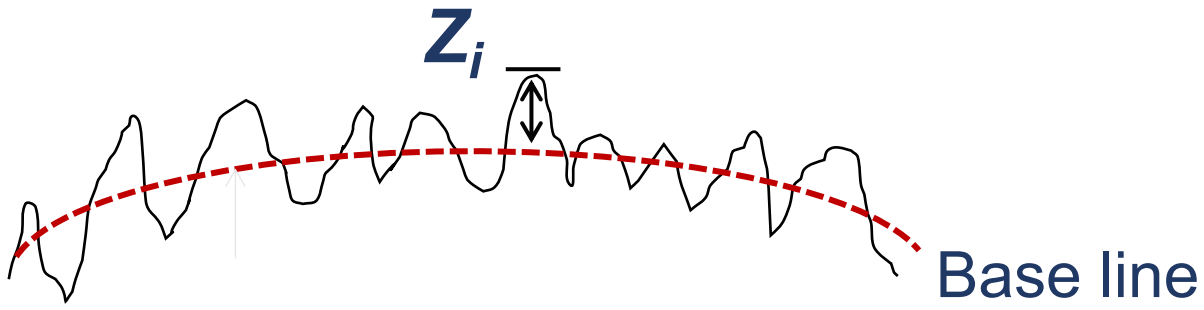

Roughened Ballotini

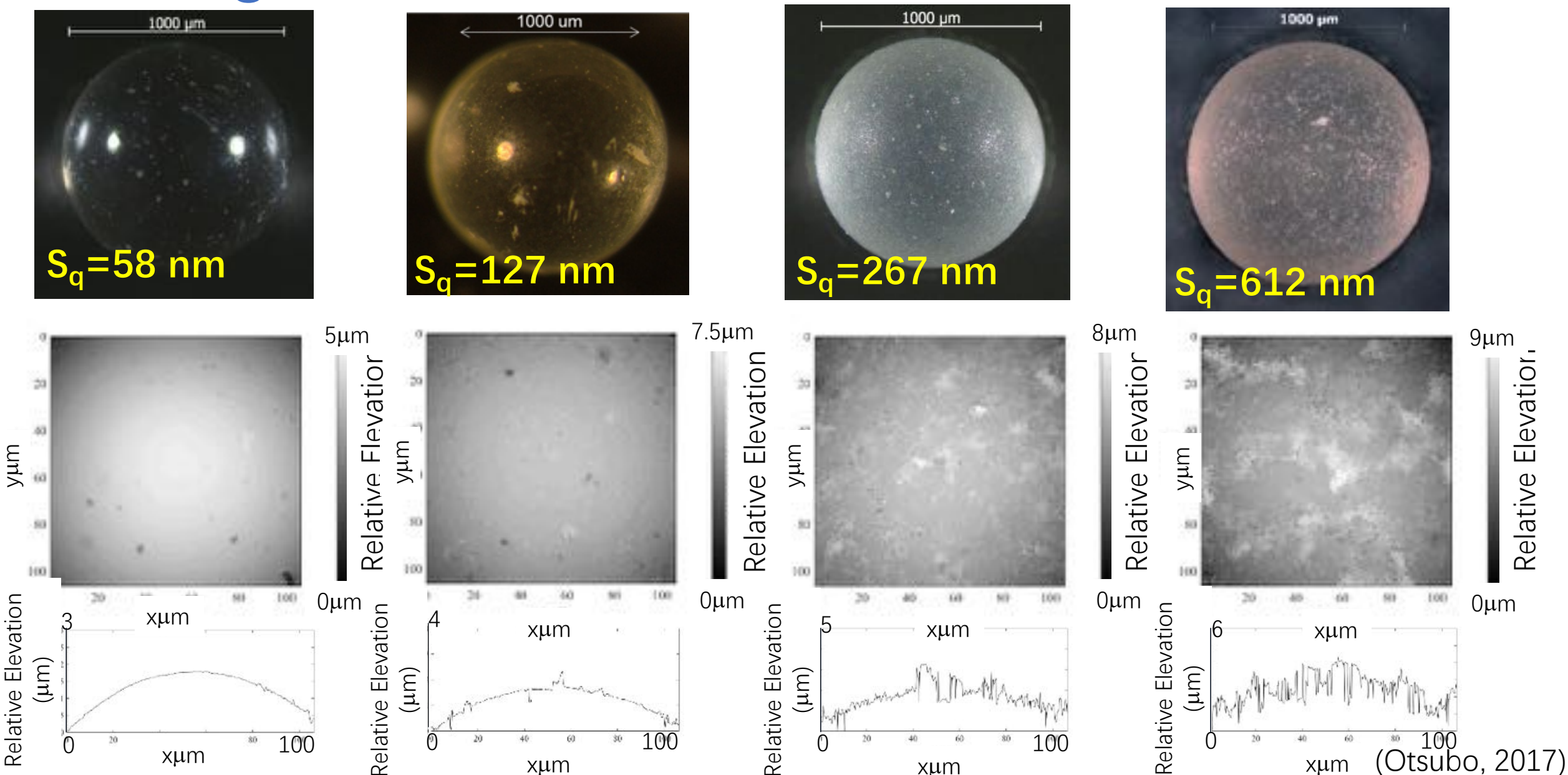

(Otsubo, 2017)

Quantifying Stiffness in Laboratory

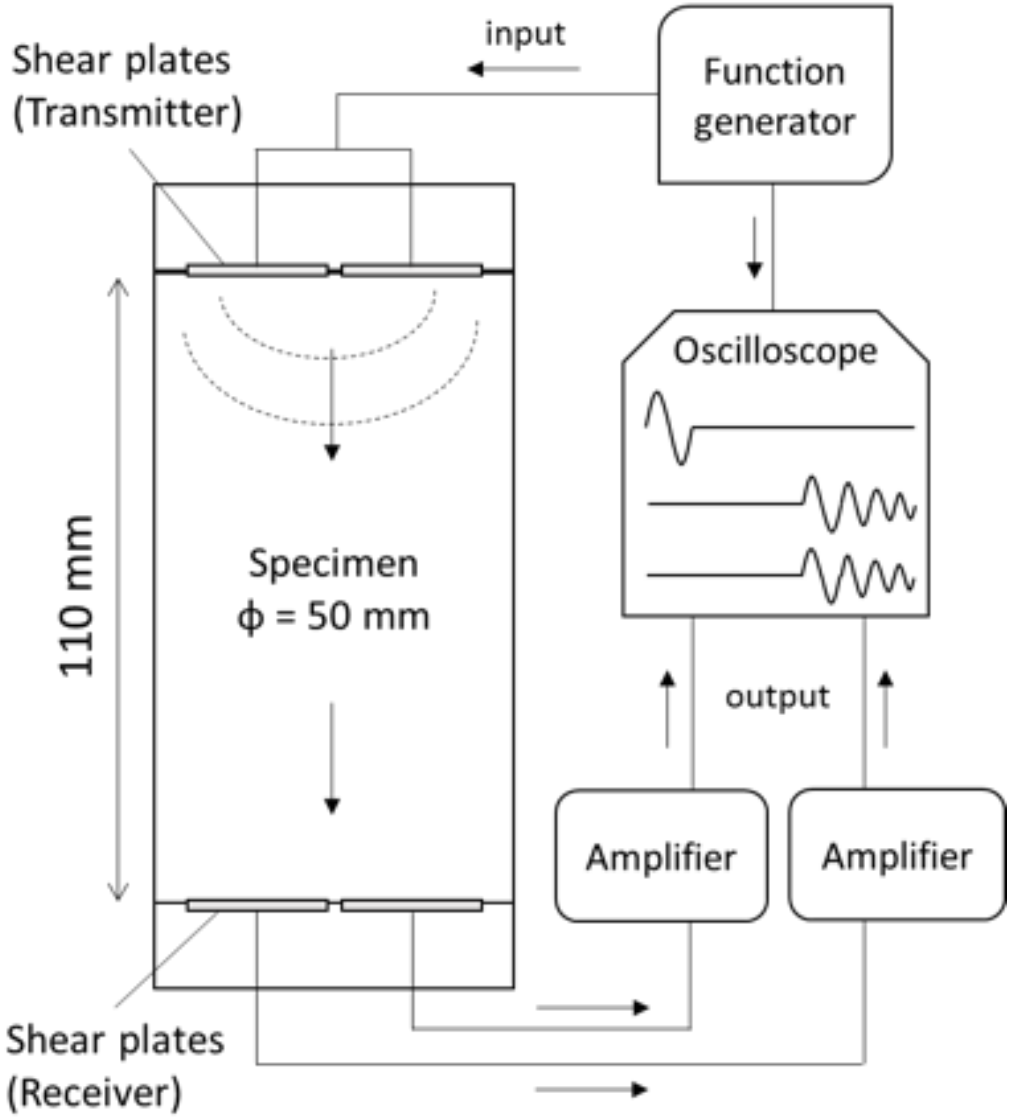

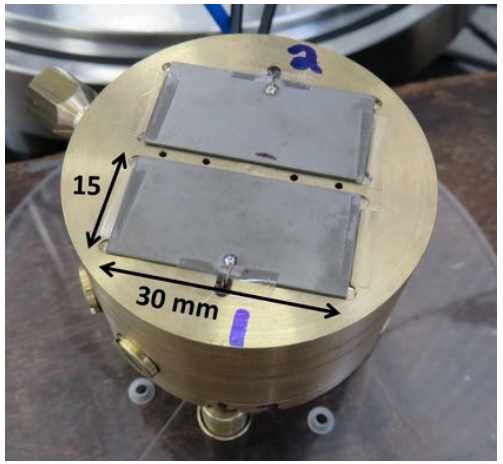

(Otsubo, 2017)

Simulating Tests using DEM

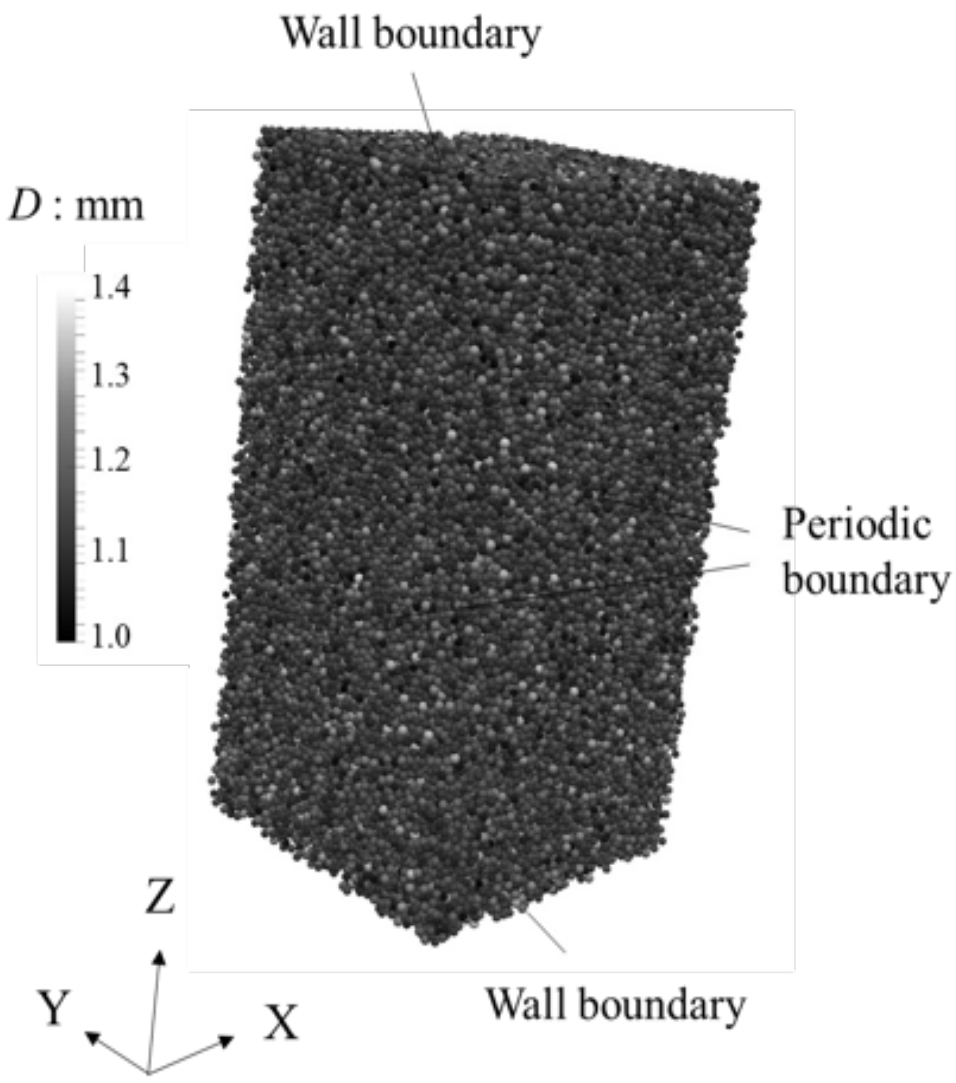

- DEM code: LAMMPS
- 155,165 particles
- Diameter : D = 2.54 mm (mono-size)
- Particle shear modulus : G_p = 25 GPa
- Particle Poisson's ratio : v_p = 0.2
- Inter-particle friction :
- μ = 0.0 (dense) 0.15 (loose)
- p′=100kPa to 10MPa
- Planar shear waves

(Otsubo, 2017)

Roughness-dependant contact behaviour

DEM Contact Model

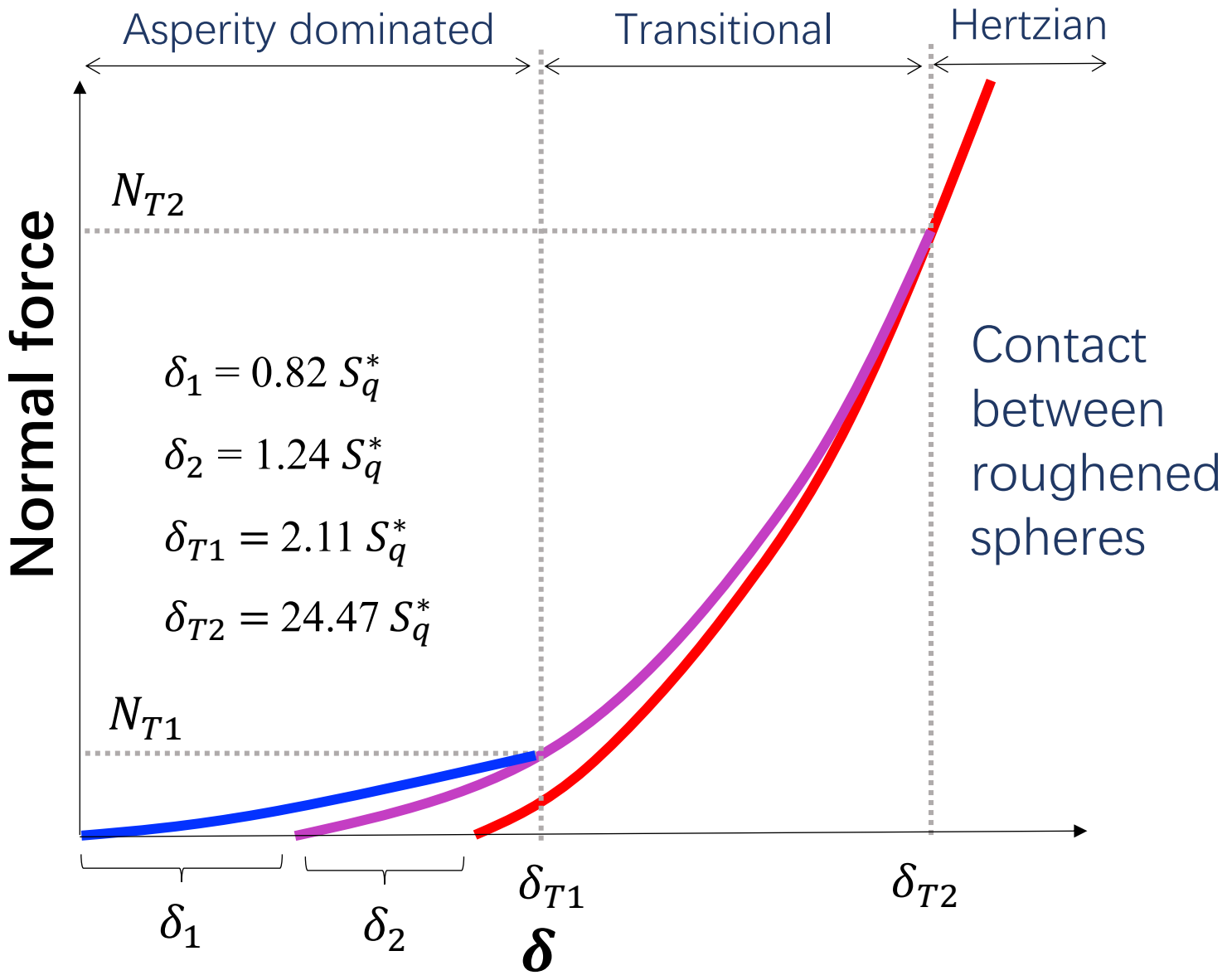

Surface Roughness and Stiffness

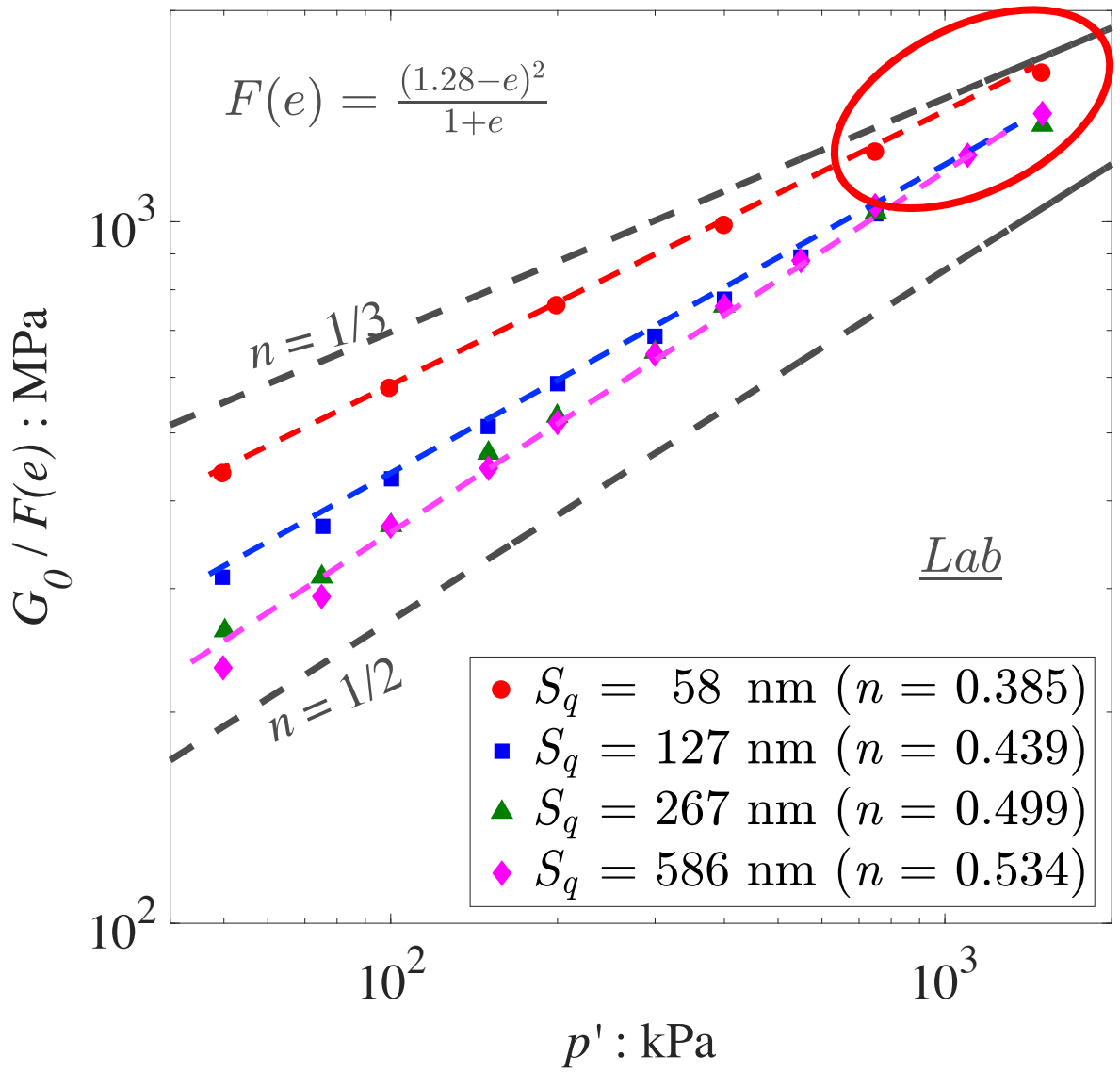

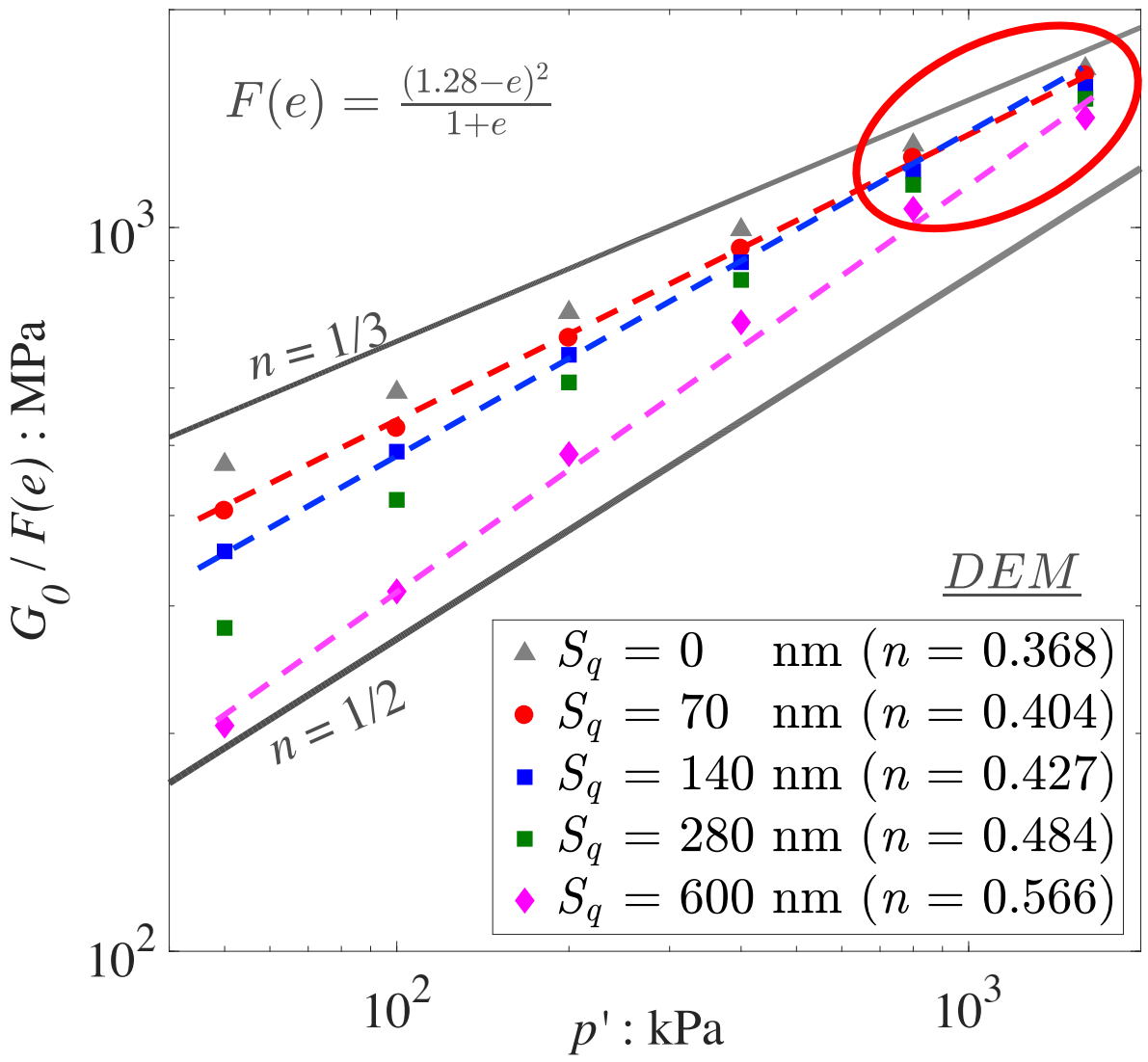

DEM data on Contact Evolution

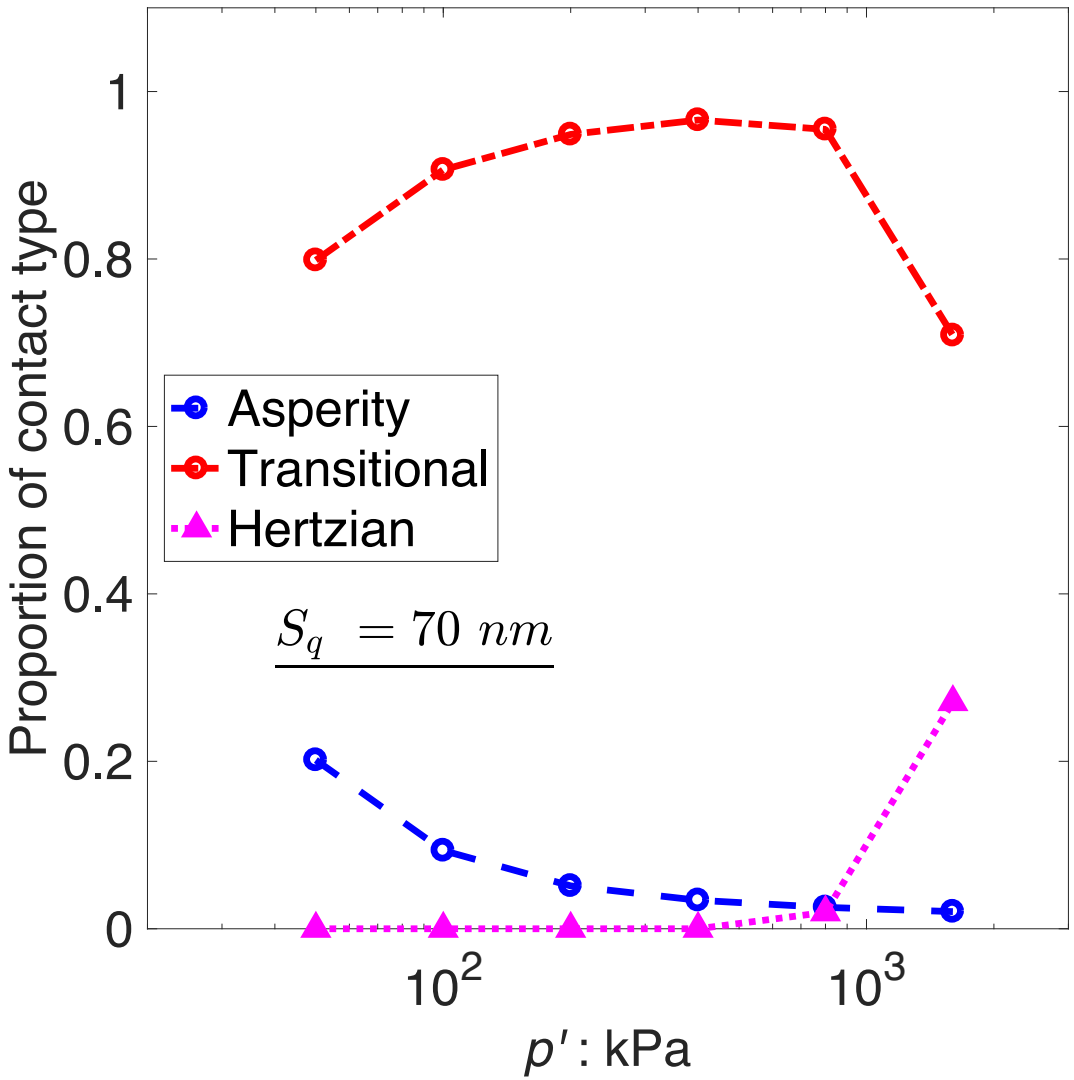

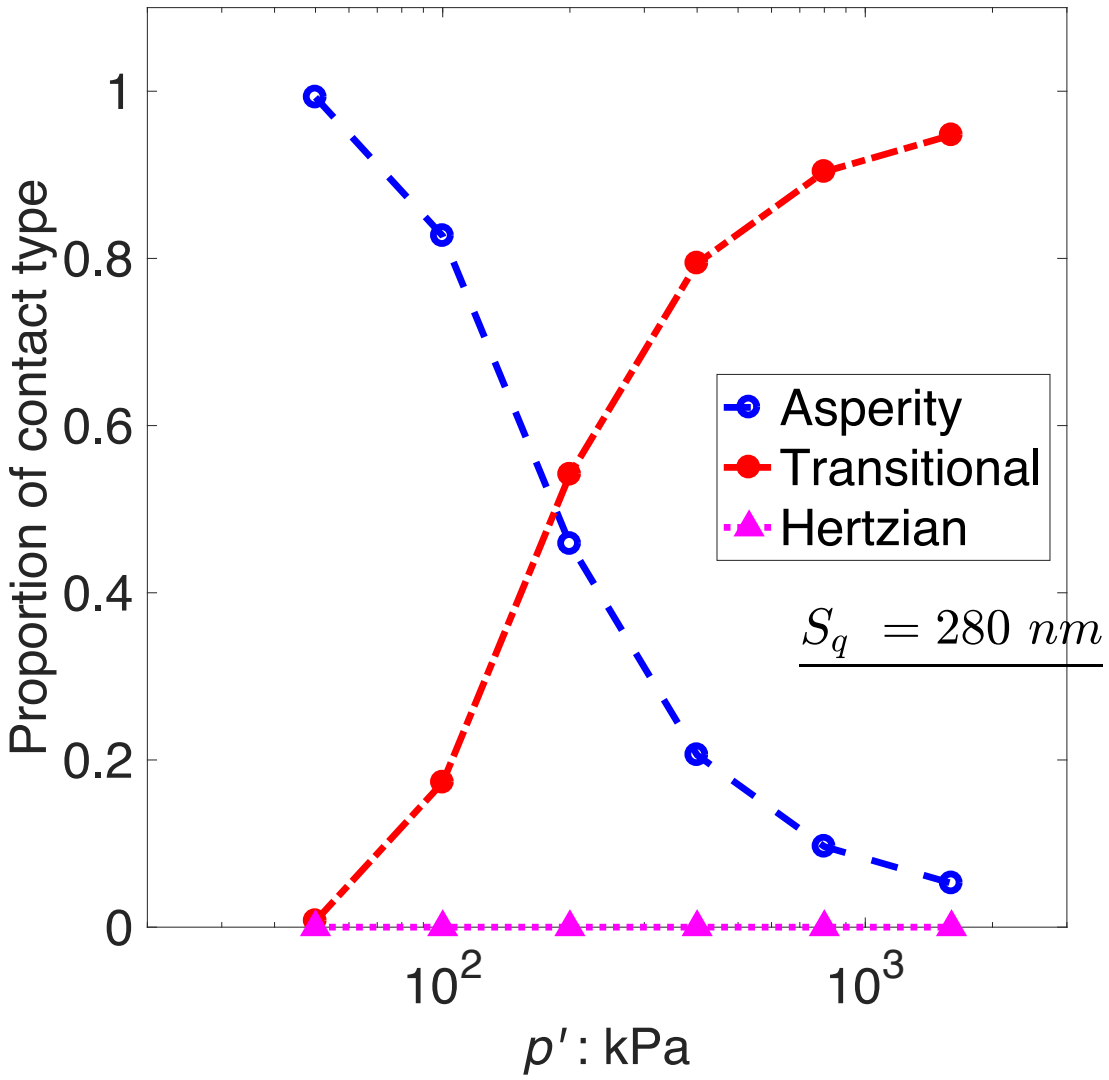

Part 3: Void space topology + fluid flow in void space

Application: Embankment dams

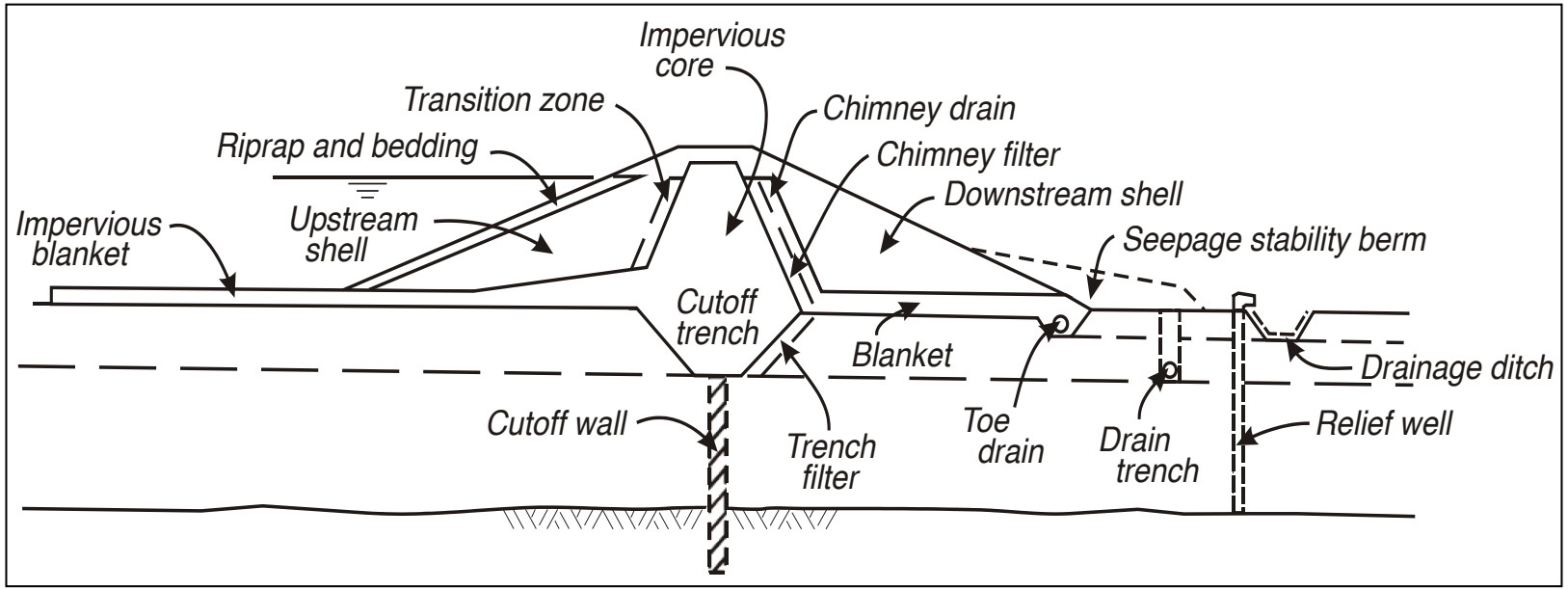

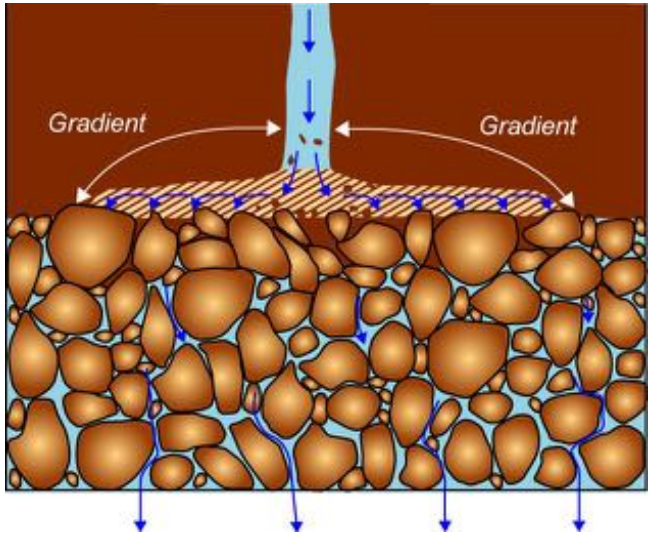

(FEMA, 2011)

Paraperios dam - May 26 2010

Filtration

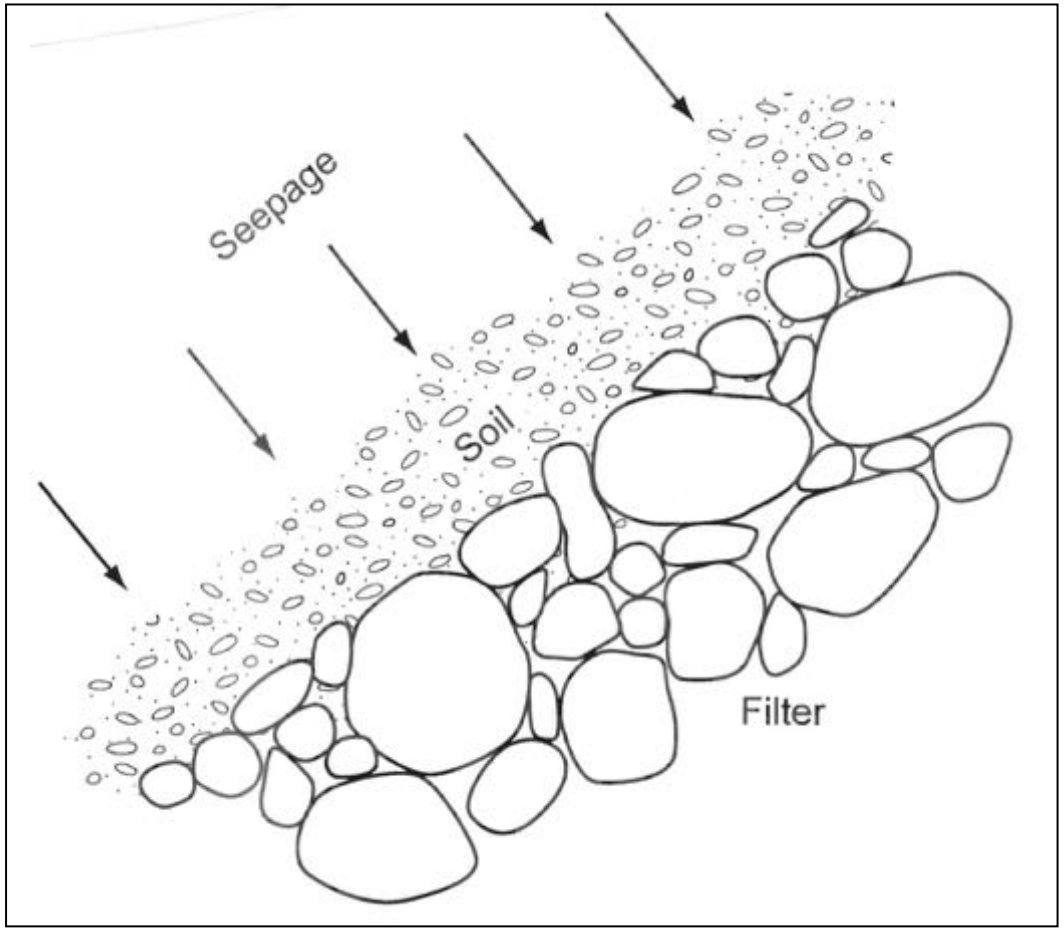

(FEMA, 2011)

- Filter should retain finer base material
- D_{15} often used as a means to infer constriction sizes
- Originates from Terzaghi' s filter rule (Sherard & Dunnigan, 1989; ICOLD, 2015)
- Supported by macro-scale filtration experiments (Kenney et al., 1985)

Research questions: Retention

- What is the relationship between the size of constrictions and D_{15F}?
- Does particle scale analysis support use of the ratio D_{15F}/D_{85B} in design?
- Is geometric partitioning of the void space relevant for fluid mechanics?
- What are the fluid – particle interaction forces?

Filtration – Samples Considered

Laboratory Experiments

DEM Simulations

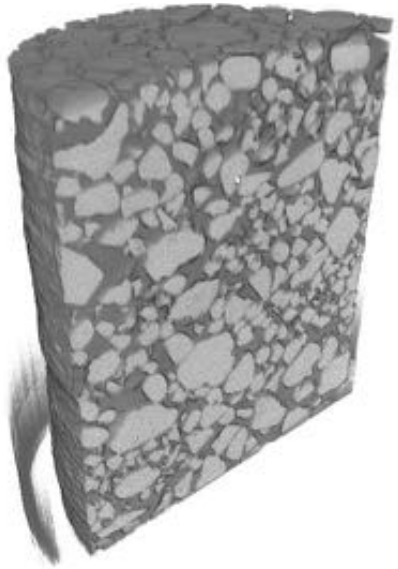

Leighton Buzzard Sand
C_u=3

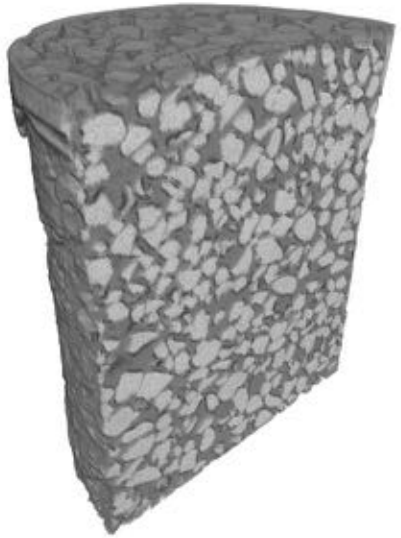

Leighton Buzzard Sand
C_u=1.5

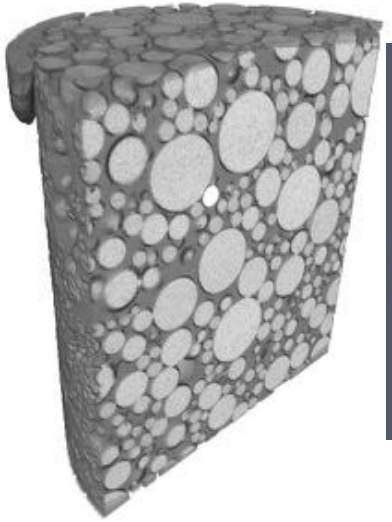

Glass Beads
C_u=3

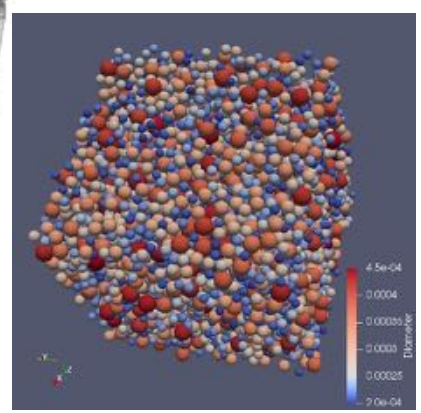

Spheres
C_u=1.2

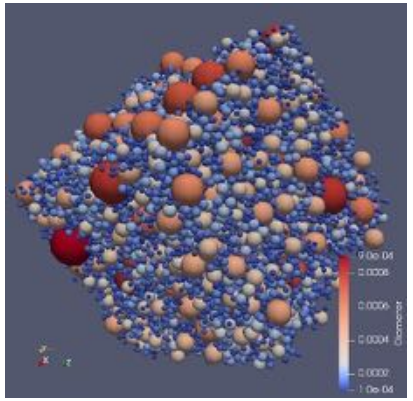

Spheres
C_u=3.0

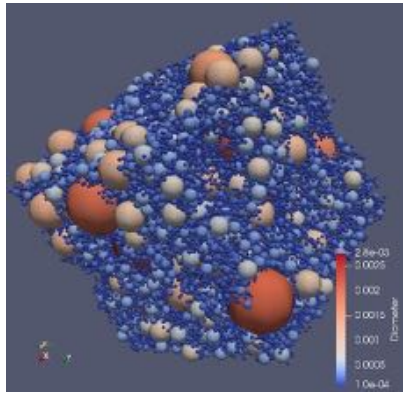

Spheres
C_u=6.0

(Taylor, 2017)

(Shire, 2018)

Determining constriction size distribution

Generate particle scale data

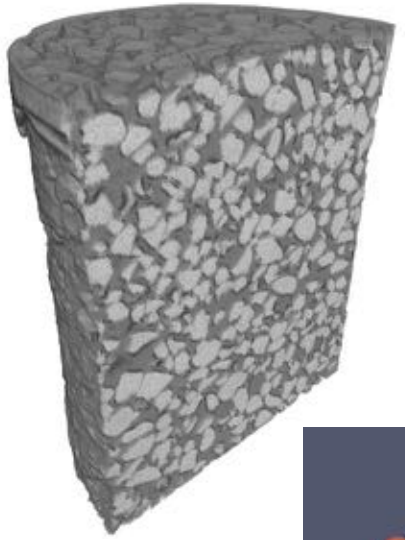

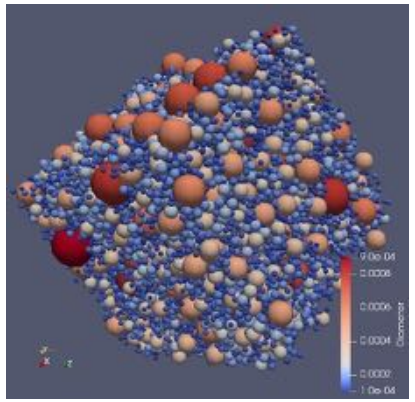

Apply void partitioning algorithm

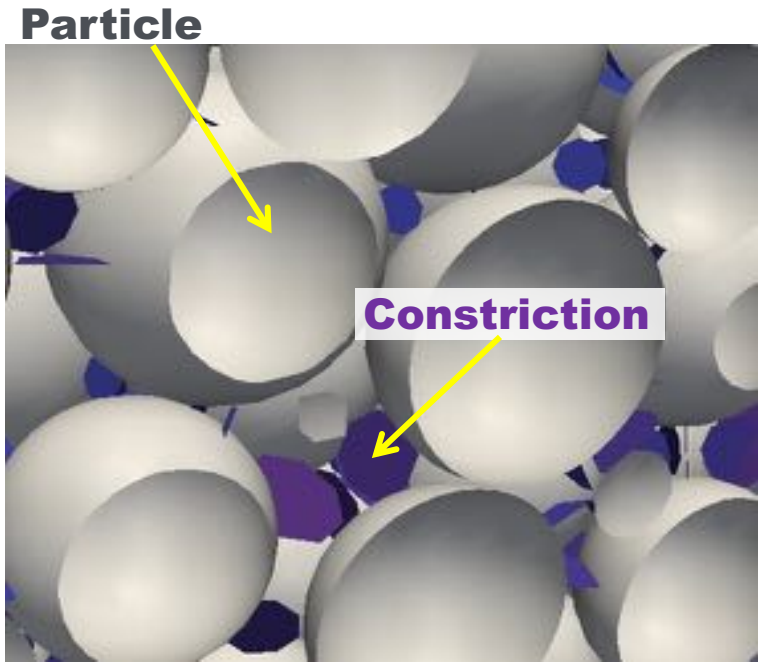

Calculate Constriction Size Distribution

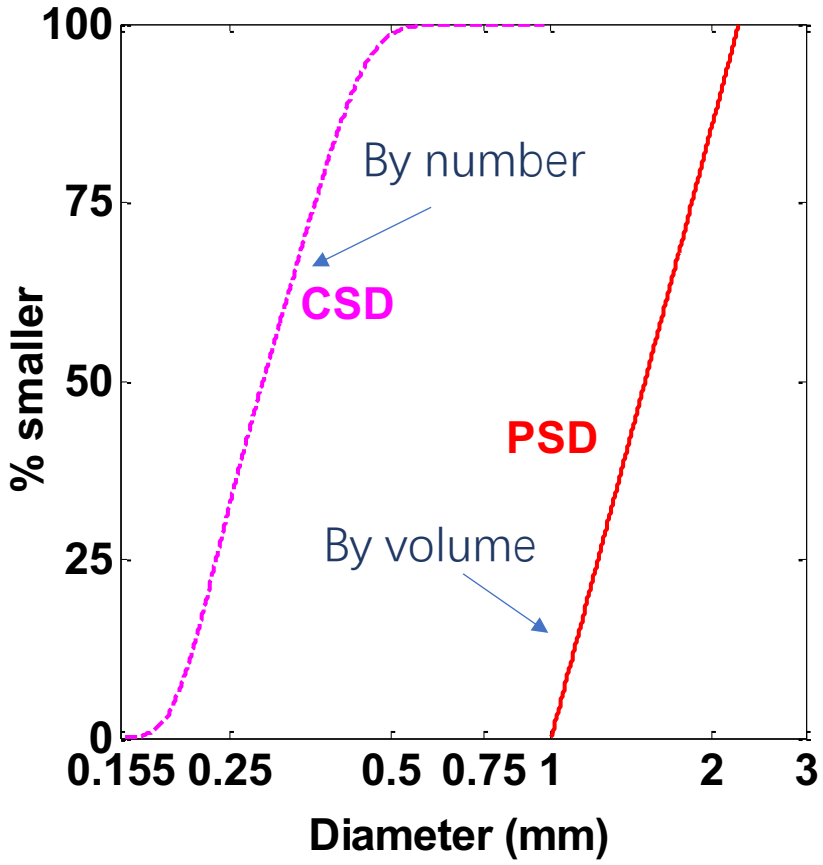

Identifying constrictions in DEM

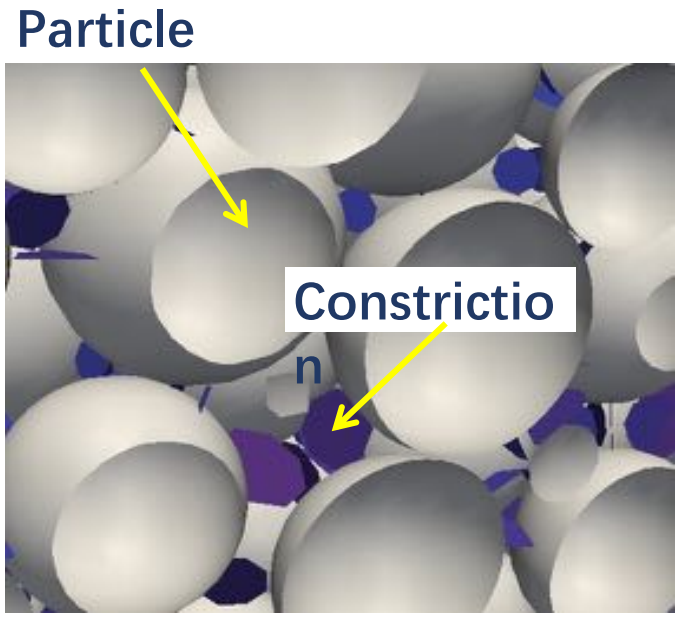

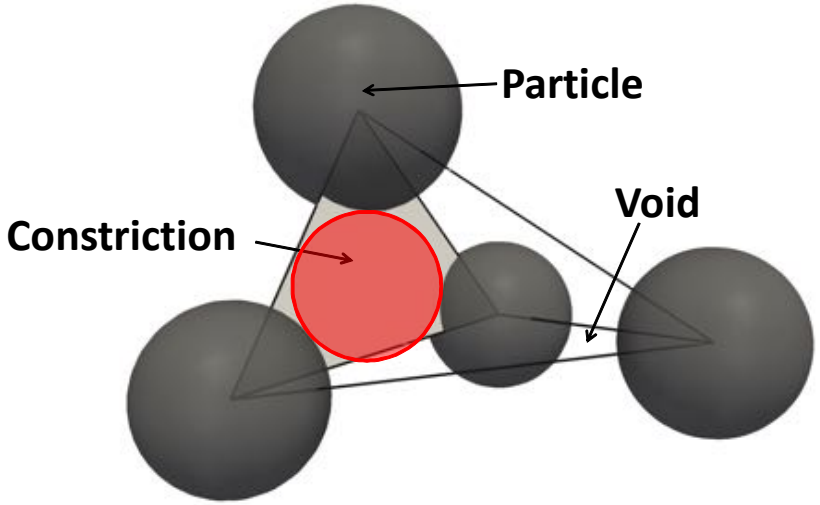

Triangulation of particle centres

Triangulation weighted by particle radii

Face of triangles are constrictions

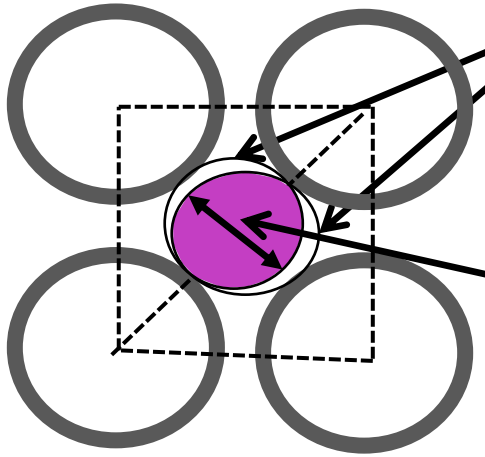

Spheres tangent to particles forming Delaunay cell

Overlap distance used to assess whether Delaunay cells should be merged

Reboul et al. (2010)

Micro Computed Tomography (microCT)

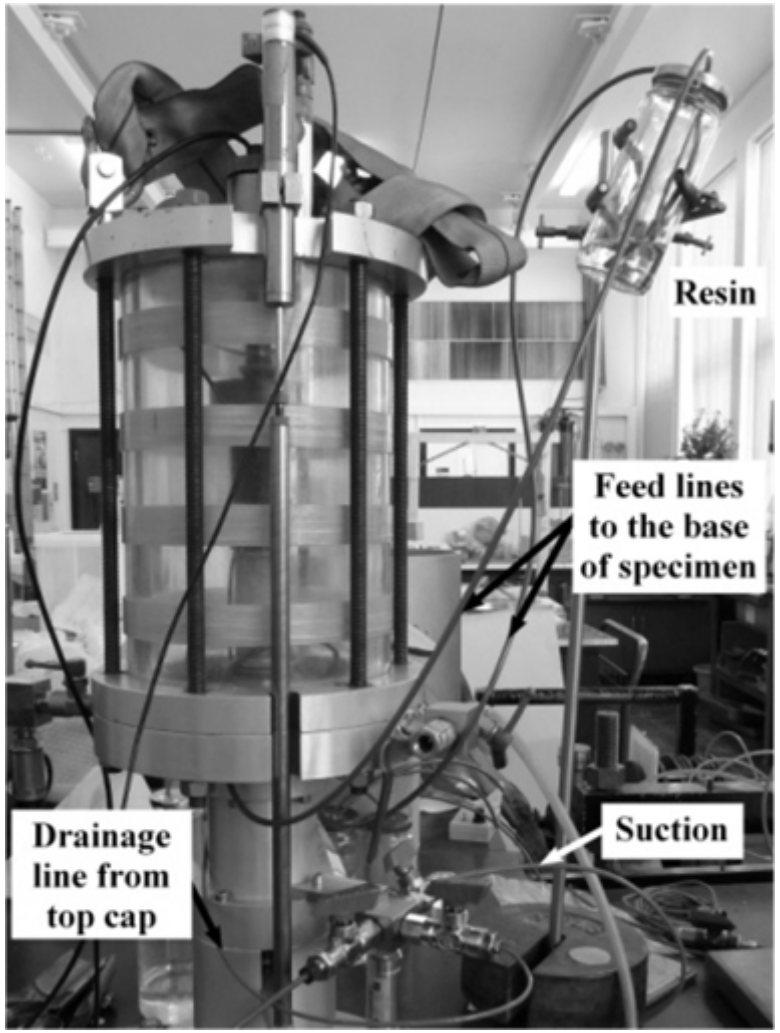

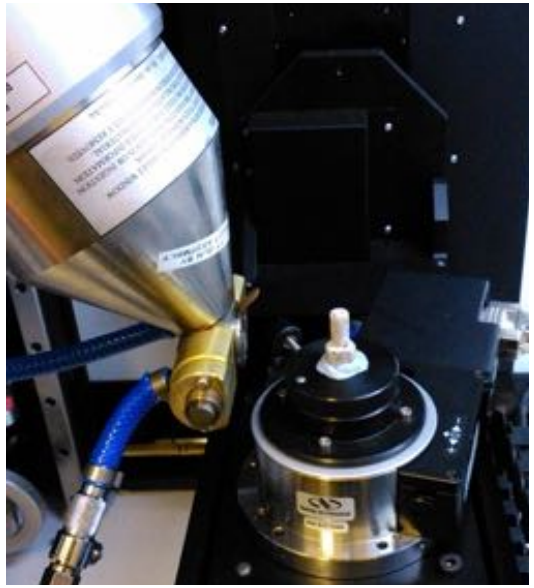

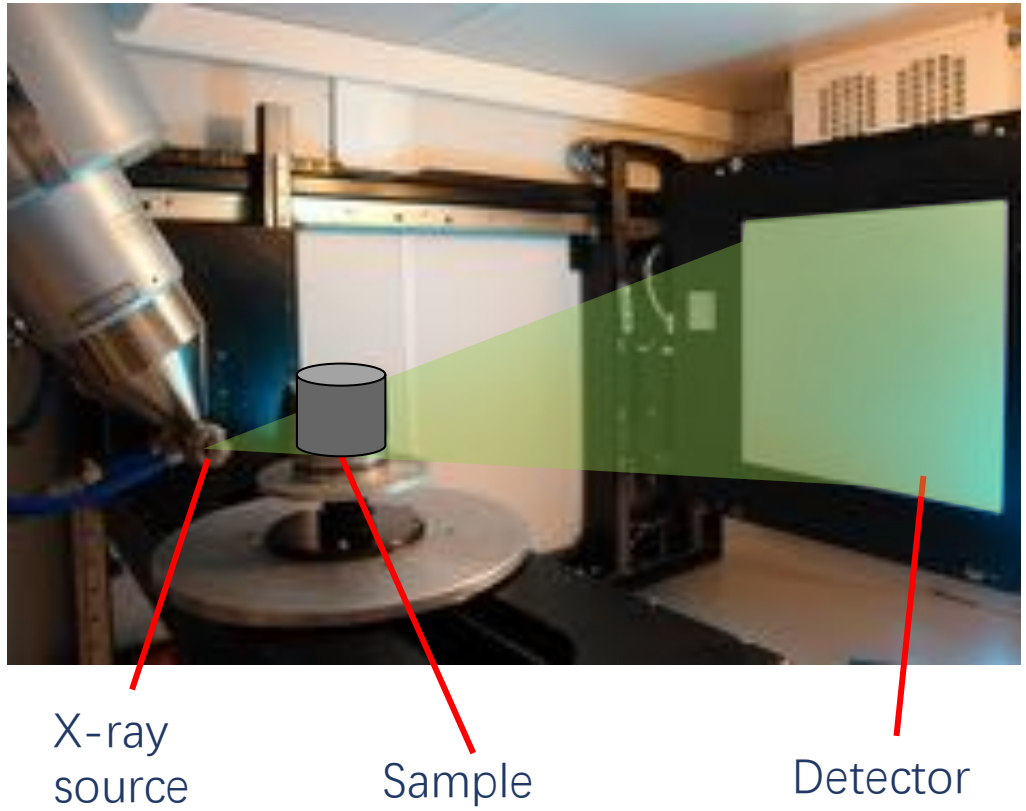

Micro Computed Tomography (Micro CT)

PhD Thesis Howard Taylor (2016)

Identifying constrictions in μCT

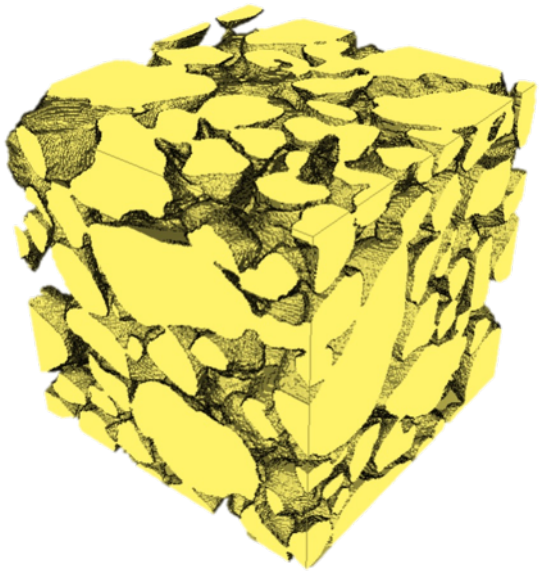

μCT image

Watershed Segmentation →

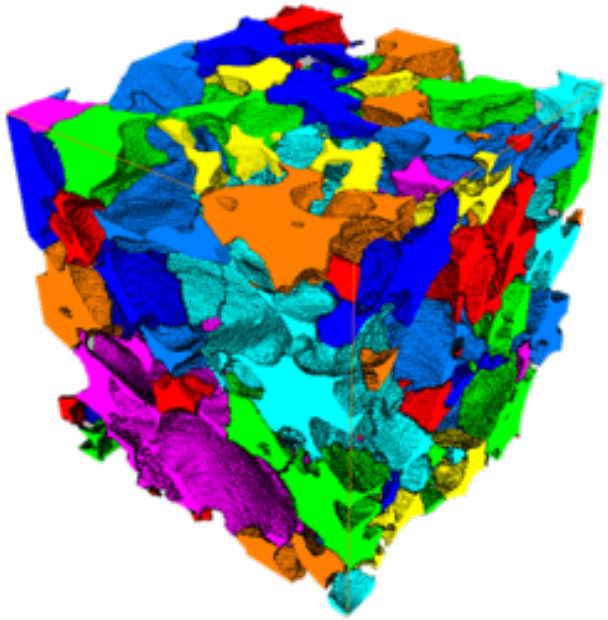

Voids

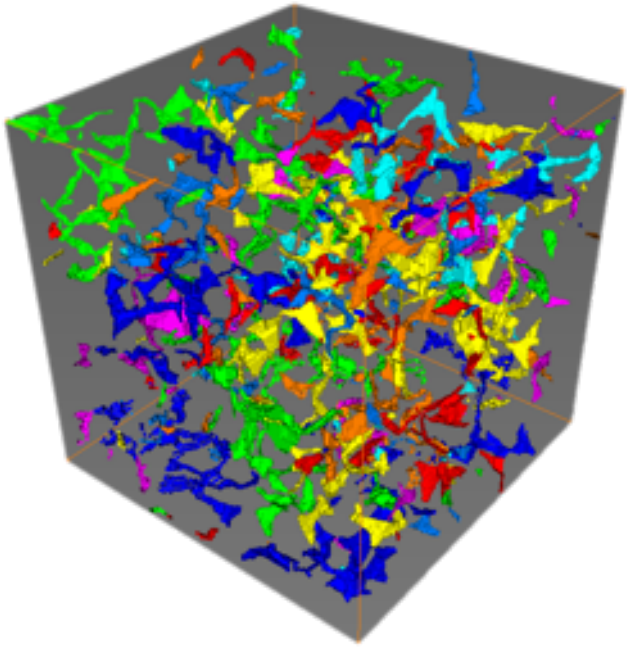

Void Boundaries

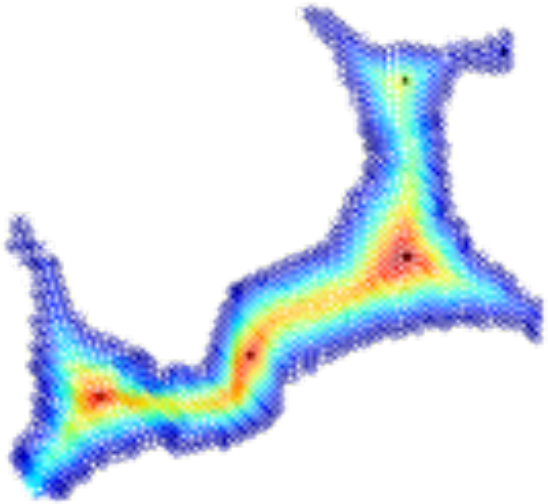

Constrictions local maxima of distances to particles

Taylor et al. (2017)

Comparing algorithms

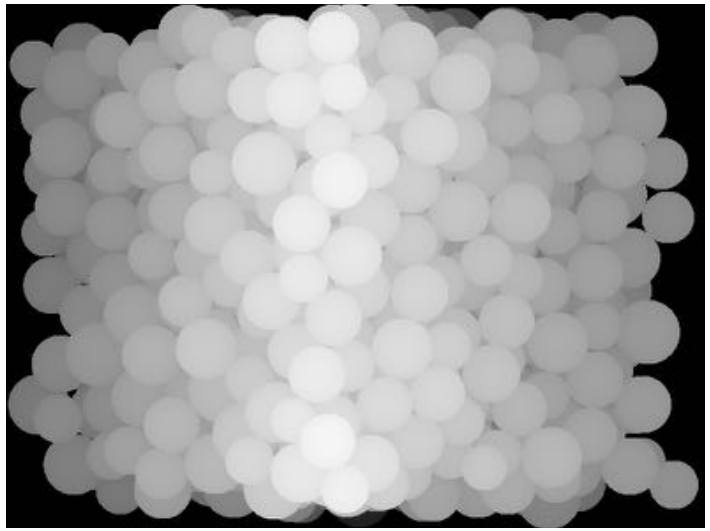

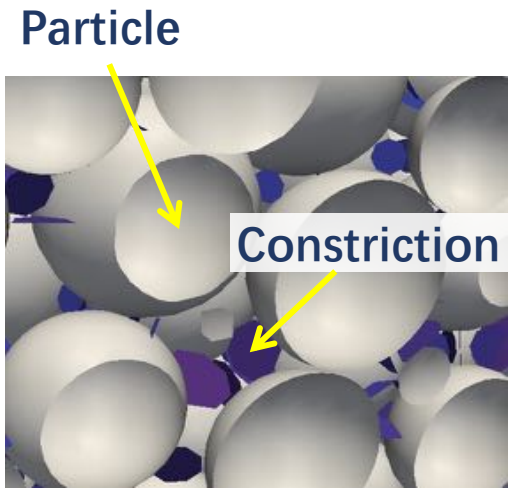

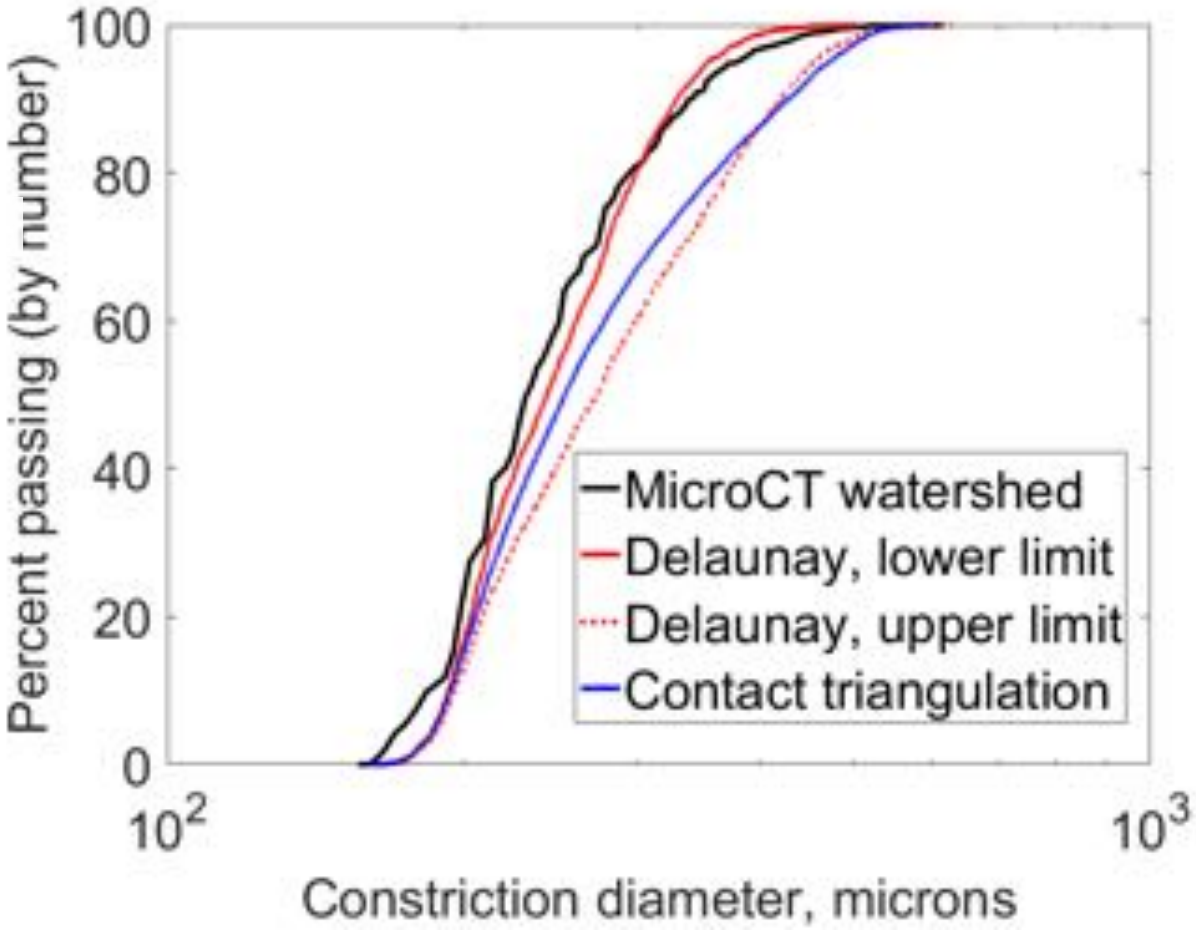

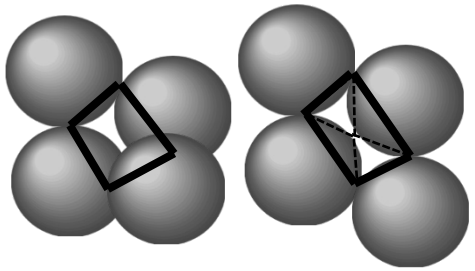

Contact triangulation

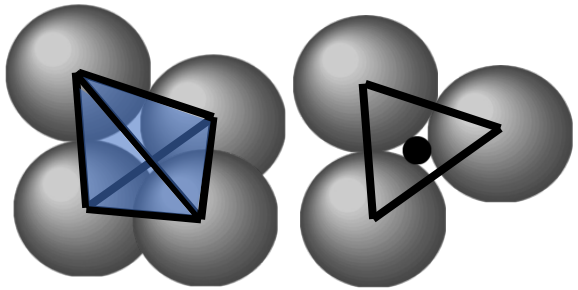

Delaunay triangulation of particles

Shire et al. (2016)

Constriction size distributions (DEM)

Particle size distribution

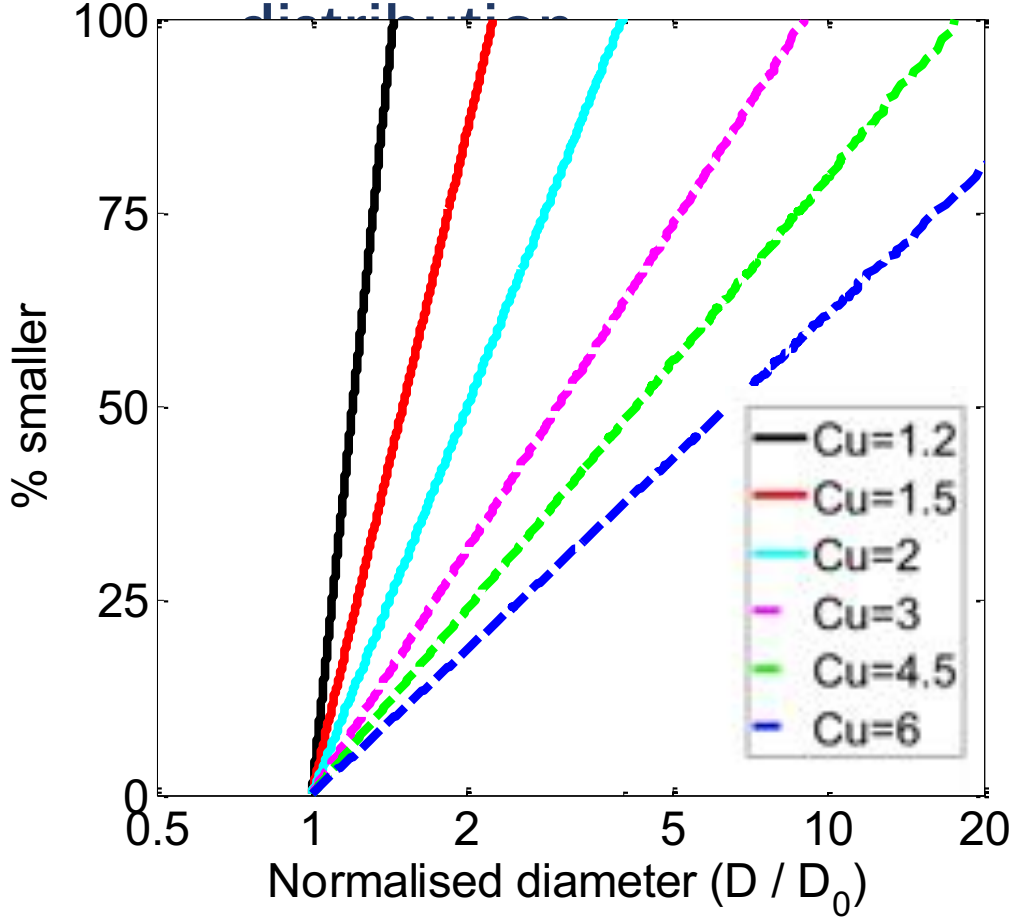

Constriction size distribution

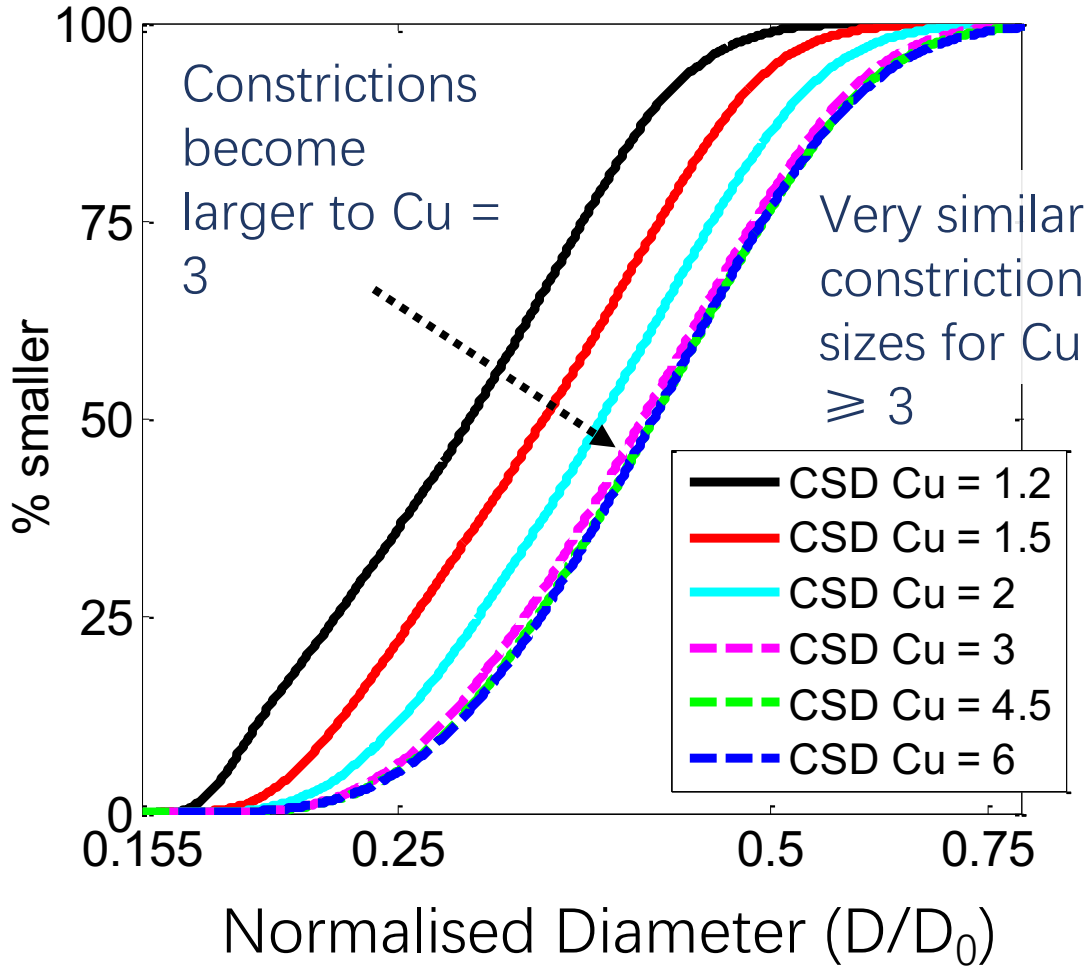

Filtration - Constriction Sizes

MicroCT Experimental data

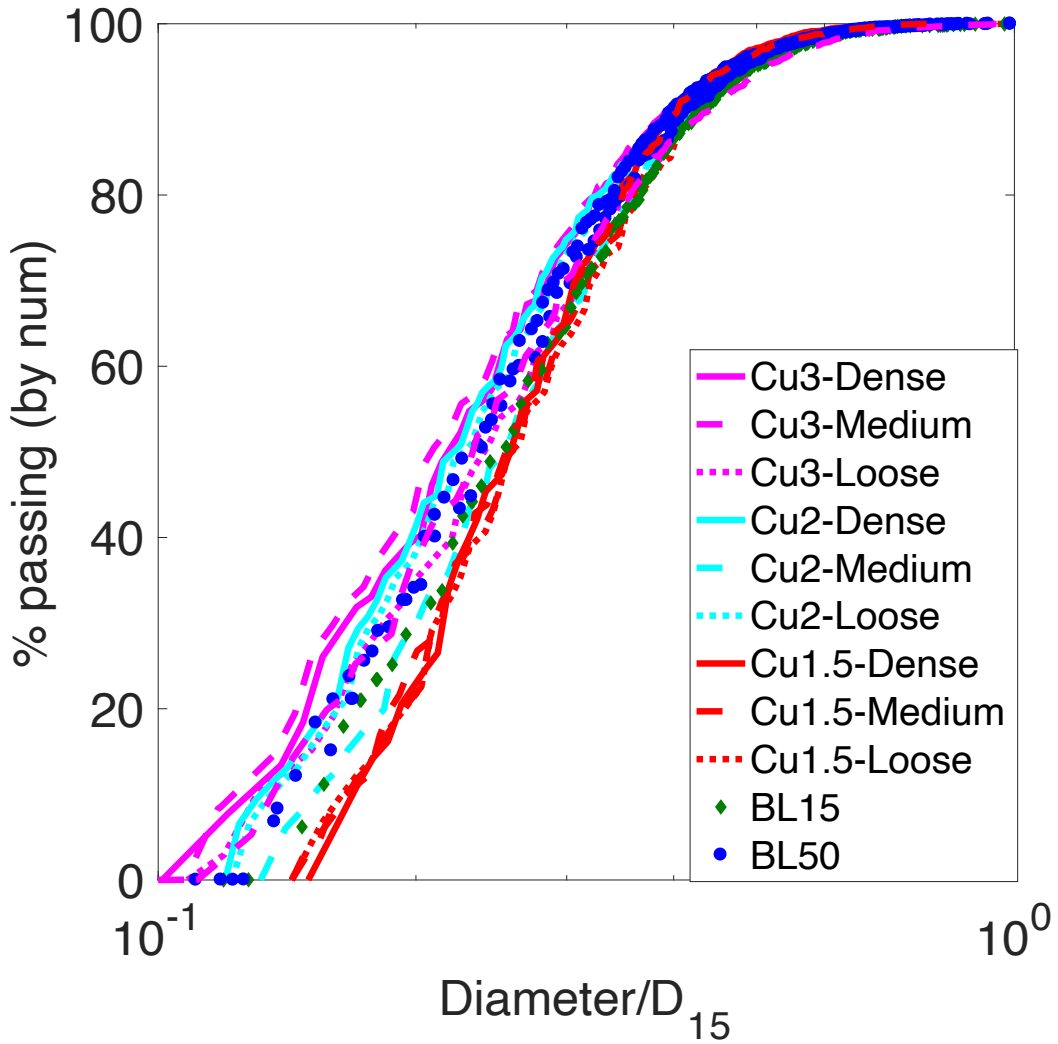

DEM Simulation data

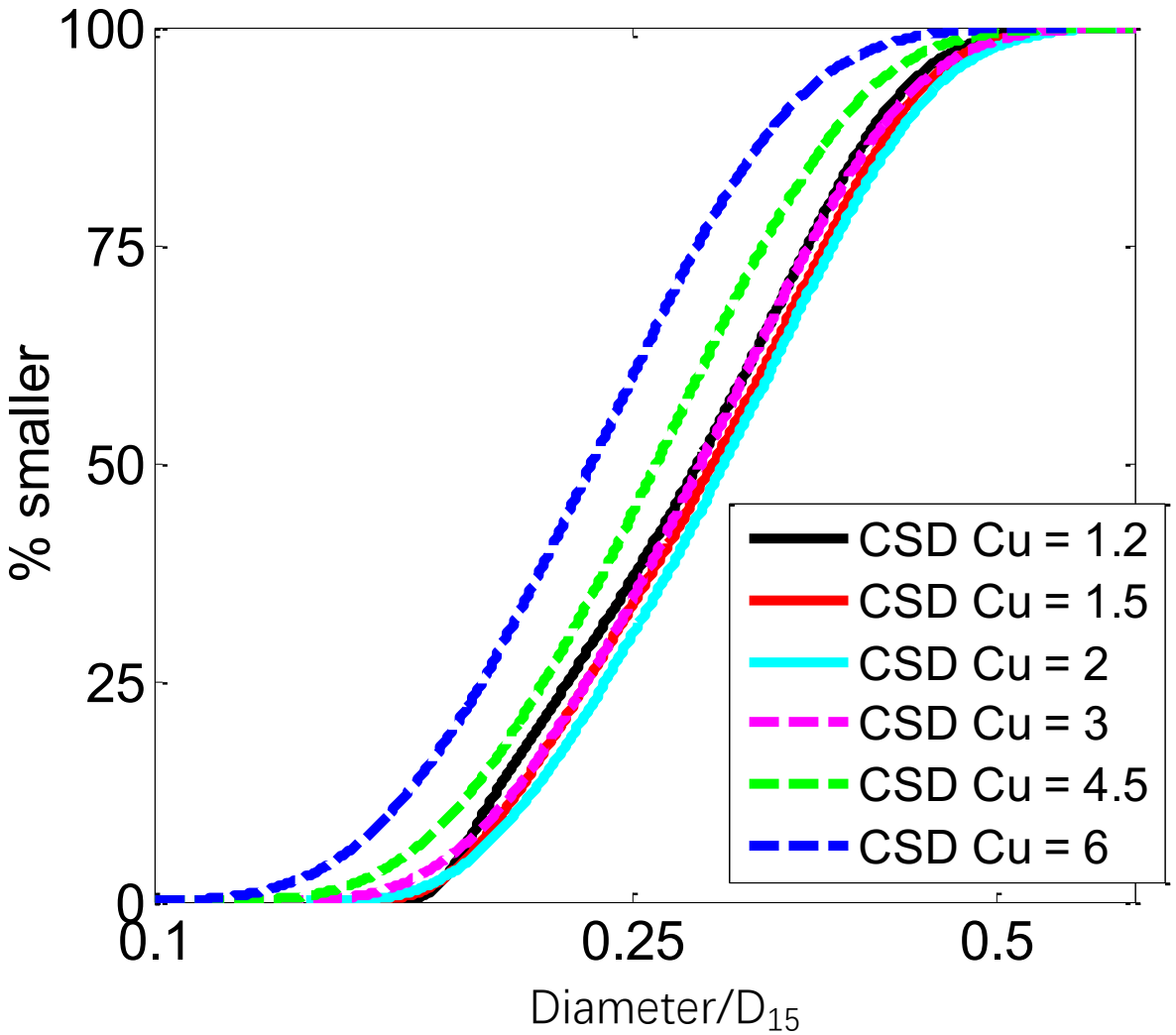

Filtration – Constriction Density / Spacing

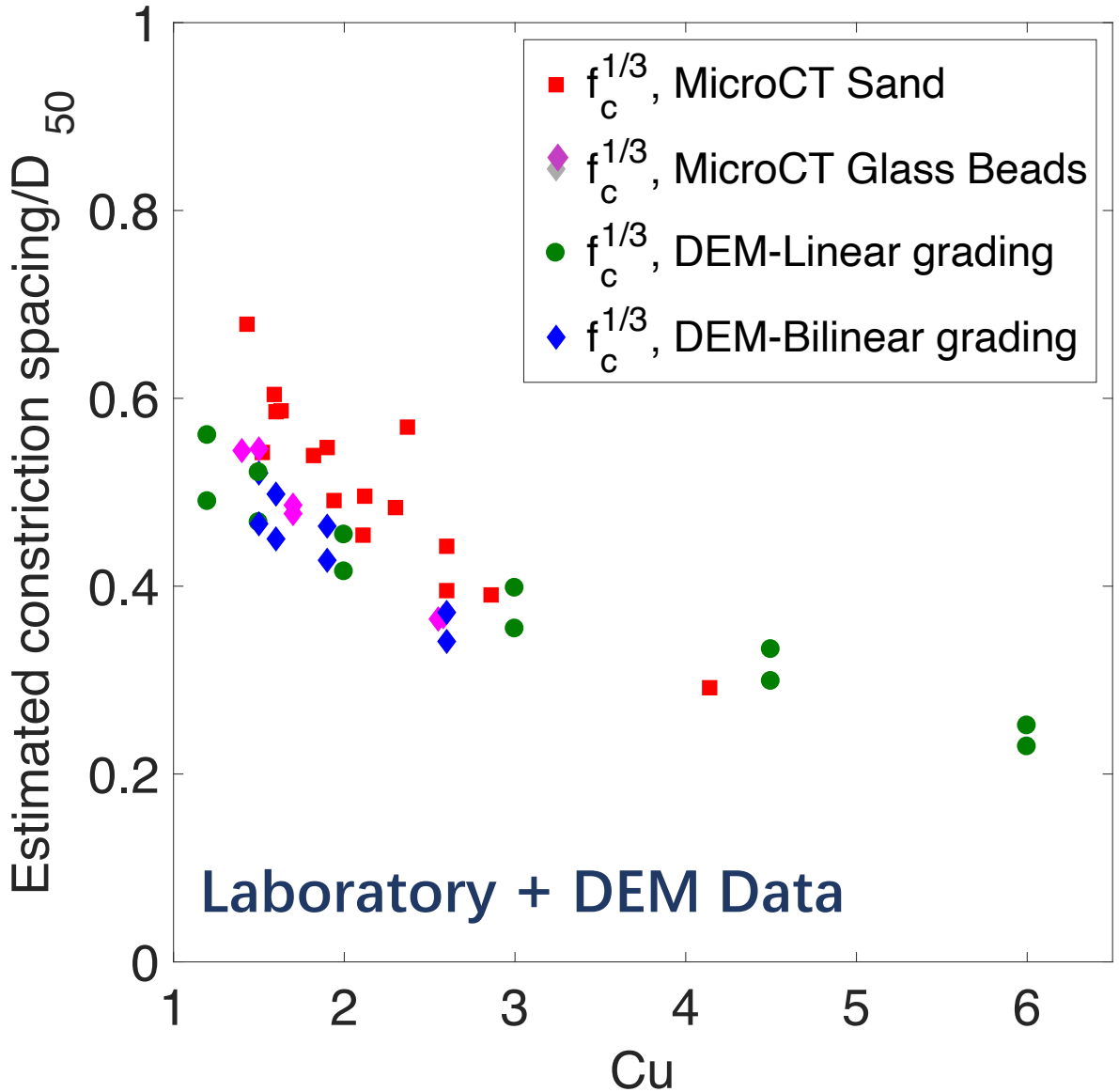

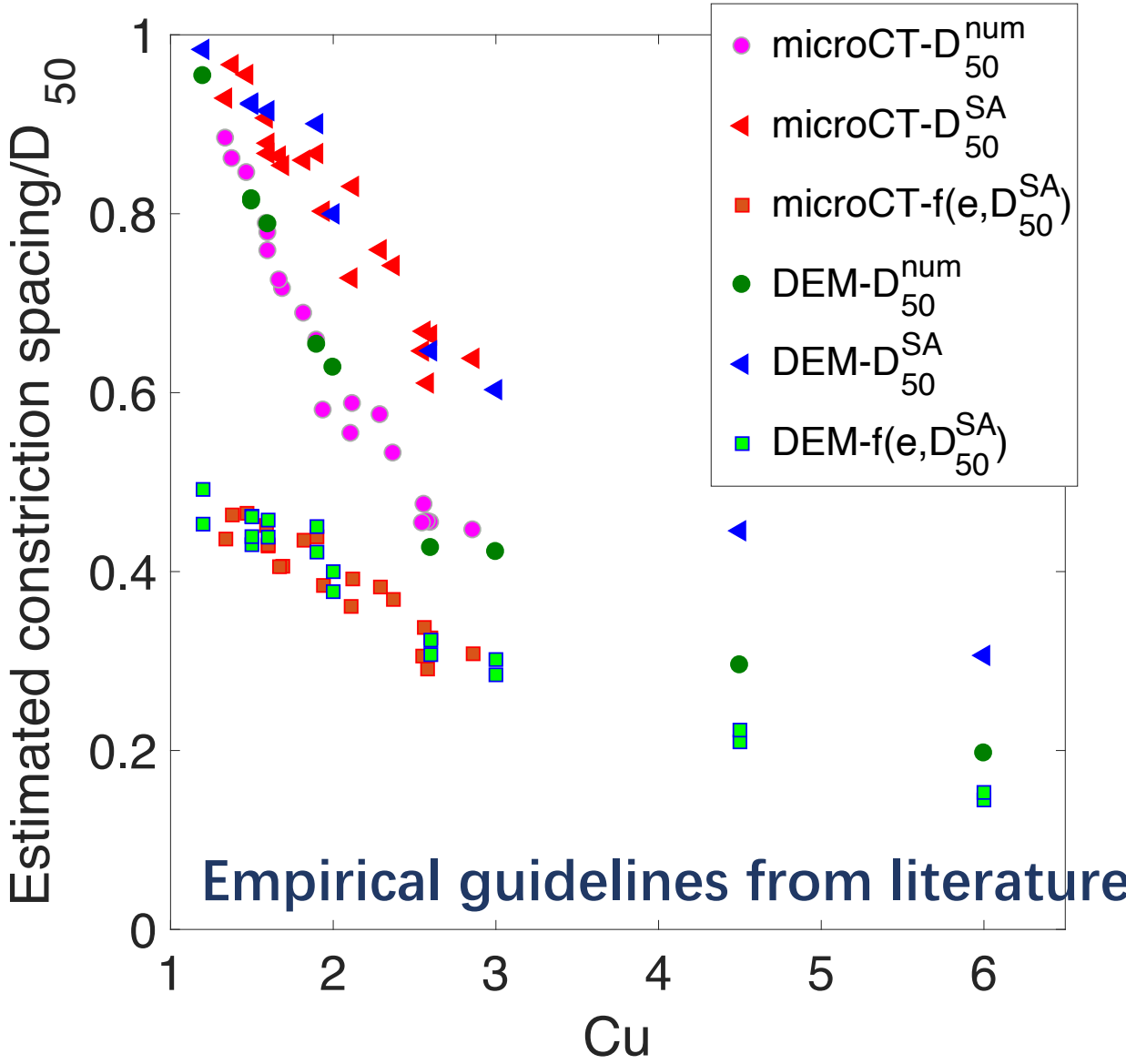

Sheffield Permeameter Experiments

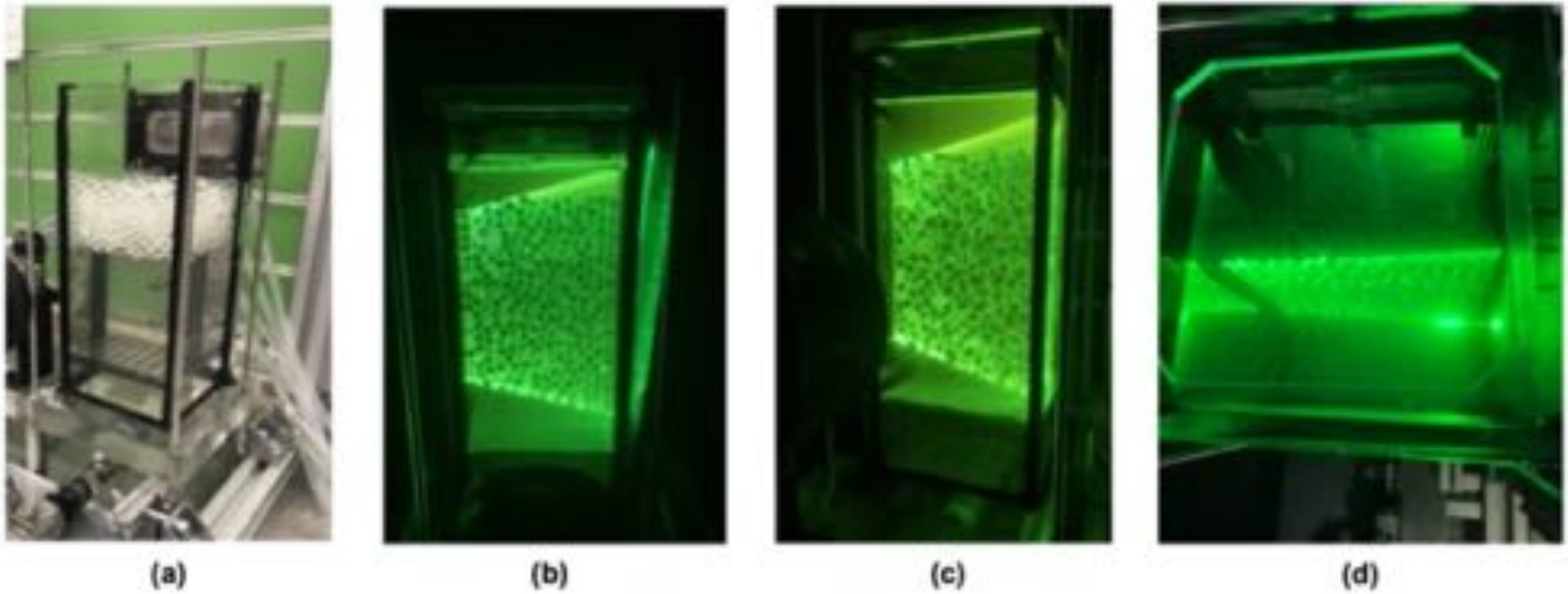

Sanvitale et al. (2021) https://doi.org/10.1680/jgeot.20.P.432

Sheffield Permeameter Experiments – CFD Mesh

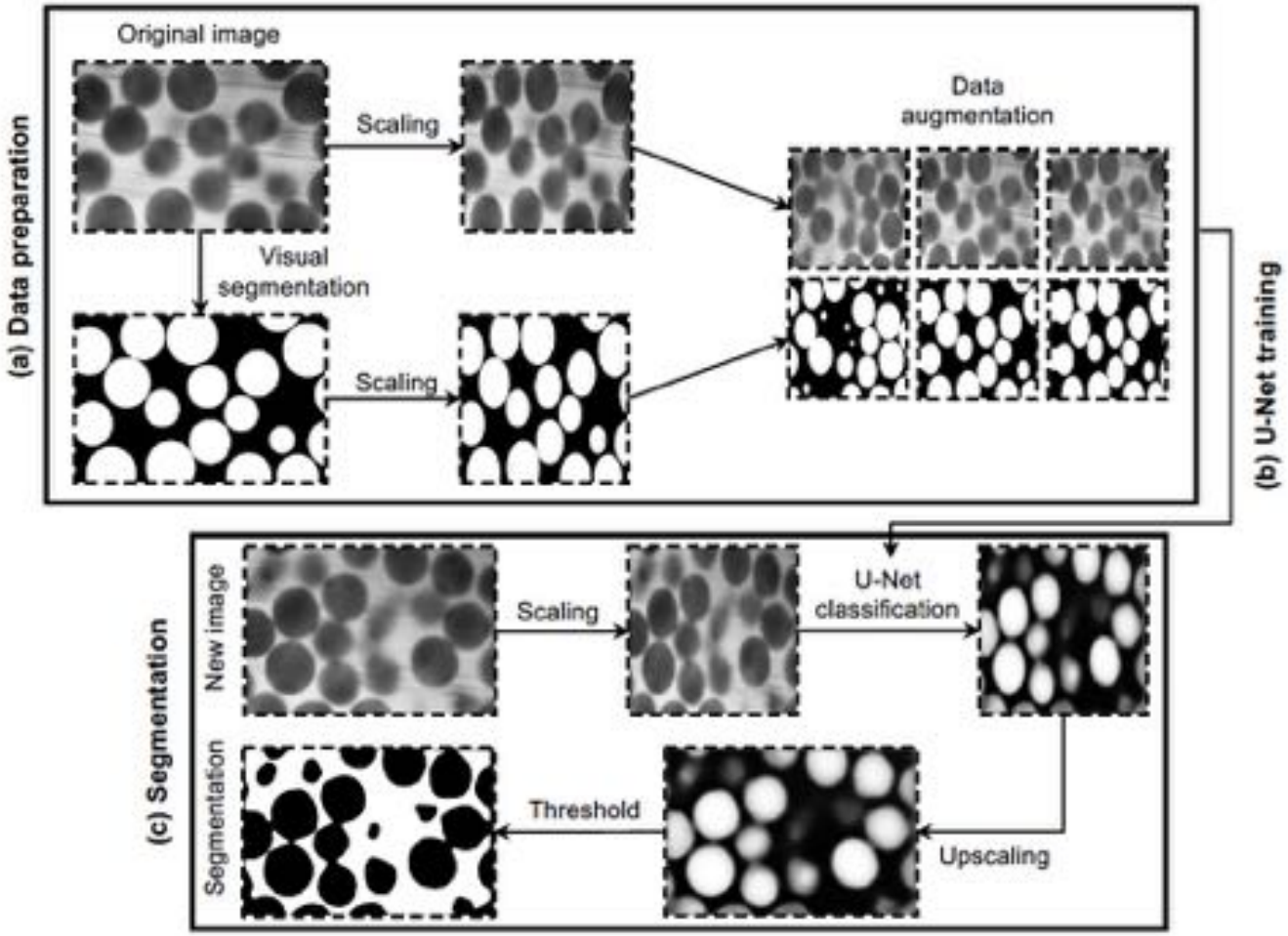

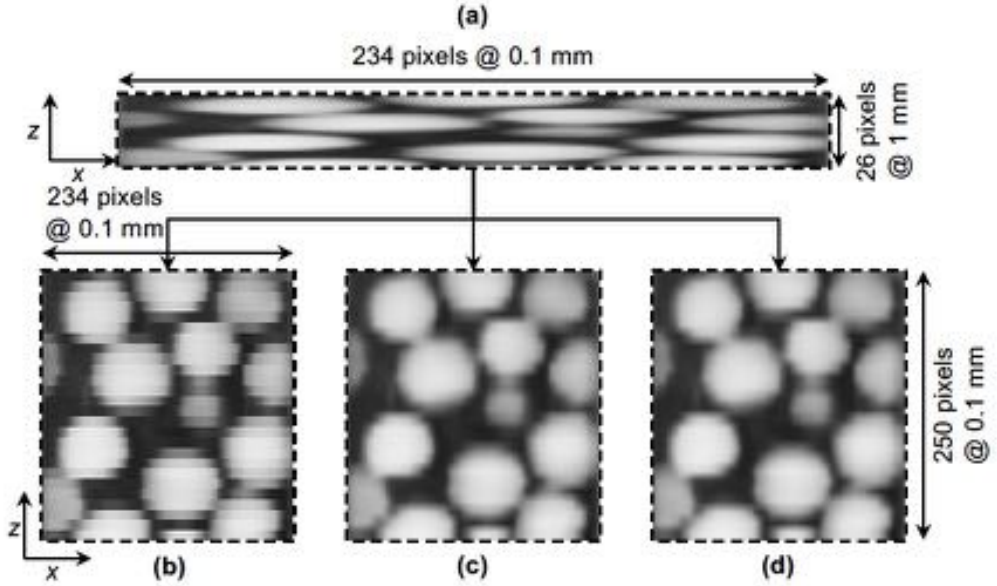

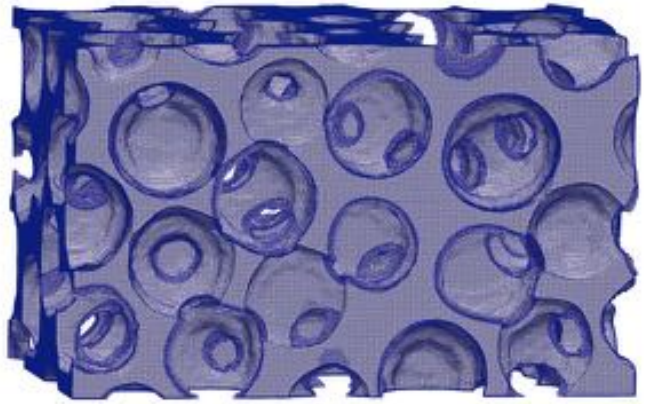

Sanvitale et al. (2021) https://doi.org/10.1680/jgeot.20.P.432

Sheffield Permeameter Experiments – PIV – CFD comparison

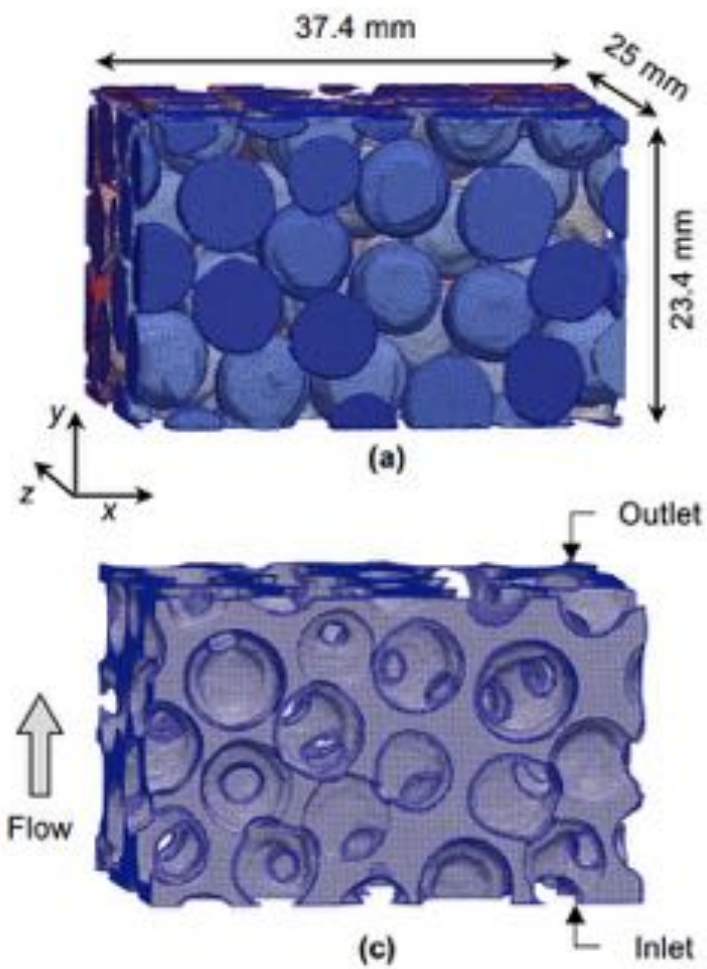

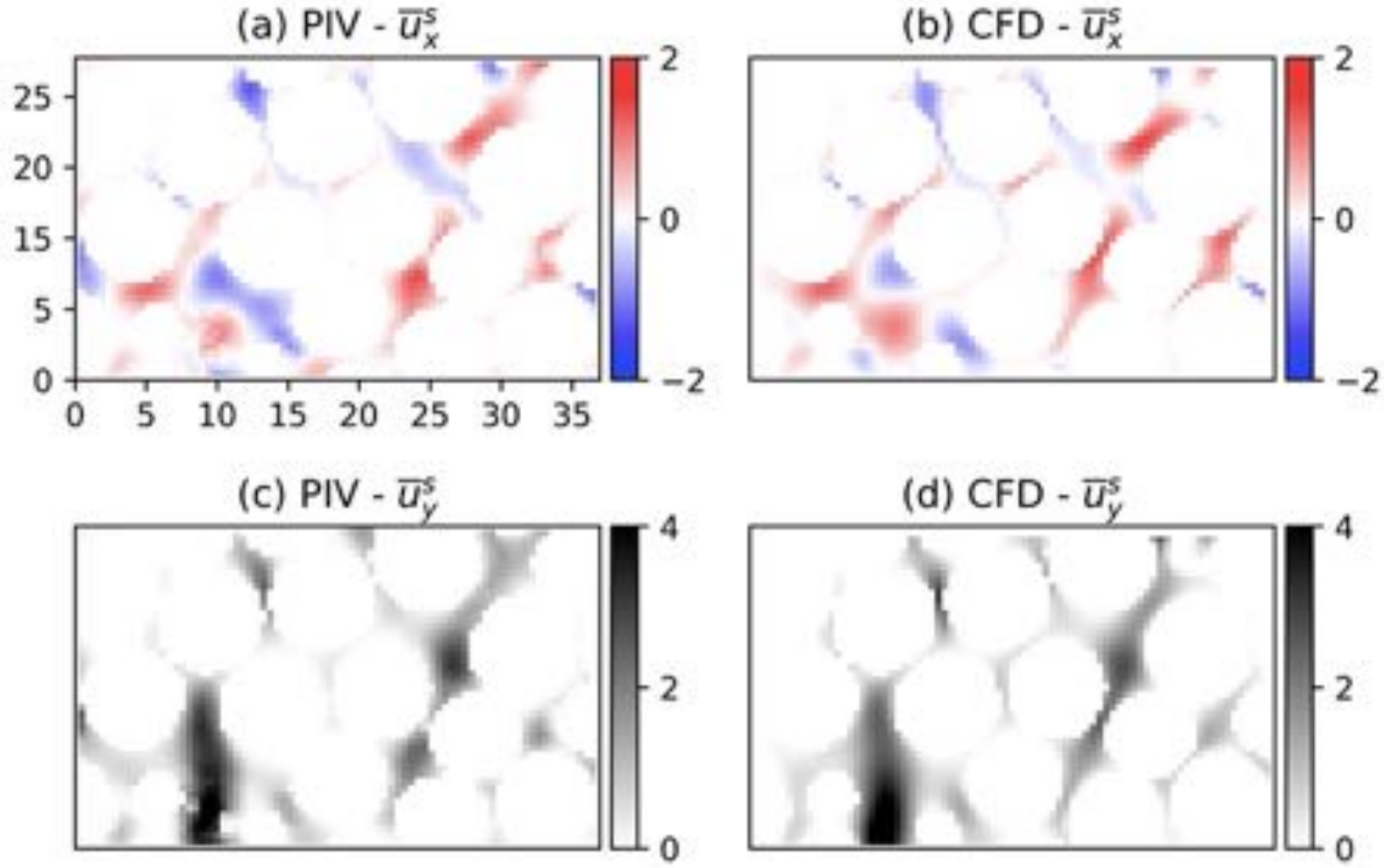

Sanvitale et al. (2021) https://doi.org/10.1680/jgeot.20.P.432

Fluid flow simulations

micro-CT image (Cu3)

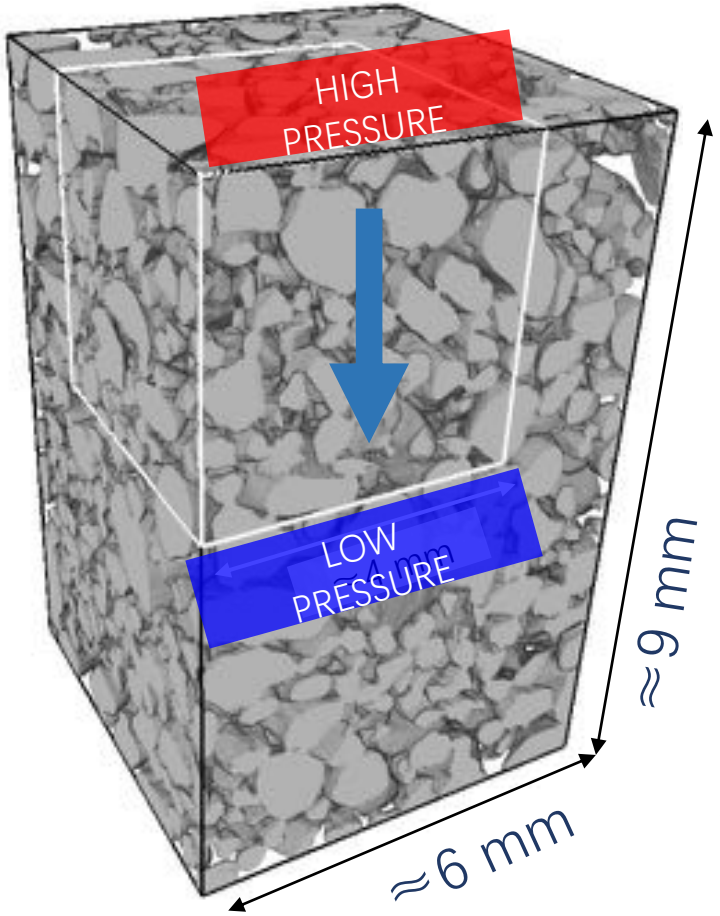

CFD Analysis

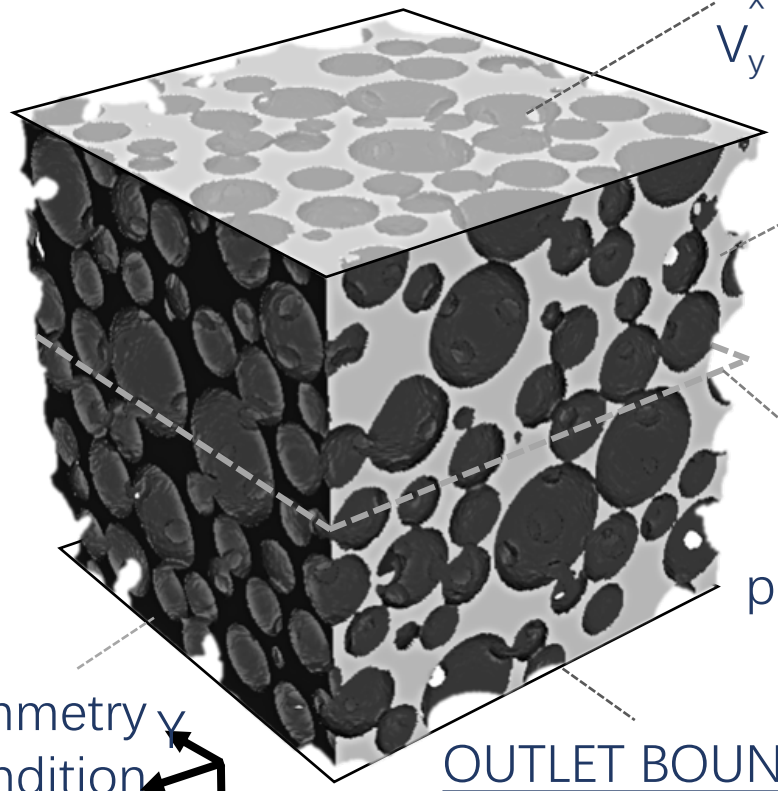

INLET BOUNDARY:

P_{in} = 0.001 kPa

V_x = 0

V_y = 0

"No slip" condition on particle surfaces

Slice, perpendicular to flow direction

"Symmetry" condition on all side boundaries

OUTLET BOUNDARY:

P_{out} = 0 kPa

V_x = 0

V_y = 0

CFD output 18-24hrs

Pressures

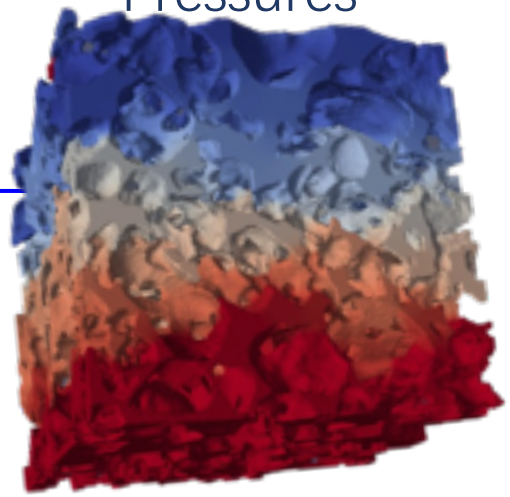

Velocities

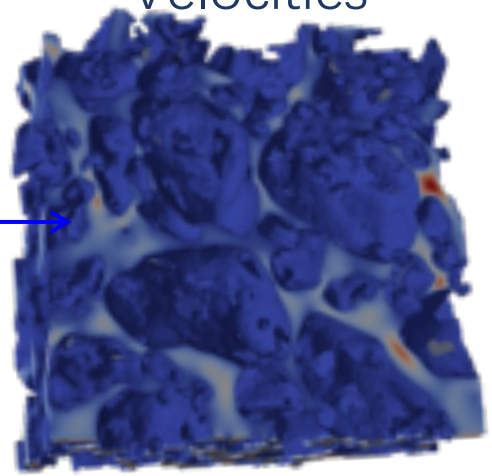

Comparison of geometric and hydraulic constrictions

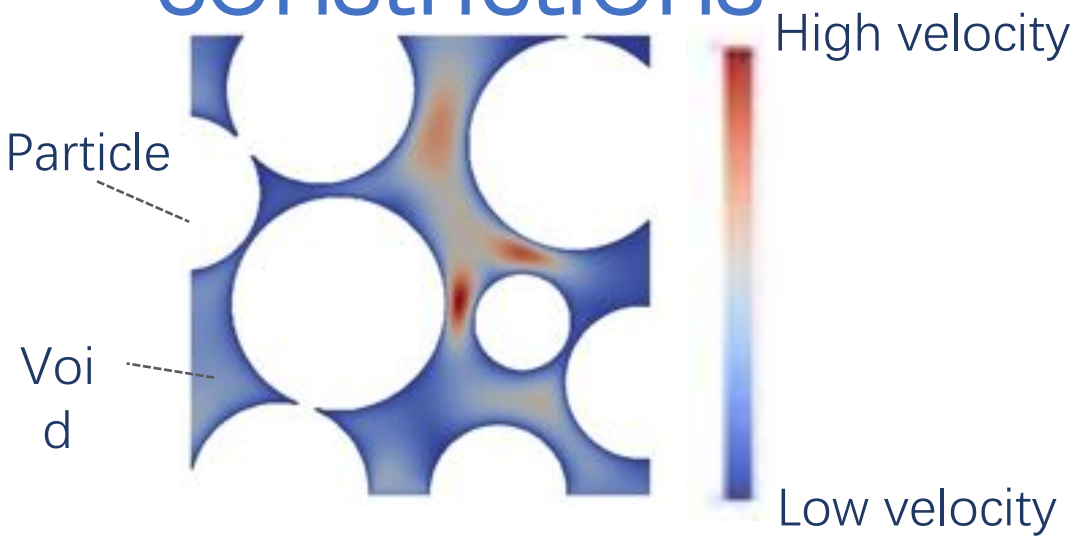

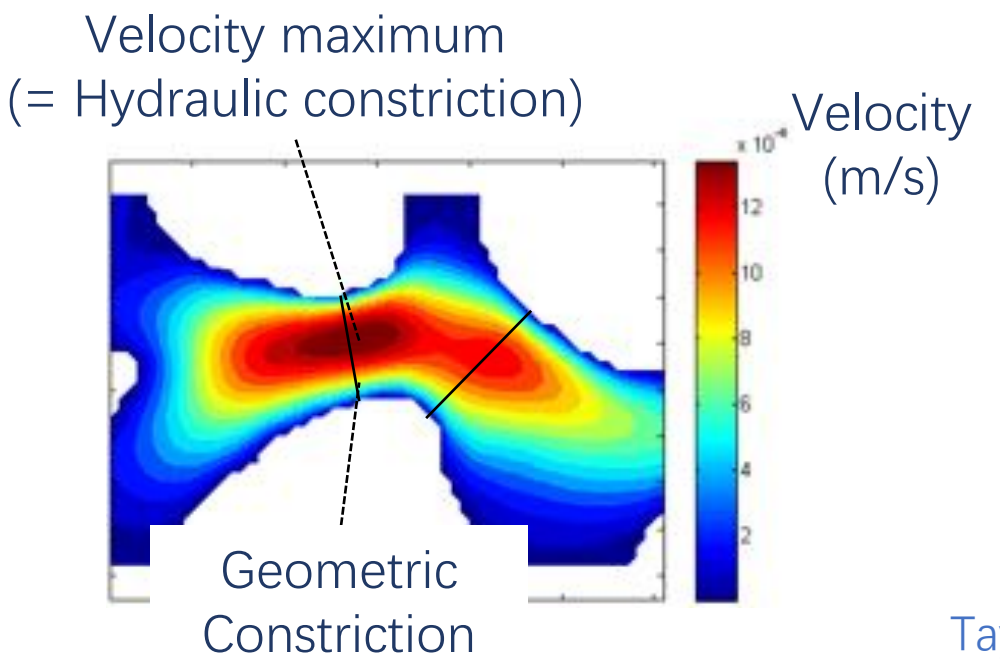

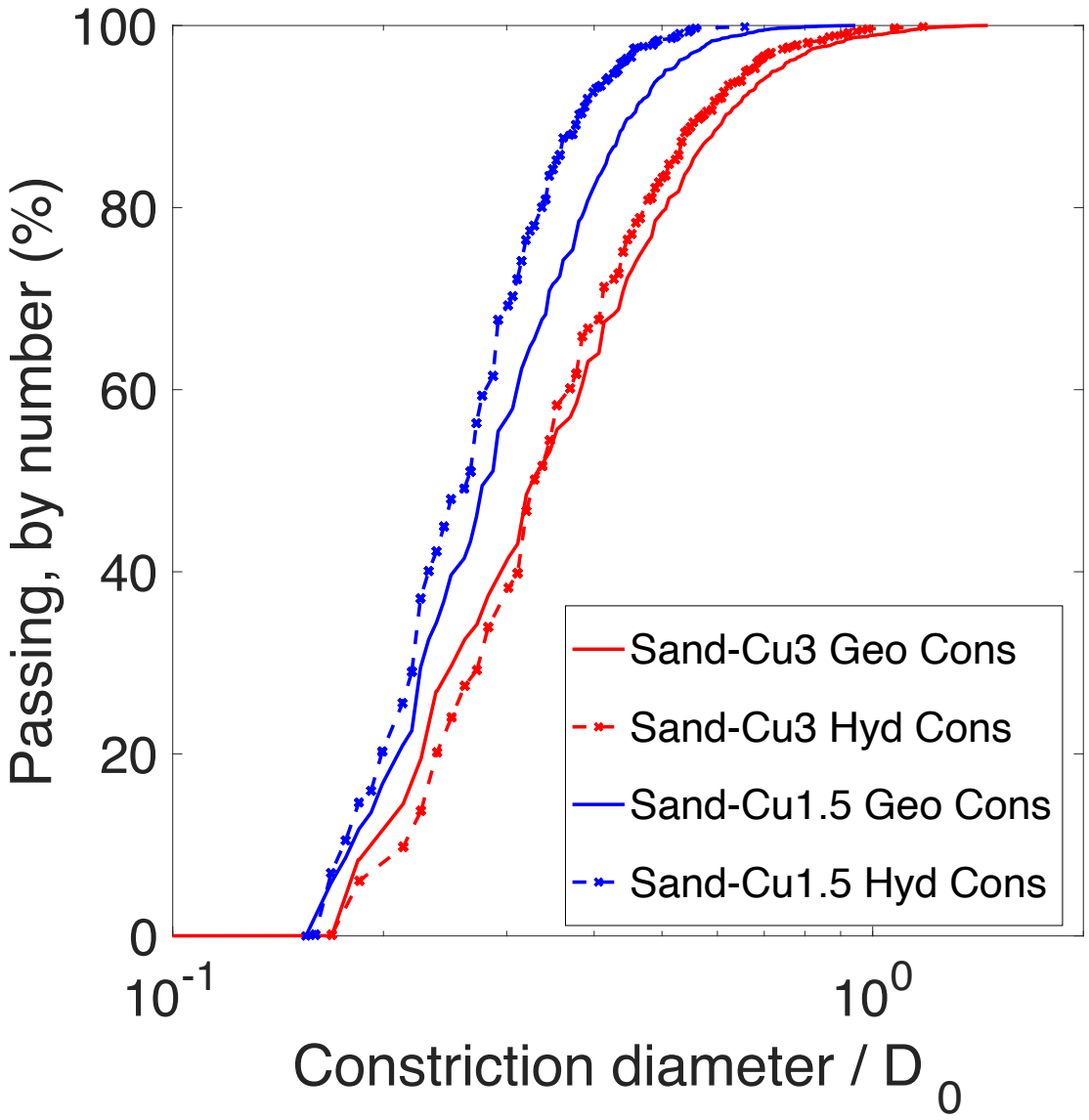

Taylor et al. (2016) https://doi.org/10.1061/(ASCE)GT.1943-5606.0001547

Headloss and streamlines

Velocity (m/s)

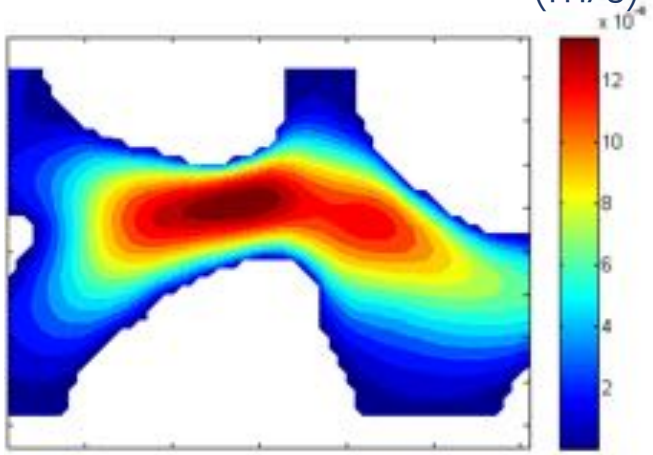

Head (m)

Particle

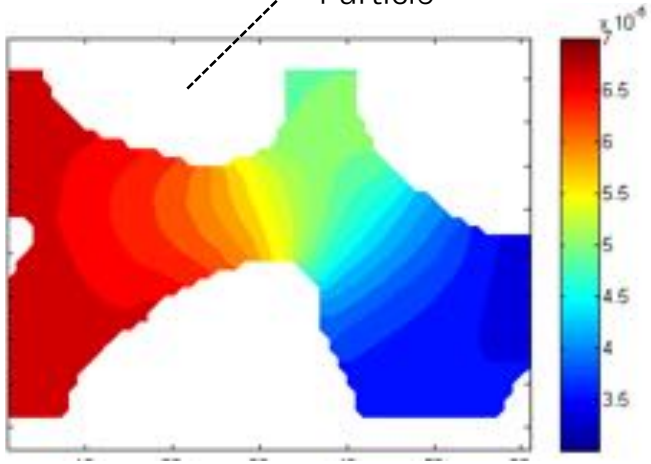

Streamline

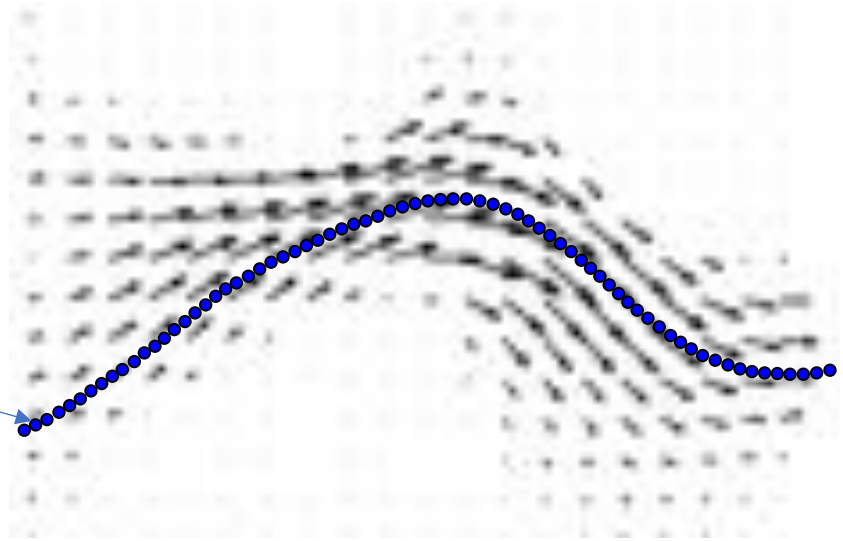

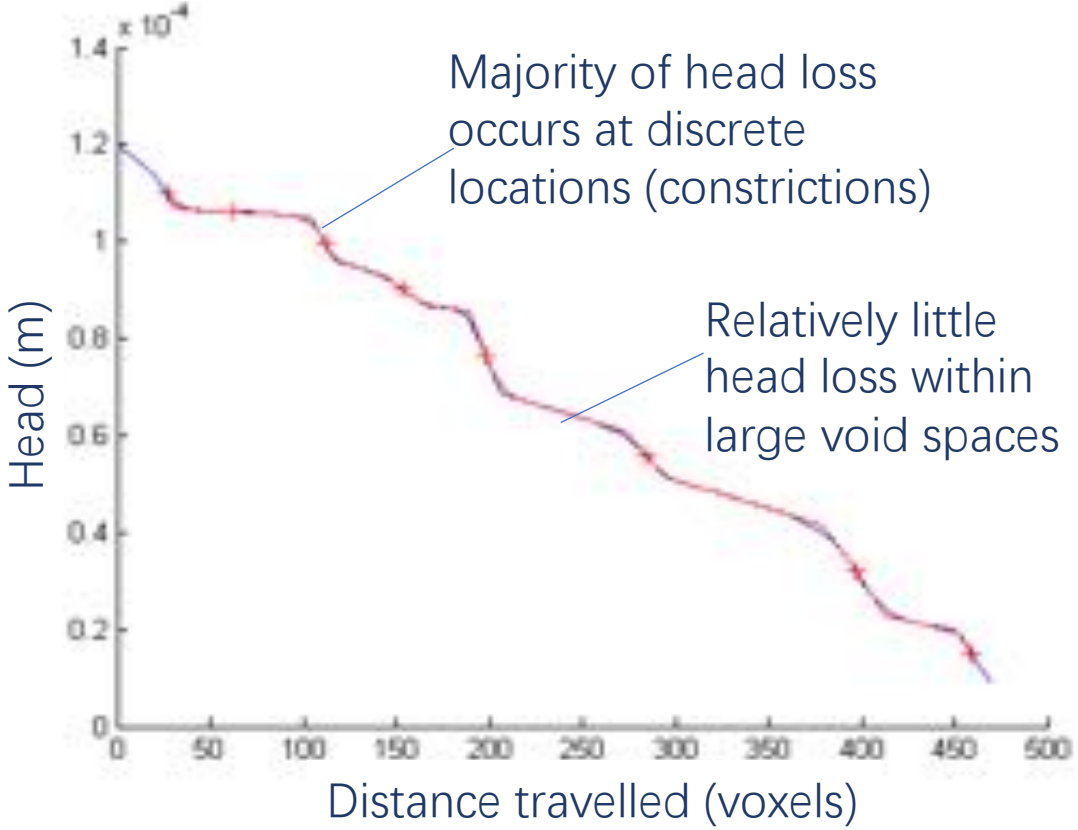

Majority of head loss occurs at discrete locations (constrictions)

Relatively little head loss within large void spaces

CFD+DEM Generated Packings

Spherical harmonics to systematically control shape

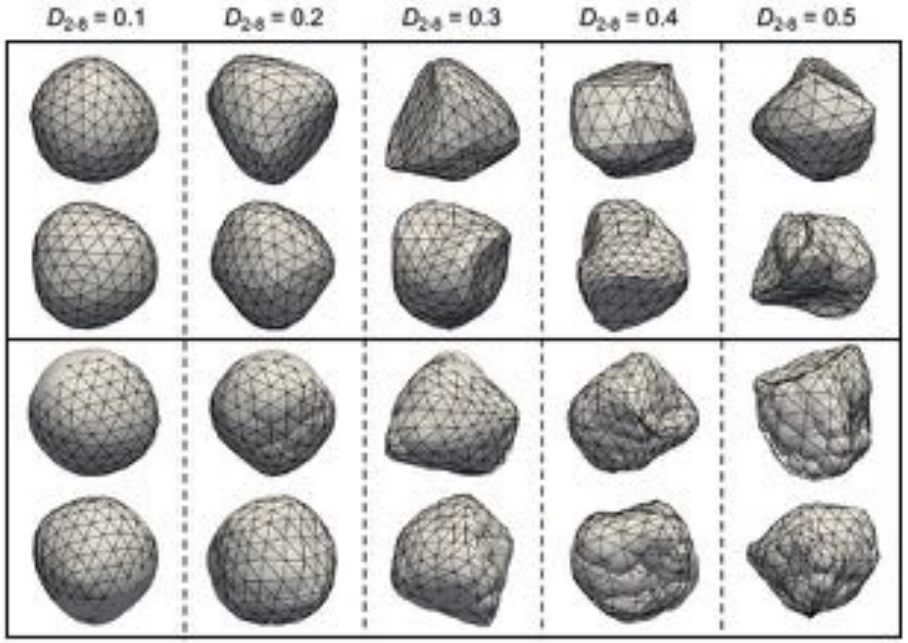

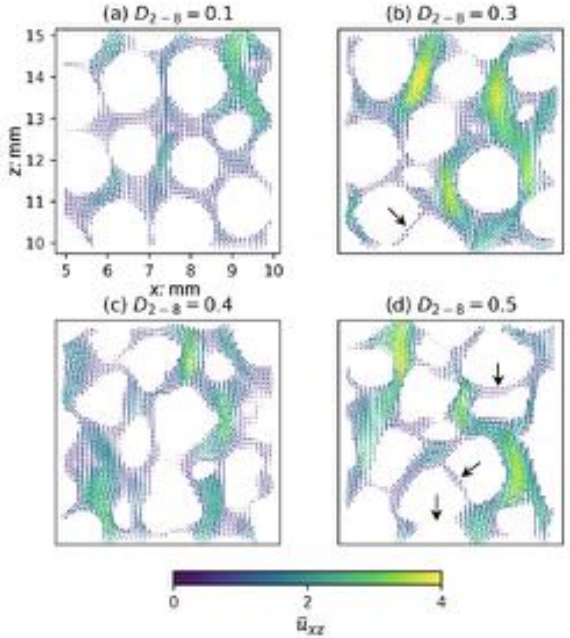

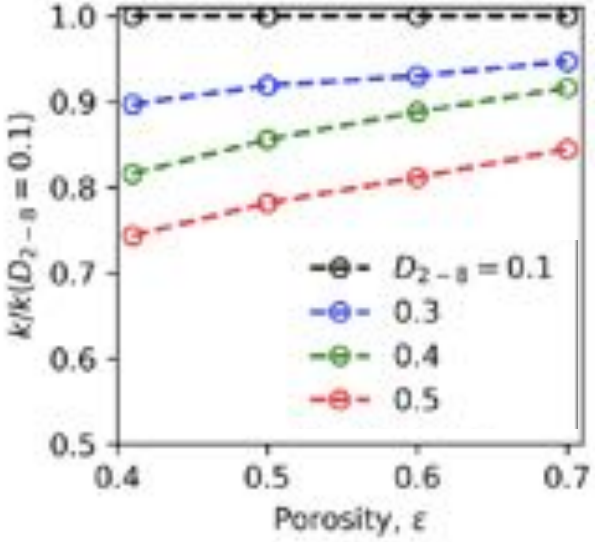

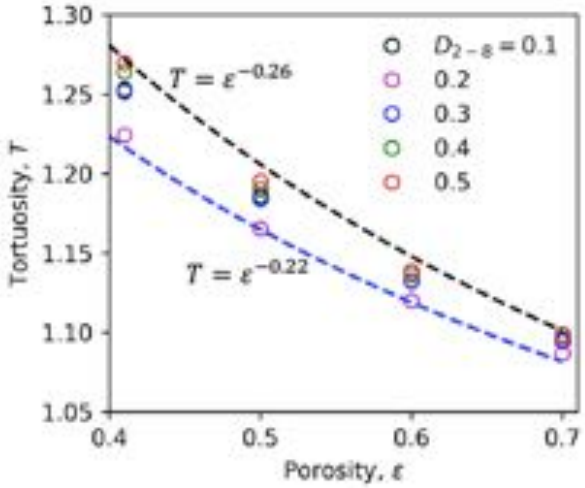

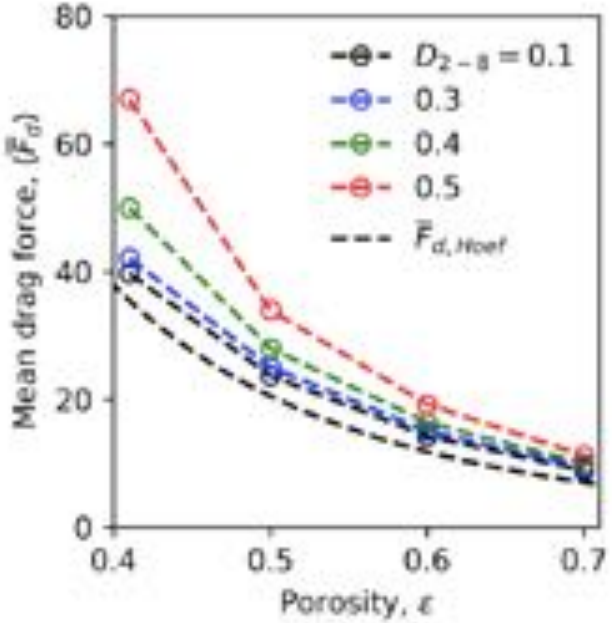

Shape no significant effect on tortuosity or flow field

Shape does affect permeability and drag

Zhao and OSullivan (2022) https://doi.org/10.1016/j.powtec.2021.09.022

Part 4: Semi-solid metals

Semi solid metals – examples of casting defects

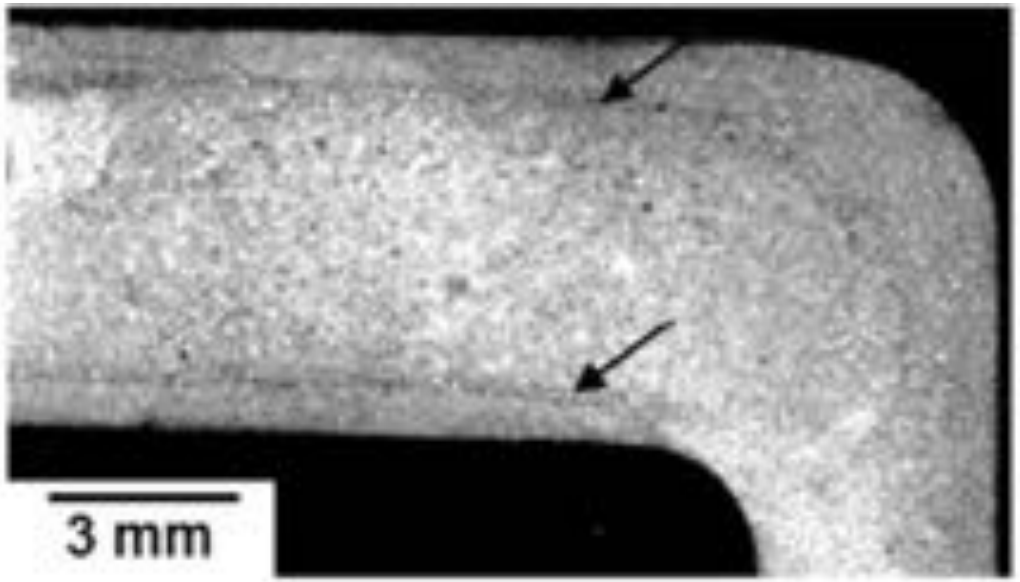

High pressure die cast Al-9Si-4Cu
PhD thesis Kristina Kareh Imperial College London

(d)

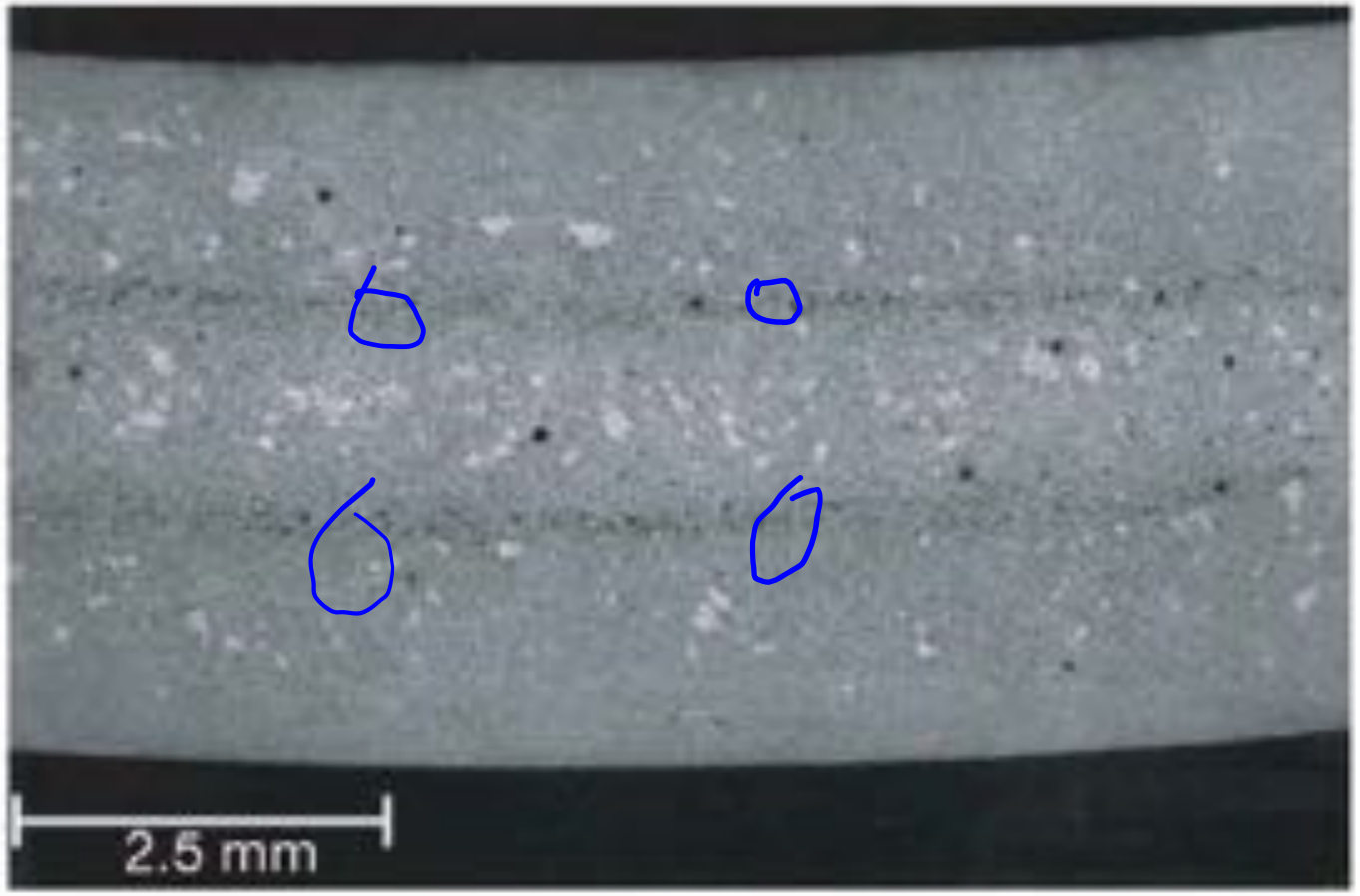

Defect bands in commercial steering wheel
PhD thesis Te-Cheng Su Imperial College London

Semi solid metals – examples of casting defects

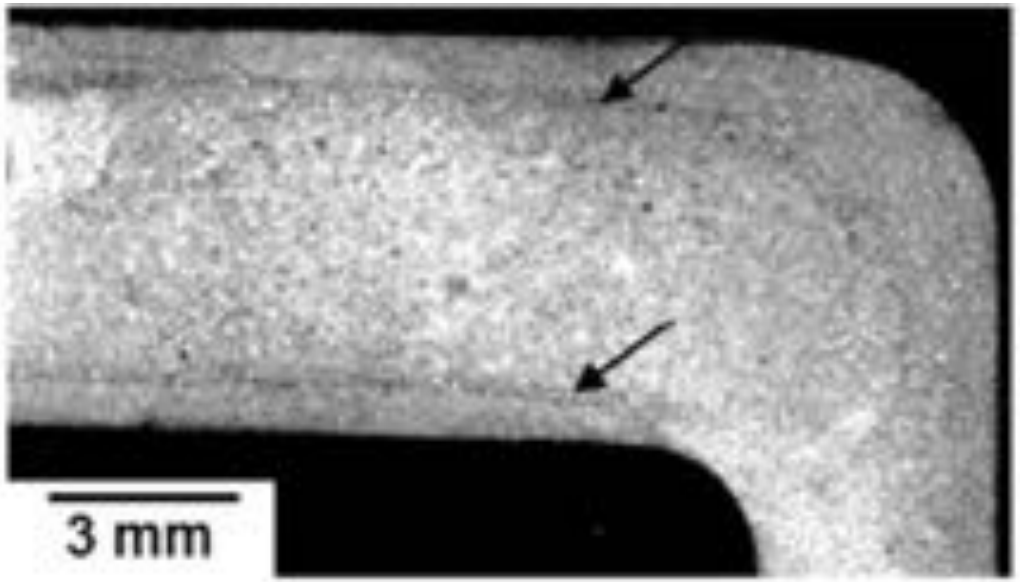

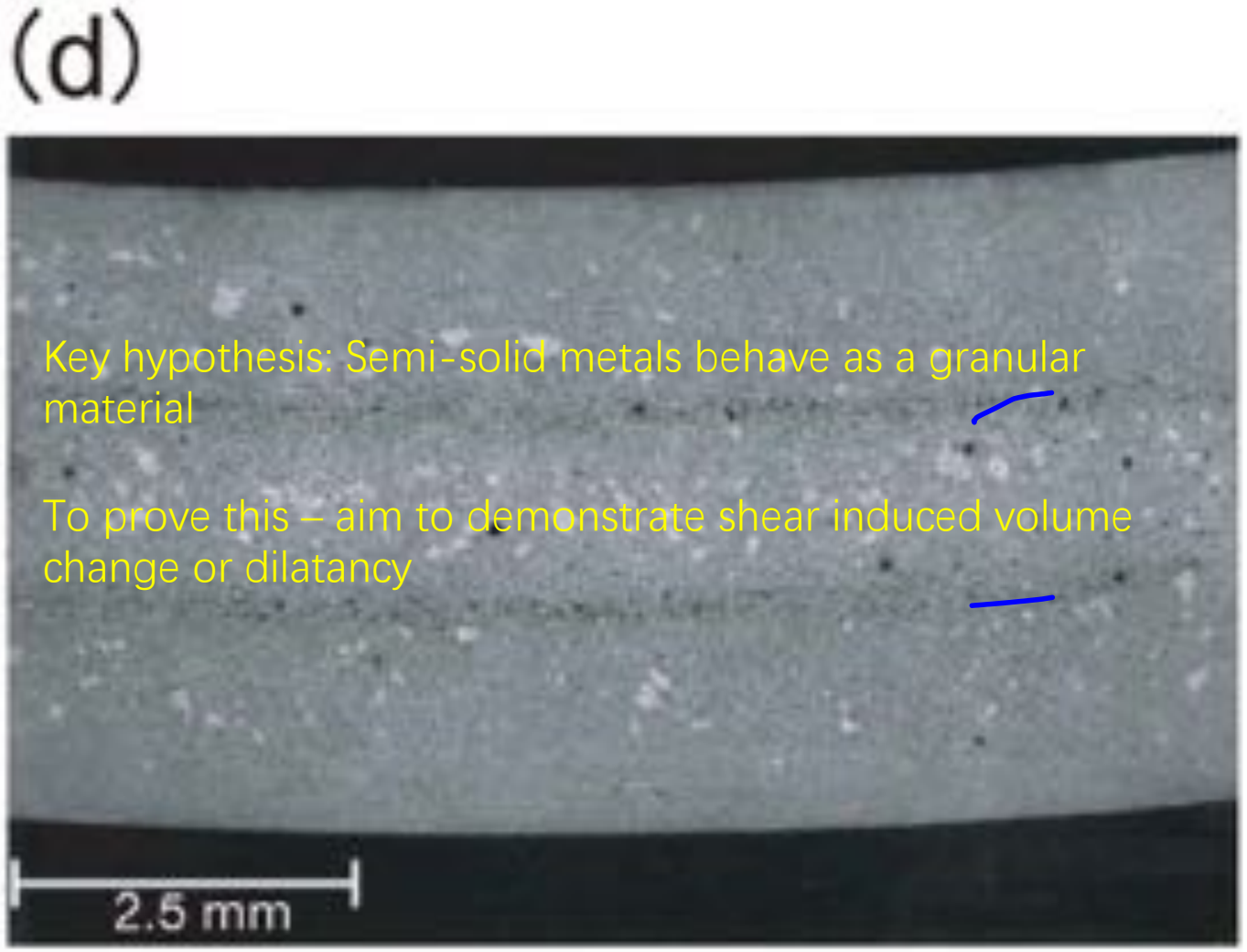

Key hypothesis: Semi-solid metals behave as a granular material

To prove this – aim to demonstrate shear induced volume change or dilatancy

High pressure die cast Al-9Si-4Cu
PhD thesis Kristina Kareh Imperial College London

Defect bands in commercial steering wheel
PhD thesis Te-Cheng Su Imperial College London

Semi solid metals - Radiographs

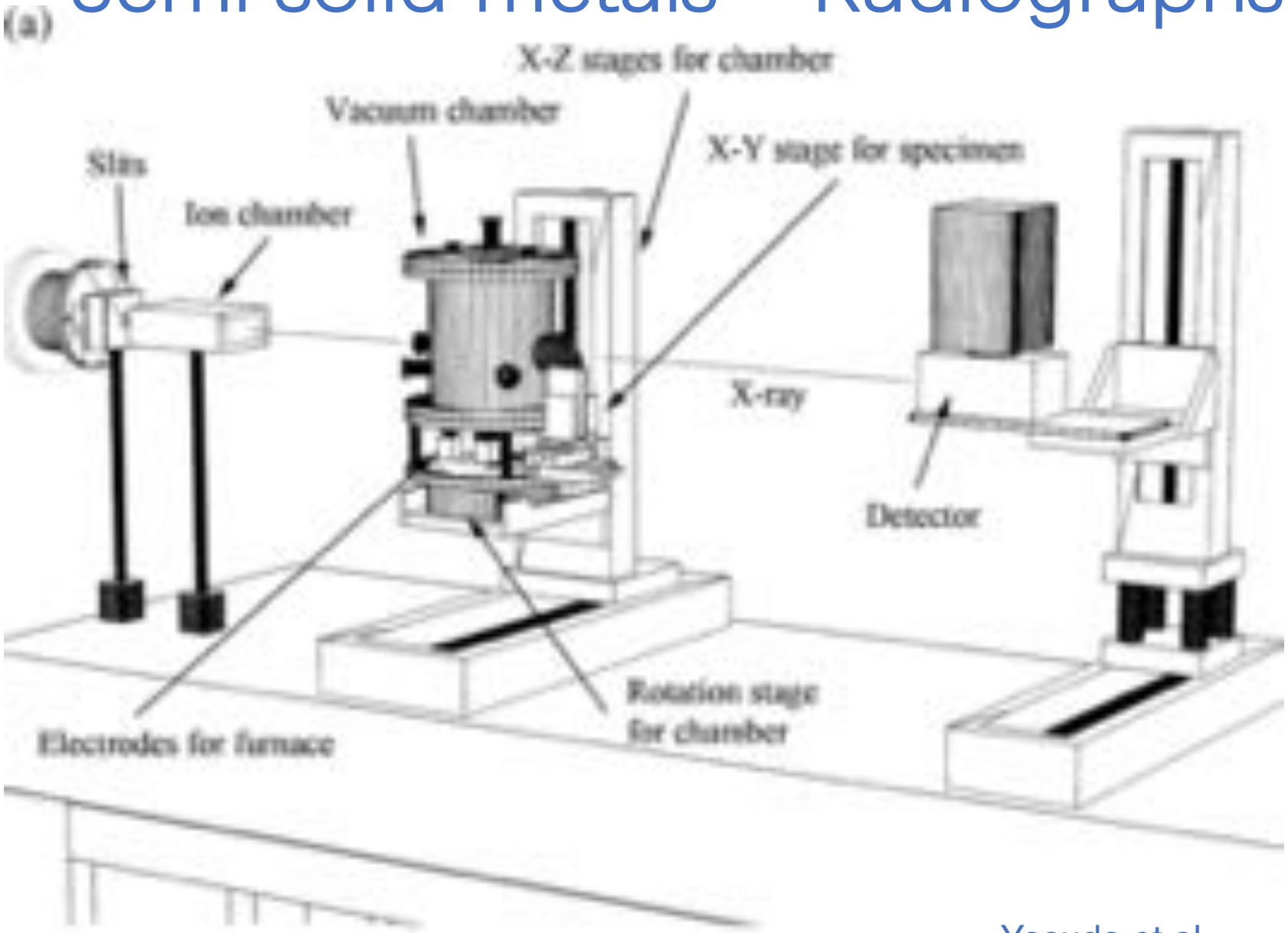

Beamlines BL20XU
and
BL20B2 at the
SPring-8 synchrotron,
Japan

Yasuda et al.
ISIJ International, Vol. 51 (2011), No. 3, pp. 402–408

Semi solid metals - Radiographs

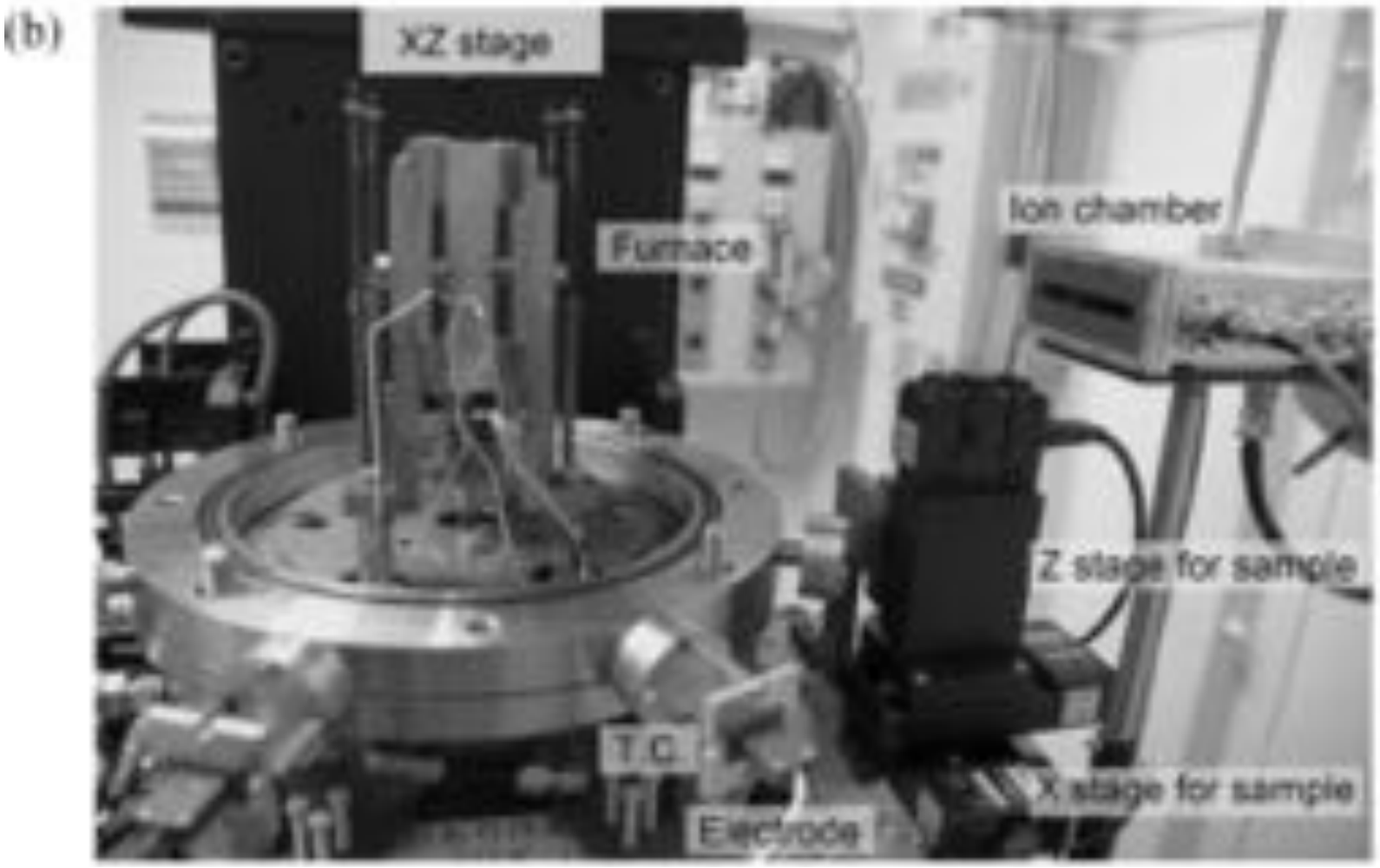

Yasuda et al.
ISIJ International, Vol. 51 (2011), No. 3, pp. 402–408

Semi solid metals - Radiographs

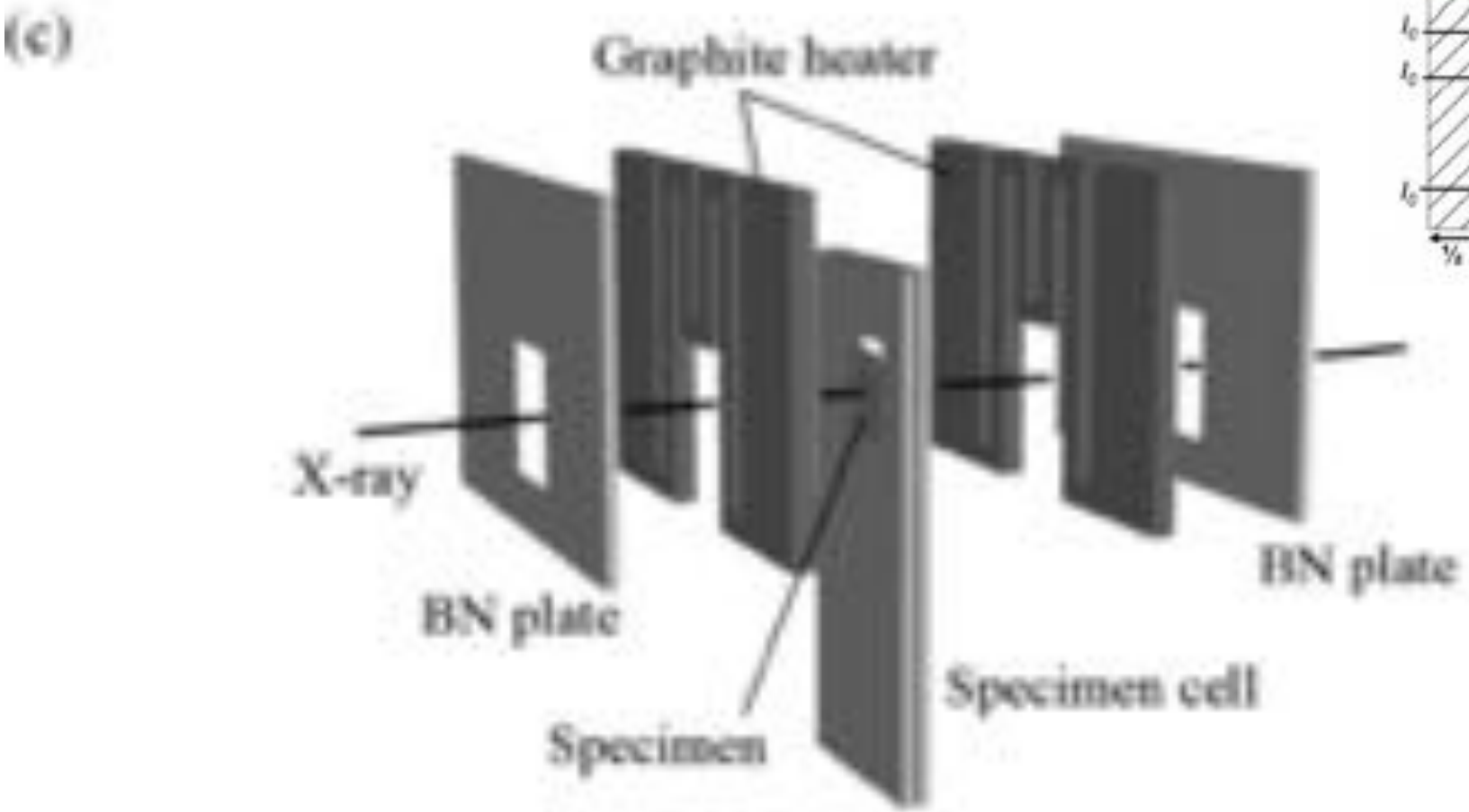

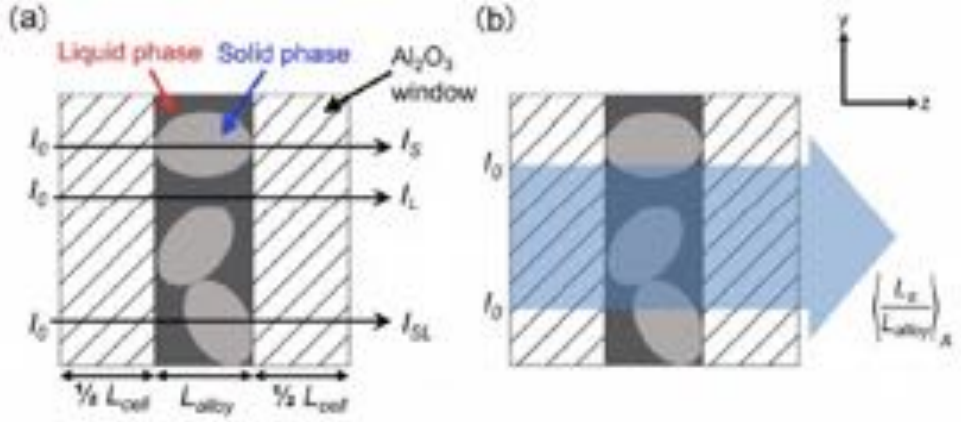

$$\frac{L_S^0}{L_{alloy}^0} = \frac{\ln I_{SL}^0 - \ln I_L^0}{\ln I_S^0 - \ln I_L^0}$$

$$g_{S.A}^0 = \langle L_S^0 / L_{alloy}^0 \rangle_A$$

Yasuda et al.
ISIJ International, Vol. 51 (2011), No. 3, pp. 402–408

Al-Cu alloys:CFD-DEM

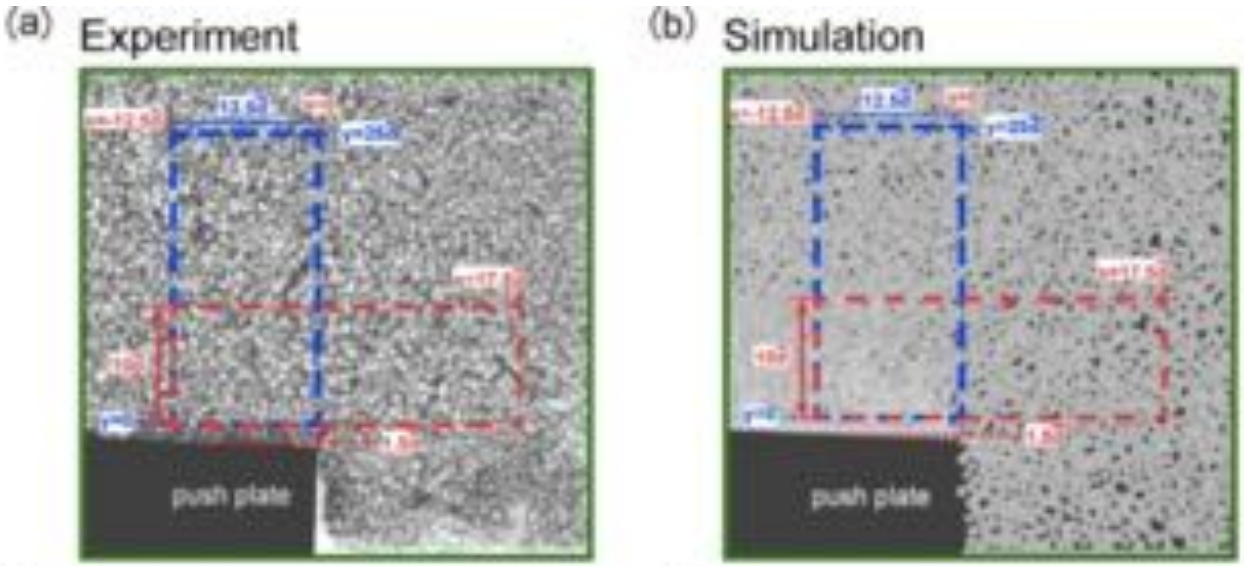

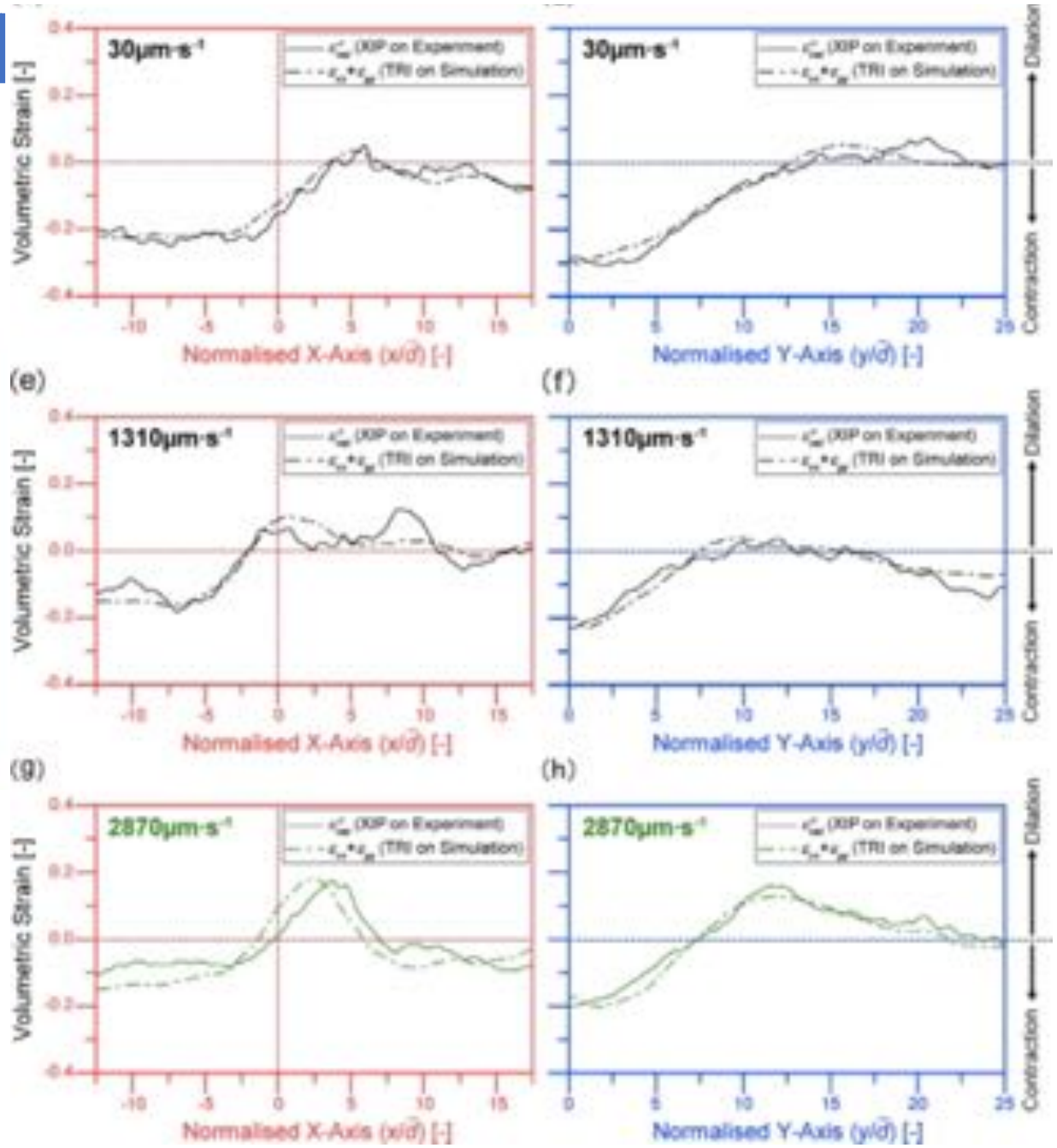

Su et al. (2020)
https://doi.org/10.1016/j.actamat.2020.03.011

Al-Cu alloys:CFD-DEM

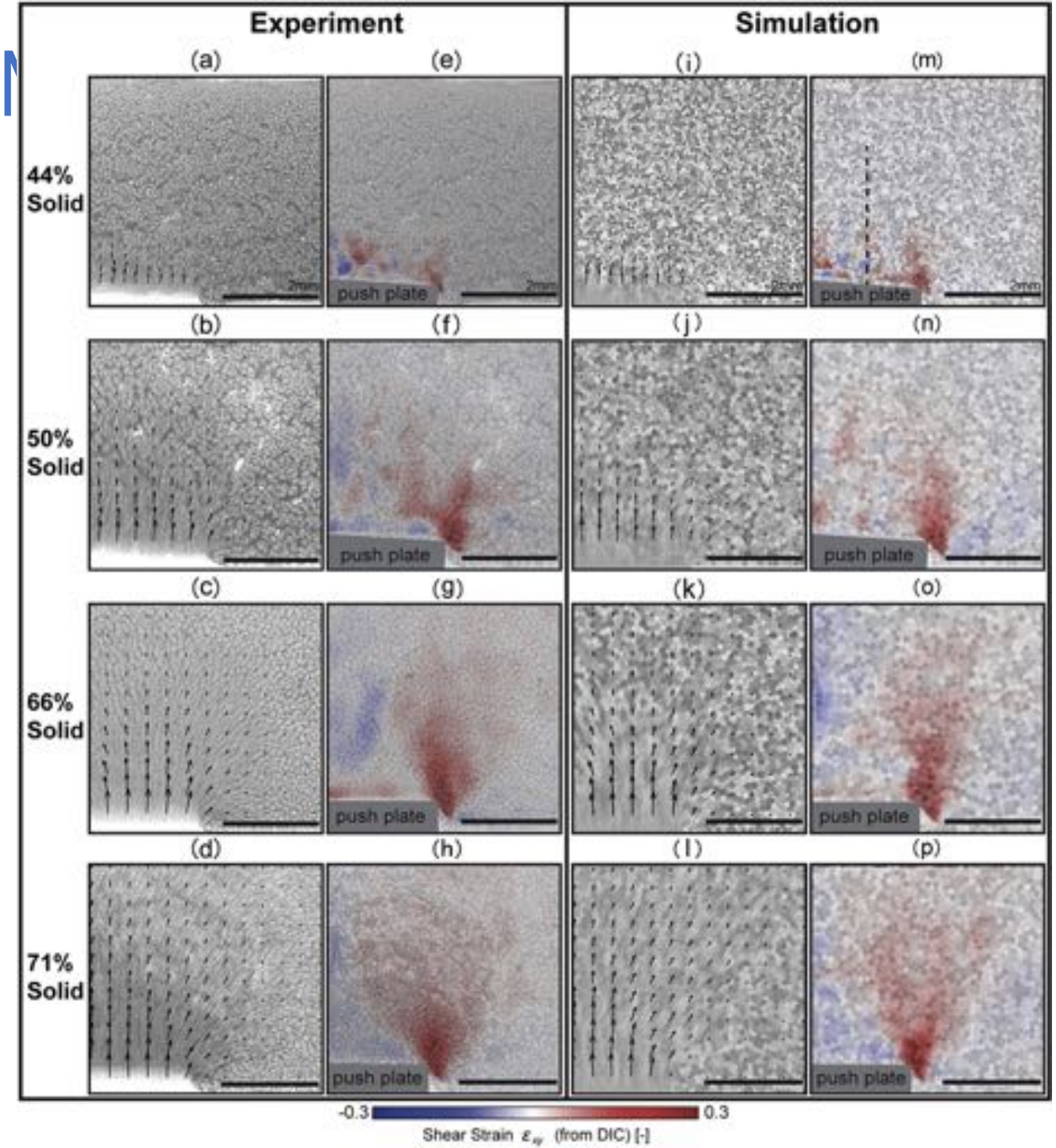

Su et al. (2019)
https://doi.org/10.1016/j.actamat.2018.10.006

Al-Cu alloys:CFD-DEM

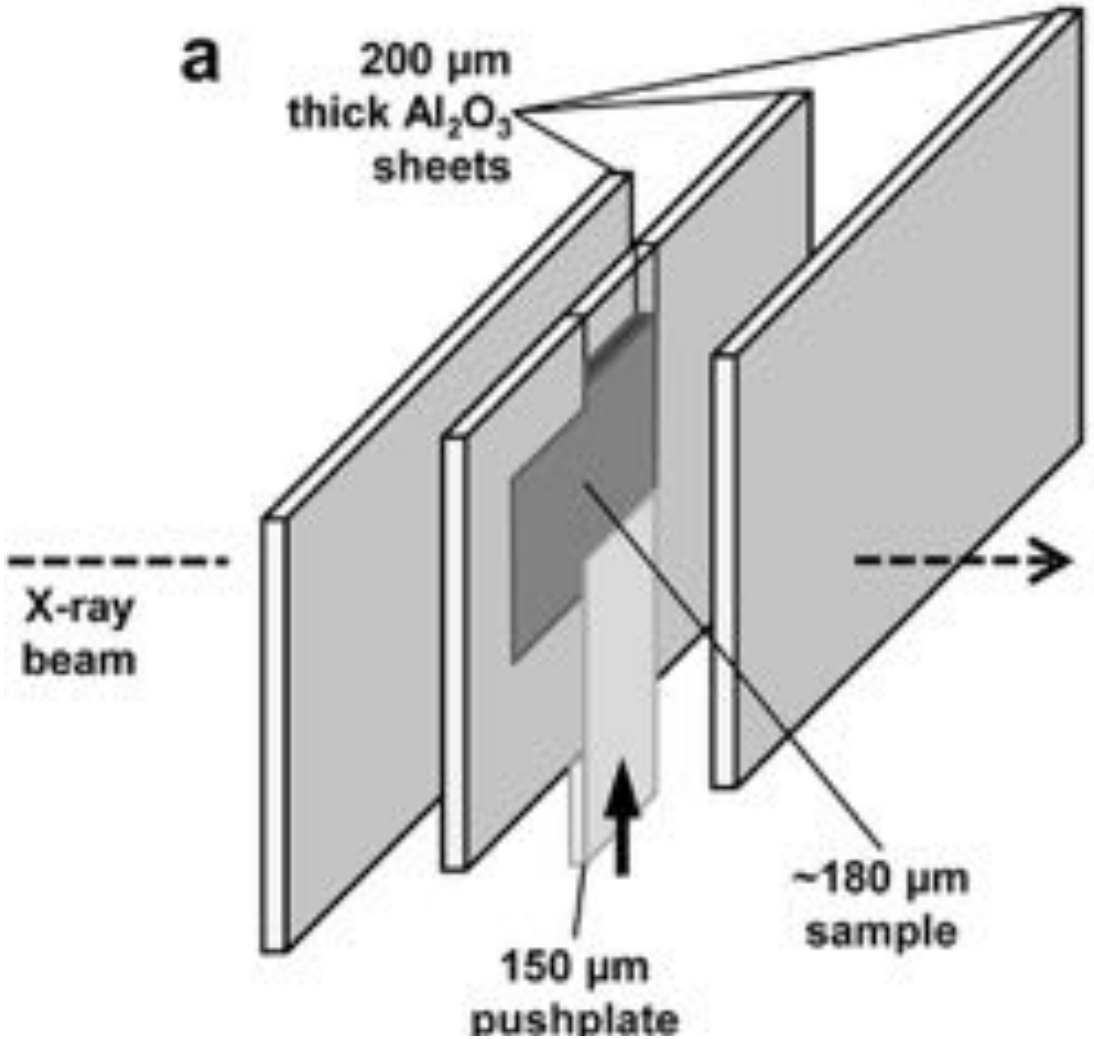

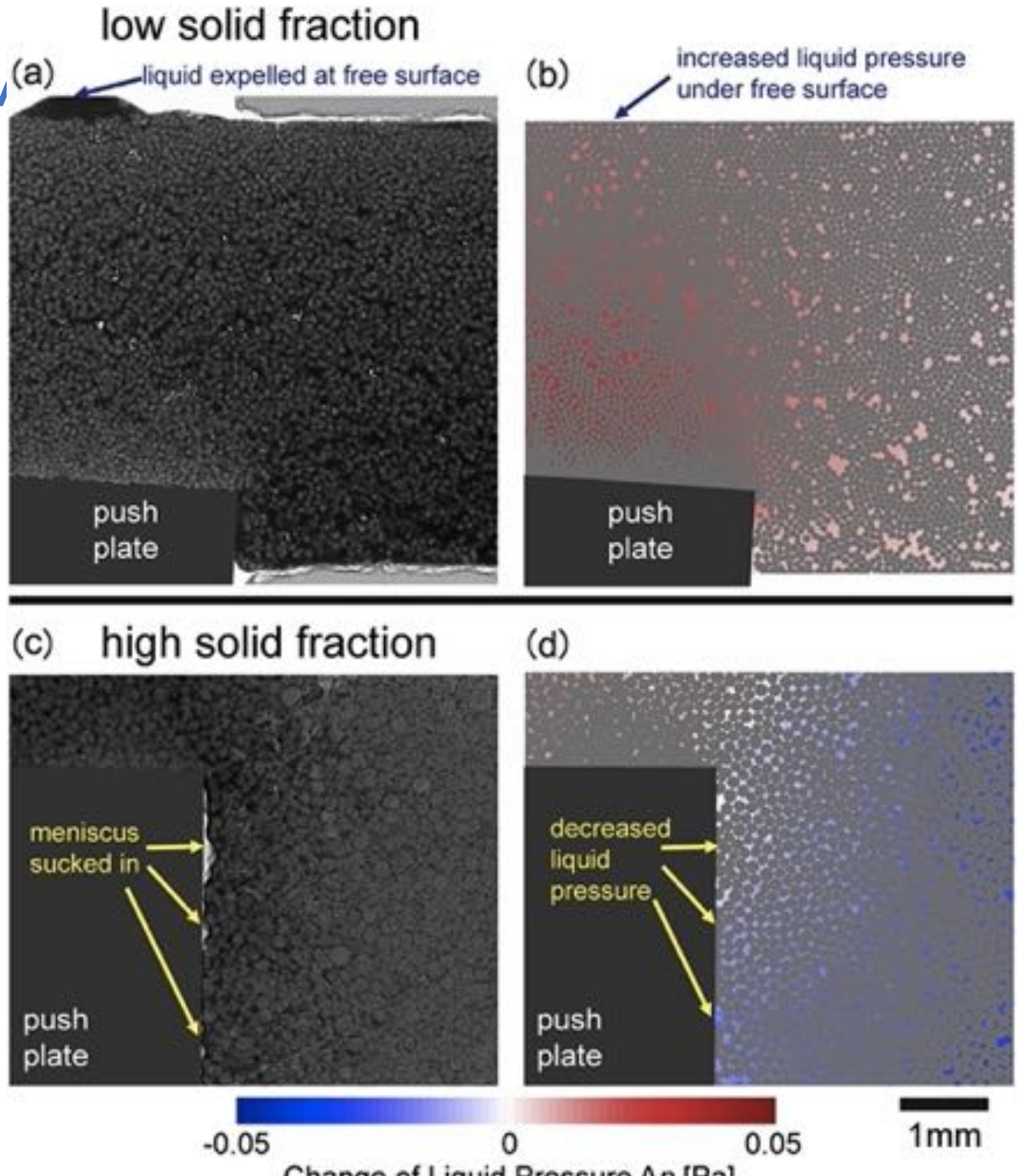

Su et al. (2019)
https://doi.org/10.1016/j.actamat.2018.10.006

Al-Cu alloys:CFD-DEM

Su et al. (2019)
https://doi.org/10.1016/j.actamat.2018.10.006

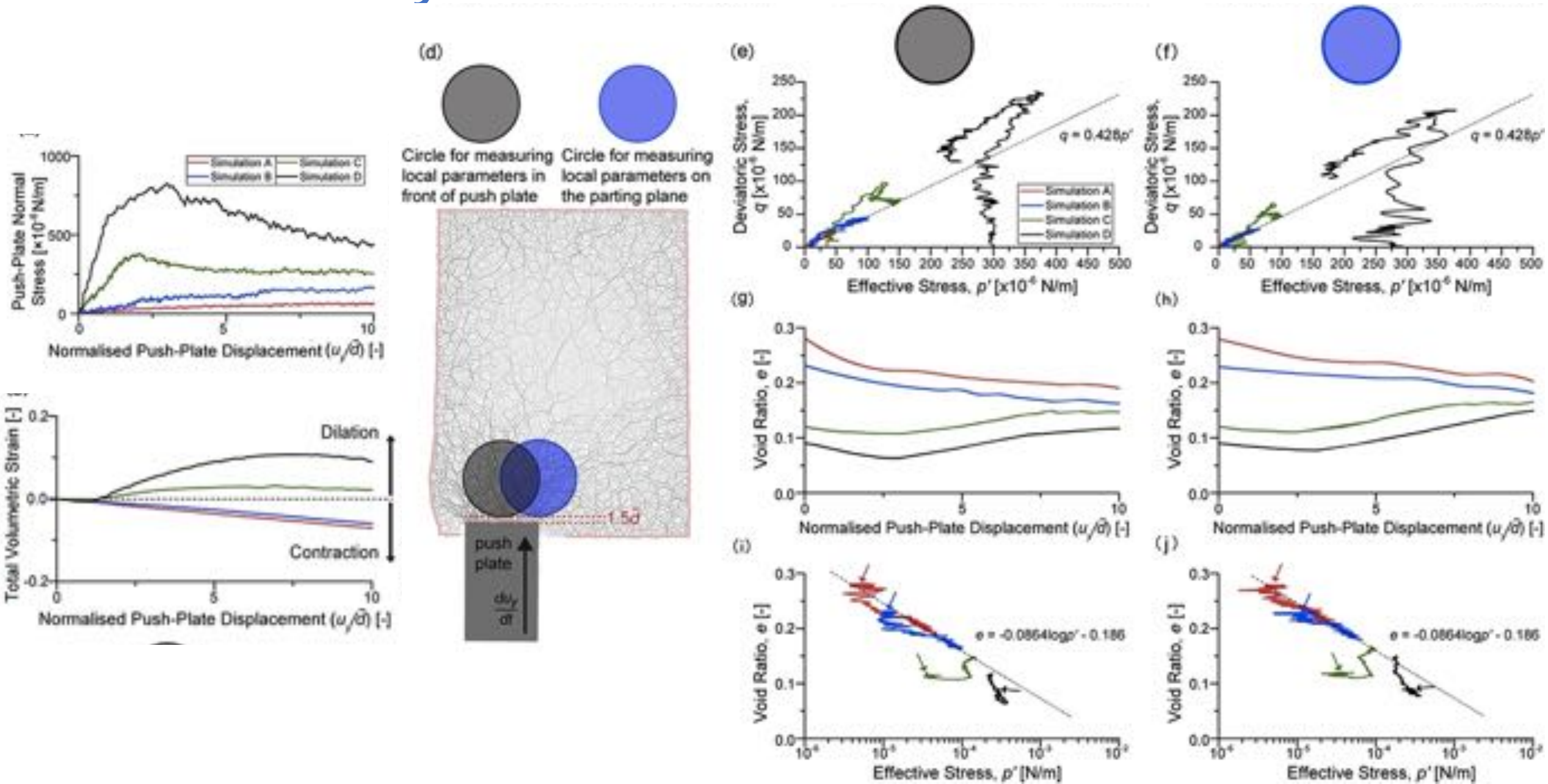

Conclusions

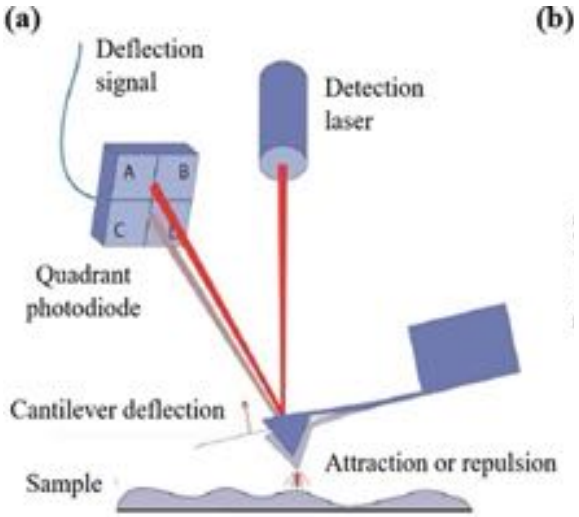

Part 1: Clay

Part 2: Surface roughness

Part 3: Void space topology

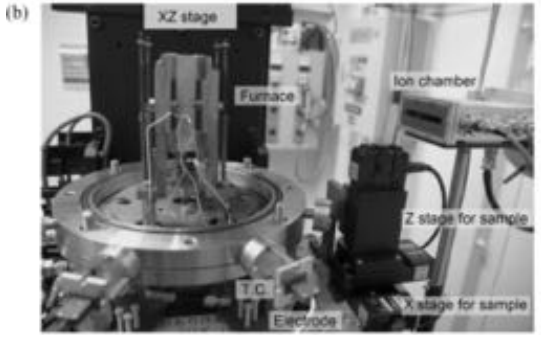

Part 4: Semi-solid metals

Acknowledgements

Tom Shire

Lis Bowman

Stefano Angioletti Uberti

Nicoletta Sanvitale

Yohei Nakamichi

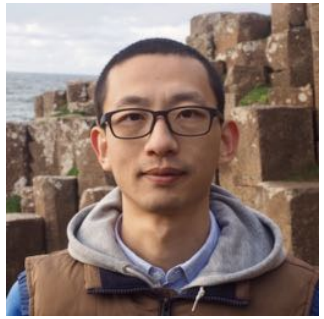

Budi Zhao

Paul Tangney

Way Way Sim

Sara Bandera

Tara Sassel

Howard Taylor

Key references

- Sanvitale et al. (2022) https://doi.org/10.1680/jgeot.20.P.432

- Zhao and O'Sullivan (2022) https://doi.org/10.1016/j.powtec.2021.09.022

- Su et al. (2020) https://doi.org/10.1016/j.actamat.2020.03.011

- Otsubo and O'Sullivan (2018) https://doi.org/10.1016/j.sandf.2018.02.020